**Universidade de Aveiro** Departamento de Biologia
**2017**

**Célia Carolina Moreira Fernandes**

# *H. portulacoides* and *J. maritimus* in a mercury contaminated salt marsh: metal accumulation, biochemical and lipidomic patterns.

# *H. portulacoides* e *J. maritimus* em sapal contaminado por mercúrio: acumulação de metal, padrões bioquímicos e lipidómicos.

**Universidade de Aveiro** Departamento de Biologia
**2017**

**Célia Carolina Moreira Fernandes**

# *H. portulacoides* and *J. maritimus* in a mercury contaminated salt marsh: metal accumulation, biochemical and lipidomic patterns.

# *H. portulacoides* e *J. maritimus* em sapal contaminado por mercúrio: acumulação de metal, padrões bioquímicos e lipidómicos.

Dissertação apresentada à Universidade de Aveiro para cumprimento dos requisitos necessários à obtenção do grau de Mestre em Biologia Molecular e Celular, realizada sob a orientação científica da Dr. Etelvina Maria de Almeida Paula Figueira, Professora auxiliar do Departamento de Biologia da Universidade de Aveiro e co-orientação científica da Dr. Carmen Bedia Girbés, investigadora de Pós-Doutoramento do Institute of Environmental Assessment and Water Research (IDAEA-CSIC) em Barcelona, Espanha.

# DECLARAÇÃO

Declaro que este relatório é integralmente da minha autoria, estando devidamente referenciadas as fontes e obras consultadas, bem como identificadas de modo claro as citações dessas obras. Não contém, por isso, qualquer tipo de plágio quer de textos publicados, qualquer que seja o meio dessa publicação, incluindo meios eletrónicos, quer de trabalhos académicos.

Aos meus pais

**o júri**

presidente

Prof. Doutora Maria de Lurdes Gomes Pereira
professora associada com Agregação, Universidade de Aveiro

Doutora Glória Cataria Cintra da Costa Pinto
professora auxiliar convidada, Universidade de Aveiro

Doutora Carmen Bedia Girbés
Investigadora de Pós-Doutoramento do Institute of Environmental Assessment and Water Research (IDAEA-CSIC)

**agradecimentos**

Primeiramente gostaria de agradecer às minhas orientadoras, Etelvina Figueira e Carmen Bedia, sem elas este trabalho não teria sido possível. Obrigada por toda a disponibilidade, apoio e até os sermões que também fazem parte para uma pessoa aprender e crescer. Um especial obrigado à minha orientadora externa e minha amiga, Obrigada!

Aos meus pais, por tudo o que fizeram, bem ou mal, e ainda o que não fizeram, pois foi isso que fez tornar na pessoa que sou hoje. Por todos os sacrifícios que fizeram, por me mostrarem todas as formas de lutar e chegar a onde queremos, não tenho como agradecer! À minha irmã Catarina, embora mais nova já aprendi muito contigo és um orgulho enorme para mim. Obrigada!
À minha restante enorme Família. Aos meus avós, especialmente aos meus avós maternos pelo exemplo e pela infância que me deram e pelos verões inteiros passados convosco. À minha tia Manuela, uma segunda mãe para mim e por todas as viagens que fizemos juntas! Aos meus primos, não vou dizer nomes pois somos imensos, todas as brincadeiras que tivemos e fazíamos a casa dos avós estar sempre cheia de vida, somos o orgulho dos nossos avós. A todos os tios e tias. Obrigada!

À minha segunda e não menos importante família: os meus amigos. Amigos como vocês, são insubstituíveis, fazem com que nunca estejamos sozinhos, mesmo em tempos difíceis. Tiago e Rogério (amigos desde da pré-escola) que literalmente crescemos e vivenciamos o sucesso um dos outos sempre lado a lado, não há forma de explicar o quão importantes vocês são para mim. À Mariana, que me deu o privilégio de ser sua “madrinha de praxe” e poder ajudar em tudo, agora é ela um exemplo de força e determinação, por todos os momentos que já vivemos, bons ou maus, os festivais, as viagens e todas aquelas experiências que ficam para a vida. Cátia, Daniela e Márcia, as minhas companheiras de casa durante os últimos 4 anos, foram sem dúvida uma família para mim e uma das melhores coisas que Aveiro me deu. À Cristina e Sofia, pelo vosso exemplo e por saber que estiveram sempre a torcer por mim nesta etapa. A todos os outros cujo o nome não está aqui, mas que contribuíram para esta etapa. Obrigada!

Aos colegas e amigos do laboratório, começando pelo Paulo, o principal mentor, que me ajudou naquela interminável noite de preparação das amostras e por toda ajuda nos softwares, és o expert! À Carina, Luísa, Simão, Zé-Tó, Anthony, Lucia e Francesaca. À Angela e Patricia pela companhia nas aventuras que foi em Barcelona! Obrigada!

Aos meus amigos e colegas do IDAEA-CSIC, obrigada por toda a experiencia e fazer da minha estadia em Barcelona inesquecível e pelo o quão cresci a nível profissional bem como pessoal! Pelos longos almoços, as conversas na máquina do café e ainda quando alguém trazia uma sobremesa.
Aos meus colegas internacionais de casa de Barcelona, Sylwia, Daniel e Vicente. Aprendi tanto convosco, desde das comidas típicas de cada país aos nossos longos serões no sofá com as nossas longas conversas, pelas viagens a descobrir a Catalunha e os seus encantos.

E por fim, e não menos importante obrigada Gonçalo por seres tão paciente, por acreditares sempre mim, mas sobretudo pelo amor sempre presente.

a todos um grande Obrigada!

**Palavras-chave**

Sapais, mercúrio, stresse oxidativo, UPLC-MS, lipidómica,resposta bioquímica, bioacumulação

**resumo**

Os sapais, considerados um dos ecossistemas mais produtivos, servem como reservatório para contaminantes, nomeadamente metais provenientes de industrias, reduzindo desta forma a contaminação dos ecossistemas circundantes.

Em ambiente aquático, a poluição por mercúrio (Hg) é principalmente devido a descargas de efluentes de industrias contendo concentrações elevadas deste metal. O mercúrio é reconhecido como sendo um metal pesado e extremamente tóxico para as plantas, interferindo desta forma em vários processos celulares cruciais.

Este estudo evidenciou a importância de compreender o processo aquando da exposição das plantas ao mercúrio e desta forma avaliar o impacto da toxicidade do Hg nas comunidades de sapais. Uma melhor compreensão sobre estes aspetos de acumulação avaliará o stress imposto pelo Hg sobre a produção primária em plantas de sapal e a adaptação das plantas no ecossistema. Adicionalmente este estudo permite também a interpretação dos mecanismos moleculares da tolerância ao mercúrio das plantas uma vez que estas são importantes para uma limpeza eficiente dos sistemas contaminados por Hg para uma restauração efetiva.

Desta forma, o trabalho incidiu em duas espécies de plantas halófitas, *Halimione portulacoides* e *Juncus maritimus* recolhidas em dois locais da Ria de Aveiro contaminados por mercúrio, s1 considerado como o local menos contaminado e s2 como o local mais contaminado. Este estudo foi projetado para (1) avaliar como a distribuição de Hg em plantas (2) de que forma as plantas iram reter a toxicidade do Hg desencadeando respostas antioxidantes. De fato, a maioria dos parâmetros bioquímicos determinaram a evidência de respostas diferentes por concentrações diferentes de Hg no sedimento (s1 e s2) e (3) as plantas poderiam ou não modificar sua composição lipídica por toxicidade de Hg através da metodologia UPLC-MS.

Este estudo demonstrou que ambas as espécies de plantas restringiam a absorção de Hg. No entanto, o processo foi mais eficiente em *H. portulacoides*. Foram observadas diferenças na quantidade de Hg acumulada por ambas as espécies. Os padrões de alocação também diferem entre as espécies. *H. portulacoides* apresentou diferentes níveis de Hg entre folhas, caules e raízes, enquanto *J. maritimus* acumulou os níveis mais elevados de Hg nas raízes. A conjugação dos processos, absorção e translocação resultou em concentrações semelhantes de Hg em caules e folhas e níveis de Hg muito elevados em raízes de *J. maritimus*.

Os resultados obtidos demonstram que o Hg gerou danos oxidativos nas raízes de ambas as espécies e nas folhas de *H. portulacoides*. As diferenças na LPO entre espécies que se obteve refletem não apenas o nível de Hg acumulado e distribuição de Hg, mas também a capacidade de desencadear mecanismos de defesa. *J. maritimus* foi capaz de aumentar os níveis proteicos e atividade DHAR em raízes e rizomas e GSTs em rizomas. *H. portulacoides* não conseguiu induzir respostas enzimáticas antioxidantes. Contudo, nas folhas as moléculas antioxidantes como carotenoides e α-tocoferol foram aumentadas.

No estudo do lipidoma, as espécies também apresentaram diferenças. Em *H. portulacoides*, os fosfolípidos diminuíram em todos os órgãos analisados, o que pode sugerir a alteração da permeabilidade da membrana. Além disso, os galactolípidos diminuíram a eficiência na fotossíntese. No entanto, o α-tocoferol aumentou, proporcionando assim uma melhor proteção às membranas de cloroplastos e manutenção da atividade fotossintética.

Em *J. maritimus*, as alterações lipídicas só foram detetadas em raízes e rizomas, aumentando a permeabilidade lipídica e explicando a maior bioacumulação de concentrações elevadas de Hg. Os fito-esteróis diminuíram significativamente nas raízes e levaram a alterações da membrana de permeabilidade. O α-tocoferol diminuiu em ambos os órgãos de *J. maritimus*, demonstrando a ineficiência para a contaminação por Hg.

Este estudo pode ser um ponto de partida para novos trabalhos, nomeadamente em outros sapais, em outras espécies e com outros metais. Compreender os mecanismos inerentes à tolerância de metais pesados em plantas de sapais e as mudanças na composição lipídica são importantes para detetar o impacto dos metais nestes ecossistemas.

**keywords**

Salt marshes, mercury, oxidative stress, UPLC-MS, lipidomic, biochemical response, bioaccumulation

**abstract**

The salt marshes, one of the most productive ecosystems, serves as the sink for contaminants, namely metals from industries, reducing in this way the contamination of surrounding ecosystems.

Although, as levels of contaminants, the ability of salt marshes to incorporate wastes can be impaired. In the aquatic environment, high mercury (Hg) pollution is mainly due to metal discharge of effluents from chloralki plants containing high concentrations of this metal. Mercury has been recognized as heavy metal and extremely toxic to plants interfering with several crucial cellular processes.

This study evidenced the importance to understand the analysis that plants under environmental exposed to Hg and to evaluate impact of Hg toxicity in plants salt marsh communities. Better knowledge on these accumulation aspects will evaluate the stress imposed by Hg on primary production in salt marsh plants and adaptation of mobility of the metal in the ecosystem. As well as the molecular mechanisms mercury tolerance, which are important to clean efficiently Hg contaminated systems in order to an effective restoration is achieved.

In this way, the work focused on two species of halophytes, *Halimione portulacoides* and *Juncus maritimus* collected at two sites of the Ria de Aveiro contaminated by mercury, considered s1 as less contaminated site and s2 as the most contaminated site.

Thus, this work was designed to (1) evaluate how Hg distribution in plants would avoid high Hg concentrations (2) which way plants would retain Hg toxicity by triggering antioxidant responses. Indeed, most of biochemical parameters determinate the evidence of different responses by different concentration of Hg in the sediment (s1 and s2) and (3) plants can or not modify their lipid composition by Hg toxicity through the UPLC-MS methodology.

This study demonstrated that both plant species restricted Hg uptake. However, the process was more efficient in *H. portulacoides*. Was observed differences in the amount of Hg accumulated by both species. Allocation patterns also differs between species. *H. portulacoides* showed different levels of Hg between leaves, stems and roots, while *J. maritimus* accumulated the higher levels of Hg in roots. The conjugation of both process, absorption and translocation resulted in similar Hg concentrations in stems and leaves and much higher Hg levels in *J. maritimus* roots.

The results obtained demonstrate that Hg generated oxidative damage in the roots of both species and in leaves of *H. portulacoides.* Differences in LPO between species obtaining for each specie reflects not only the level of Hg accumulated and Hg distribution but also the ability to trigger the defense mechanisms. *J. maritimus* was able to increase the protein levels and DHAR activity in roots and rhizomes and GSTs in rhizomes. *H. portulacoides* was not able to induce the antioxidant enzymatic responses. Although in leaves antioxidant molecules such carotenoids and α-tocopherol were enhanced.

In lipidome study, species also showed differences. In *H. portulacoides*, phospholipids decreased in all the organs analyzed, which can subject an alteration of membrane permeability. In addition, galactolipids decreased, reducing the efficiency on photosynthesis. However, α-tocopherol increased, and so better protection to chloroplast membranes and maintenance of photosynthetic activity provided. In *J. maritimus*, lipid changes were only detected in roots and rhizomes, increasing lipid permeability and explaining the higher bioaccumulation at high Hg concentrations. Phyto sterols decreased significantly in roots and lead to alterations of permeability membrane. α-tocopherol was detected in both organs of *J. maritimus*, a decrease that demonstrate an ineffective Hg contamination.

This study may be a starting point for further work, namely in other marshes, in other species and with other metals. Understanding the mechanisms inherent to in heavy metal tolerance in marsh plants and the changes in lipid composition are important to detect the impact of metals in these ecosystems.

# Index

# Abbreviations

| | |
|---|---|
| α – toc | α – tocoferol |
| Aas | Atomic absorption spectrometry |
| AsA | Ascorbate |
| AMA | Advanced Mercury Analyzer |
| ATSDR | Agency for Toxic Substances and Disease Registry |
| BAF | Bioaccumulation factor |
| BRs | Brassinosteroids |
| CAT | Catalase |
| Cer | Ceramide |
| CoQ9 | Ubiquinone |
| DG | Diacylglycerol |
| DGDG | Di-Galactosyl-Diacyl-Glycerol |
| DHA | Dehydroascorbate |
| DHAR | Dehydroascorbate redutase |
| FA | Fatty-acid |
| GC | Gas chromatography |
| GPx | Glutathione peroxidase |
| GR | Glutathione reductase |
| GSH | Gluthathione |
| GSSH | Oxidized glutathione |
| GST | Glutathione-S-transferase |
| LC | Liquid chromatography |
| HPLC | High-performance liquid chromatography |
| LPC | Lysophosphatidyl-choline; |
| LPI | Lysophosphatidyl-inositol |
| LPO | Lipid peroxidation |
| MCR-ALS | Multivariate curve resolution by alternating least squares |
| MDHA | Monodehydroascorbate |
| MG | Monoacylglycerol |

| | |
|---|---|
| MGDG | Mono-Galactosyl-Diacyl-Glycerol |
| MS | Mass spectrometry |
| MSI | Mass spectrometry imaging |
| $Na^+$ | Sodium ion |
| PA | Phosphatidic Acid |
| PC | Phosphatidyl-Choline |
| PCA | Principal Component Analysis |
| PCO | Principal coordinates |
| PE | Phosphatidyl-Ethanolamine |
| PG | Phosphatidyl-Glycerol |
| PI | Phosphoinositide |
| PII | Photosystem II |
| ROI | Regions of interest |
| ROS | Reactive Oxygen Species |
| SOD | Superoxide dismutase |
| SDQG | Sulfoquinovosyl-Diacyl-Glycerol |
| TF | Translocation factor |
| TG | Triacylglycerol |
| TLC | Thin-layer chromatography |
| TOF | Time-of-flight |
| UPLC | Ultra-performance liquid chromatography |

# Chapter 1: Introduction

## 1.1 Salt marsh

Salt marshes are complex coastal environments where tidal flooding with seawater leads to a partial or total submergence of vegetation, high sediment salinity and sediment anoxia (Rebora et al., 2008; Armstrong et al., 1991). These ecosystems are located in estuaries, and coastal lagoons and frequently receive large inputs of nutrients and contaminants coming from nearby urban areas, river transportation and tidal inundation (Doyle and Otte 1997; Williams et al., 1994). The reduced flux of tides helps the deposition of detritus in suspension, increasing organic matter which after decomposition supports salt marsh contaminants. Salt marshes have a huge importance for migrating birds and many invertebrates (Hughes, 2001). The nutrients come to marshes naturally, taken by the constant movement of tidal flow, the sediment from the continental zone, the living microorganisms that are fixed and died there decomposed (Pedro, 1986). They are dynamics, influenced by water action, sedimentation and vegetation, which leads to having ecological and economic importance (Silva, 1993). With all these features makes it the most productive ecosystem of the planet (Mitsch & Gosselink, 2000). All these features make salt marshes the most productive ecosystem on planet and emphasize their ecological and economic importance (Mitsch & Gosselink, 2000; Silva, 1993).

## 1.2 Salt marsh vegetation – Halophytes

Salt marsh vegetation has a wide geographic distribution due, not only to its long-distance dispersal, but also to the similarities between salt marsh environments around the globe (Adam, 2002).

The physical-chemical conditions of salt marshes are relatively adverse for growth and reproduction of most vascular plants, thus limiting the number of species capable to survive in these environmental conditions. Thus, the vegetation of these ecosystems includes a reduced number of species, belonging to few genus but with morphological and physiological features well adapted to the habitat conditions (Adam, 1993). Most of the plants are classified as halophytes, since they complete their life cycle in habitats with a high salt content (Waisel, 1972).

These species have anatomical and morphological features allowing them to survive in these adverse conditions, namely, leaf area reduction due to decrease water loss by transpiration, increased leaf and stem succulence as strategy to accumulate sodium ion ($Na^+$)

absorbed, protection of aerial organs from water loss through a thick cuticle, presence of secretory salt glands to eliminate the accumulated $Na^+$ and the presence of aerenchyma to allow growth in anoxic sediments (Carvalho, 2009; Marschenner, 1995, Grigore et al. 2014).

*Halimione portulacoides* (L.) is a dicotyledonous salt marsh halophyte belonging to the Chenopodiaceae family which is the most represented halophytic family, with a large number of genus and species and has a C3 metabolism. Flowering is from August until November. Regarding its distribution, it is scattered along the coast of the Iberian Peninsula, including *Ria de Aveiro* (Silva, 2000), in salt marshes and estuaries along the Mediterranean, European Atlantic cost (until Denmark) Southern Africa and North American Atlantic coasts (Silva, 2000). Leaves are succulent with vesicular hairs. Roots superficial is on waterlogged sediment. These superficial epidermal structures involved in the accumulation and subsequent elimination of excess salt (Grigore et al. 2014).

*Juncus maritimus* (Lam), is a monocotyledoneous species belonging to the *Juncaceae* family with a C3 metabolism and is usually found in high marshes. Its flowering period is from June to August and is widely spread in salt marshes in the Atlantic coast of Europe, growing in costal lagoons and estuaries in the northwest of Portugal (Figueira et al., 2012; Rose et al., 1989). *J. maritimus* has a well-developed aerenchyma, thick roots and well-developed endodermis once that allows survival in saline anoxic sediments (Grigore et al., 2014). These two species are the most abundant in *Ria de Aveiro*, occupying more than 2/3 of this Ria area (Lillebø et al., 2013).

## 1.3 Absorption, translocation and accumulation of mercury in plant tissues

Mercury (Hg) belongs to group 12 of the periodic table and its atomic number is 80, atomic mass is 200.59 g/mol and it has a density of 13.6 $g.cm^{-3}$. This metal can be present in three distinct forms, all toxic, with different solubility and reactivity (Clarkson, 2002). In aquatic ecosystems, Hg may be in elemental form (Hg0), a divalent ion $Hg^{2+}$ or as methylmercury (MeHg) (Mason and Fitzgerald, 1993). The Agency for Toxic Substances and Disease Registry (ATSDR) considered Hg the third substance in the priority list (ATSDR 2015). Phytoremediation is a new approach for the decontamination of soils. The use of phytoremediation, in which plants absorb, extract and/or sequester metals, decreasing the contamination of an area (Raskin, 1996). In addition, phytoremediation offers a promising alternative since the plants naturally dominate the majority of ecosystems, use solar energy, have reservoirs with high reducing power, possess extended root systems capable of extracting a variety of metal ions and can stabilize and

rehabilitate damaged environments. Like any method of environmental remediation, phytoremediation has some limitations: it is a slow process and not completely efficient (USEPA, 2000). Regarding to Hg, several studies showed that roots of some plants such *Eriocaulon septangulare, Glodea densa* and *Ludwigia natans* accumulate Hg when grow in sediment contaminated by this metal (Coquery et al., 1994; Lenka et al., 1992; Ribeyre et al., 1994).

Metal contamination of salt marshes is reflected in the concentrations of these elements in colonized plants in these areas (Otte, 1991; Rozema et al., 1990).

In salt marsh plants, metals accumulation varies between organs of the same plant, generally with a higher retention in roots (Fitzgerald et al., 2003; Matthews et al., 2004; Otte, 1991). The concentration of metals in the different plant organs results from processes of uptake and translocation process (Singh and McLaughlin, 1999). Plant species may differ in the rates of absorption, excretion and translocation of metals. Thus, the dynamics of these contaminants in marshes can be influenced by the composition of the plant communities presents therein (Verkleij and Schat, 1989).

Monocotyledonous and dicotyledonous plants were shown to differ in Hg allocation probably due to their different taxonomy (Castro 2009). In monocots (such as *J. maritimus*), the majority of Hg were allocated in belowground organs (Castro et al., 2009, Fitzgerald et al., 2003). In dicots (such as *H. portulacoides*) a higher proportion of Hg is accumulated in aboveground organs (Castro et al., 2009).

## 1.4 Hg toxicity – targets

High levels of Hg are reported to be extremely phytotoxic. Zhang and Tyerman, (1999) reported that Hg can bind to water channel proteins and consequently induce physically obstruct water flow into plants and leaf stomata to close. Moreover, Gothberg (2004) showed a inhibition nitrogen and phosphorous uptake of *Spinacia oleracea* seedling exposed to Hg (Gangwar et al., 2014). Metals, Hg included, originate an excessive accumulation of ROS (reactive oxygen species) leading to oxidative stress, lipid peroxidation, protein oxidation, inactivation of enzymes and DNA damage (Anjum and Duarte et al., 2014). Mercury can bind to sulfhydryl groups in proteins and consequently inactivate SH-dependent enzymes (Hameed et al., 2016). Mercury has been to show to decrease *Nostoc muscorum* growth by inhibiting chlorophyll synthesis, photosynthetic electron transport chain and $CO_2$ fixation by enhancing ROS generation and causing damage to lipids (Singh et al., 2012a; Singh et al., 2012b). Mercury ions complexed with organic compounds causing deterioration of polypeptides of photosystem II (PII) submembrane leading to decrease of photosynthetic pigments (Hameed et al., 2016).

## 1.5 Response of plants to metals

There were several studies that showed that plants from salt marshes have the ability to accumulate mercury and exhibited different mechanism of tolerance to metals allowing to classify plants in different types. (Castro 2009). When plants can effectively prevent the accumulation of metals, especially in their aerial parts, they are classified as excluders. Other basic strategy of plants is the accumulation of metals in their tissues reflecting of the metal levels existing in the soil/sediment and in this way defined as indicators. Finally, the accumulators described as plant species may concentrate metals in their tissues (hyperaccumulators) at levels much higher than those existing in the sediment (Figure 1.1) (Baker 1981).

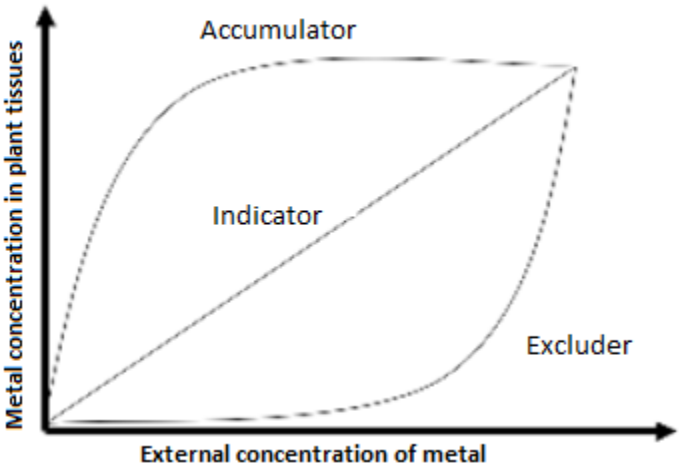


**Figure 1.1**: Types of metallic absorption in plants and relation with the external concentration of the metal (Prasad and Hagemeyer, 1999).

Furthermore, several works have shown that plants have mechanisms to tolerate metal contamination without apparent toxicity allowing plants survival in most adverse areas ((Lasat, 2002). The mechanism developed by plants can avoid or minimize the toxicity of metal ions contributing to metal tolerance.

### 1.5.1 Mechanism of metal avoidance

One of the most common mechanism of tolerance of metals is restriction. This mechanism occurs by extracellular secretion of chelating agents or uptake restriction at the plasma membrane, deposition of metals in wall components (Meharg et al., 1990). Other way is through restriction of xylem loading and acropetal movement. The retention of metals in roots

is a strategy providing protection to the photosynthetic organs from the harmful effects of metals (Lozano-Rodriguez et al., 1995). According by most of the studies establish that plants exposed to mercury tend to prevent high metal concentrations, accumulating lower metal concentrations in their organs than those present in the sediments (Godbold and Hiittermann, 1988; Windham et al., 2003; Lodenius, 1995) and preferentially accumulating Hg in belowground organs, especially roots (Castro et al., 2009).

Other important factor in the assessment of toxicity in the plant is the subcellular distribution of metals in organs. Thus, a high accumulation of metals in the cell walls functions as a protective barrier, reducing its concentration in the cytoplasm (Zornoza et al., 2002; Castro et al., 2009).

### 1.5.2 Intracellular mechanism of tolerance: metal chelation and induction of antioxidant systems

Intracellular sequestration of metals is an efficient mechanism to minimize the toxic effects that metals have on plants (Rauser, 1999). However, when they are not effective oxidative stress overcomes.

One of the main effects of metal contamination is the oxidative stress generated by an increase in the production of reactive oxygen species (ROS). Once formed, plants need to eliminate rapidly the ROS with the main aim to minimize cellular damage (Moller, 2001).

The main defense against oxidative stress is the induction of antioxidant response. At cellular level, the non-enzymatic antioxidant response includes antioxidant molecules such as ascorbate, glutathione (GSH), flavonoids, carotenoids and α-tocopherol. Ascorbate is present in chloroplast, cytosol (Gangwar et al., 2014) and mitochondria (Anjum et al., 2014) and reacts with ROS, generating products such as monodehydroascorbate (MDHA) and dehydroascorbate (DHA) and the rate of synthesis and recycling is fundamental in the process of ROS scavenging (Gangwar et al., 2014; Zhang, 2013). Degradation of DHA occurs by dehydroascorbate reductase (DHAR) and uses glutathione (GSH) to reduce dehydroascorbate (DHA) and regenerates reduced ascorbate (AsA) (Gangwar et al., 2014).

Chlorophyll and carotenoids content are often measured in order to evaluate the impact of a stress in plants, as changes in pigment content are linked to photosynthetic productivity (Kalaikandhan, 2014). Carotenoids, as antioxidants, play a key role as scavengers to protect the chloroplasts against photo-oxidative damage, by quenching singlet state of chlorophyll an ROS and inhibiting lipid peroxidation under stress conditions (Hameed et al., 2016; Hou et al., 2007).

α-tocopherol is the most active form of vitamin E and is produced in the thylakoid membranes of chloroplasts and other plastids (Hasanuzzaman et al., 2014; Munné-Bosch 2005). Toc is a lipophilic antioxidant that stabilizes the membrane structure involved in polyunsaturated fatty acyl chains and consequently protect the photosynthetic apparatus from the oxidative stress and lipid peroxidation, by reducing lipid peroxyl radicals to their corresponding hydroperoxides (Hasanuzzaman et al., 2014; Singh et al., 2016).

Glutathione-S-transferases (GSTs) are a large heterogenous family of biotransformation enzymes that catalyze the conjugation GSH to a variety of hydrophobic, electrophilic and cytotoxic substrates (Marrs, 1996), removing potentially genotoxic or cytotoxic compounds which react with lipids, DNA, RNA and proteins (Edwards et al., 2000; Moons 2005; Noctor and Foyer 1998).

Antioxidant response, is also accomplished by enzymes with antioxidant activity such as superoxide dismutase (SOD), catalase (CAT), glutathione peroxidase (GPX), the dehydroascorbate reductase (DHAR), glutathione reductase (GR) and other (Sharma et al., 2012; Cargnelutti et al., 2006; Moreno et al., 2008; Zhou et al., 2008). Altogether antioxidants compounds and enzymes act to prevent uncontrolled oxidative cascades and to minimize the toxic effects of ROS.

Lipid peroxidation result in products such aldehydes, which are highly toxic to cells and constitute and constitute an import source of toxicity to cells under oxidative stress (Pizzimenti et al., 2013; Gangwar et al., 2014). These products can react with DNA leading to DNA damage. GSTs has the function to reduce aldehydes to alcohols (Regoli and Giuliani 2014) or catalyze their conjugation with gluthathione (Halliwell and Gutteridge 2007).

When antioxidant defense is not able to scavenge ROS efficiently, damage overcomes and lipids, proteins and DNA are oxidized with severe consequences to membrane integrity, metabolic homeostasis and gene mutagenesis (Birben et al., 2012).

## 1.6 Lipids

Lipids are considered as fundamental cellular constituents of all living cells that have critical roles in cellular function (Fouillen et al., 2013; Hummel et al., 2011; Sethi and Brietzke 2017; Tenenboim et al., 2016a). Structurally, there are components of cell membranes including phospholipids, glycolipids, sphingolipids and sterols and do compartmentalization of cell. They are also involved in energy storage, in the form of using triacyclglycerols (Fouillen et al., 2013). In addition, these molecules participate in cell signaling as second messengers, such as lysolipids, diacylglycerols phosphatidic acid and sphingolipids (Barh et al., 2015; Fouillen et al., 2013).

Plant membrane structure is considered the first target for metals since one the main effects of toxicity occurs on the membrane structure resulting from the alteration in lipid composition (Elloumi et al., 2014). These alterations can be as adaptive responses of plant to changes in environmental conditions (Maciel et al., 2016).

Estimations on lipid diversity described more than 1,000 lipid species (Sud et al., 2007). LIPID MAPS Consortium classifies lipids based on their biosynthetic origin. Commonly 8 functional subclasses of lipids are found: fatty acids, glycerolipids, glycerophospholipids, sphingolipids, sterols, prenols, saccharolipids and polyketides (Sud et al., 2007).

Due to the importance of lipids, a new field of investigation emerged the lipidomics. This area, defined as a field within the metabolomics, aims to analyze the cellular lipids in a quantitative and comprehensive way defining the lipidome from different biological sources, from organelles to whole organisms (Sethi and Brietzke 2017; Tenenboim et al., 2016b; Zhao et al., 2014). However, the study of the role of lipids has been hampered by their diversity as well as the technical challenges associated with their identification due to the panoply of functions that lipids play and the detection in lipid composition due to environmental and internal changes changes, lipidomics became an area of great relevance for in-depth understanding of biological events.

Lipids have been analyzed by diverse chromatography-based separation methods and no single analytical technology is enough to identify and quantify all the lipids species in single experiment. The common technologies to successfully perform the quantitative and qualitative analysis of lipids comprises thin-layer chromatography (TLC), gas chromatography (GC), liquid chromatography (LC) coupled to mass spectrometry (MS) (Hummel et al., 2011; Sethi and Brietzke 2017; Tenenboim et al., 2016a). The results obtained from these methods generate big amounts of data and new bioinformatic tools have been developed to extract the relevant information to yield biological insight.

Among the liquid chromatography, different chromatographic technologies exist such as high-performance liquid chromatography (HPLC) or ultra-performance liquid chromatography (UPLC).

For our study, we choose UPLC coupled to a time-of-flight (TOF) high-resolution mass spectrometer. This method has been described as versatile and reproducible with an accurate qualitative and semi-quantitative targeted analysis (Tenenboim et al., 2016a).

## 1.7 Objectives

In literature, there are studies that assess the effect of Hg accumulation in salt marsh plants. Although, the detection and identification of salt marsh plants metabolites from an untargeted study is a challenging task due the complexity of the data, the wide range of existing metabolites and due to literature, there is no prior knowledge about the metabolites contained in analyzed samples. For this reason, we propose the combined use the powerful analyses approaches with chemometric strategies to see halophytes metabolites changing their concentration due to mercury toxicity.

This thesis presents a holistic approach in order to assess the effects of Hg contamination in two salt marsh species with different taxonomic and anatomical features, the monocotyledonous *J. maritimus* and the dicotyledonous *H. portulacoides*, the patterns of Hg accumulation, the biochemical differences and the lipidome alterations in plants of both species colonizing two sites differing in Hg contamination were evaluated.

To achieve the main goal, we hypothesize that:

1. Hg distribution in plants would avoid high Hg concentrations in the most vulnerable organs (the leaves) in order to decrease the interference with metabolic processes sensitive to metals like photosynthesis and respiration.
2. Plants would counteract Hg toxicity by triggering antioxidant responses, especially in tissues accumulating high Hg concentrations (roots) or in tissues more vulnerable to Hg toxicity (photosynthetic tissues).
3. *H. portulacoides* and *J. maritimus* would evidence different lipid profiles in membranes due to Hg toxicity and to mechanisms counteracting Hg toxicity.

# Chapter 2: Materials and methods

## 2.1 Study area

The study was conducted in Ria de Aveiro (Portugal), a costal lagoon located in the northwest coast of Portugal. The lagoon has a complex network of channels with extensive intertidal zones and is surrounded by several urban aggregates and industrial centers. One of these industrial centers includes a chloralkali plant located in Ria the Aveiro complex industry nearby Estarreja. This industrie discharged an effluent rich in mercury to a confined area, the Laranjo basin between the 1950s and the 1990s (Pereira et al., 1998). Due these discharges, Laranjo Basin is considered one of the most Hg contaminated coastal sites in Portugal. In the last two decades, the Hg discharge diminished considerably, but Hg concentration in the surface sediments of Laranjo basin is still higher than pre-industrial levels (Válega et al. 2008).

## 2.2 Sampling

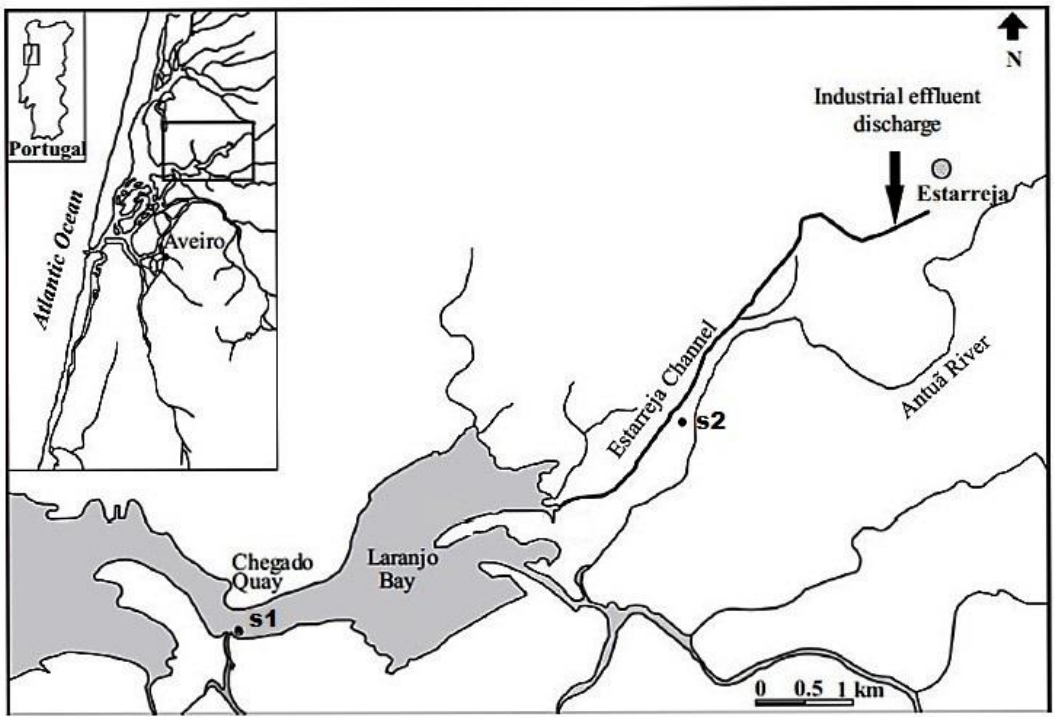


**Figure 2.1** Schematic plan of Aveiro lagoon and Laranjo basin (the study area). Locations (S1 and S2) and the mercury industrial discharge are marked.

Two sampling areas were selected in the Laranjo basin. One more contaminated near the discharge point (s2). The other, at the opposite side of the basin as (s1) (Figure 1). At each site two plant species, a monocotyledonous (*J. maritimus*) and a dicotyledonous (*H. portulacoides*) were chosen given their abundance (they comprise more than 70% of plant cover

at each site). Plants and sediment were collected in the two sites. At each site plants were collected with roots. Rhizosphere sediments of each plant (10–15 cm depth) were collected and non-vegetated sediment were also collected at each site during low tide on July 2016. Samples were transported to the laboratory under refrigerated conditions. After sampling, plants were wash and organs were separated (leaves, stem and roots for *H. portulacoides* and leaves, rhizome and roots for *J.* maritimus). Each organ was again washed with deionized water to remove soil particles still adherent to plants surface. After the excess of water was removed, plants were stored at -80°C until further use.

## 2.3 Mercury determination

### 2.3.1Total mercury in sediments

Sediment samples vegetated and non-vegetated from two collecting areas were disaggregated, homogenized and lyophilized overnight until dryness. Mercury concentration of sediment was measured by Advanced Mercury Analyzer (AMA), model AMA-254, manufactured by Altec (Prague, Czech Republic) and distributed by Leco Corp. (St. Joseph, MI, USA), which uses catalytic combustion of the sample, preconcentration by gold amalgamation, thermal desorption, and atomic absorption spectrometry (AAS). Every sediment sample was put in a nickel boat, placed in the instrument and automatically introduced into the AMA. The sediment samples were analyzed in triplicate and always with blank procedures run in parallel.

### 2.3.2 Total mercury in plants

Before extraction, the different plants organs of each species were ground under liquid $N_2$ to a fine powder using mortar and pestle and lyophilized overnight until dryness. After weighted (10-200 mg), mercury content in samples was measured as previously described for sediments (2.3.1).

For each sample, Hg was calculated the mean ± the standard deviation from triplicate determinations.

### 2.3.3 Data Analysis

To evaluate the differences in accumulation and translocation of Hg in the two species, several factors were calculated. The tables 3.1 and 4.1 show the relations between Hg concentration in sediment and roots (bioaccumulation factor: root/sediment) and translocations between different organs of plant (translocation factor: rhizome/root; stem/root; photosynthetic organs/root). Several factors were, independently, submitted to hypothesis

testing using permutational multivariate analysis of variance with the PERMANOVA+ add-on in PRIMER v6 (Anderson et al., 2008). Thus, the t-statistic of the pair-wise comparisons for each descriptor were evaluated in terms of significance among different areas. Values lower than 0.05 ($p<0.05$) were considered as significantly different.

## 2.4 Biochemical parameters

### 2.4.1 Lipid peroxidation (LPO)

Lyophilized samples were extracted by adding 10% trichoroacetic acid (TCA) (1:2 v/w) and sonicating during 15s at 0.5 cycles. LPO was measured by quantification of thiobarbituric acid reactive substances (TBARS), according to the protocol described by Ohkawa et al. (1979), based on the reaction of lipid peroxidation products such as malondialdehyde (MDA), with 2-thiobarbituric acid (TBA), forming TBARS. The amount of TBARS was quantified spectrophotometrically at 532 nm and calculated using the molar extinction coefficient of MDA (1.56 × 105 M−1 cm−1). Results were expressed in nmol of MDA equivalents per g dry tissue million cells (nmol MDAeq d.w.).

### 2.4.2 Determination of enzyme activity

**Preparation of cell extracts:**

Lyophilized samples were weighted, buffer (0.1 M Tris-HCl pH 7, 15% (w/v) PVP) was added (1:2 v/w) and samples were lysed by sonication during 15 s at 0.5 cycles $s^{-1}$. After sonication cell extracts were centrifuged at 10 000 g for 10 min at 4°C and the supernatant used immediately or frozen (-80 °C) until further use.

**Protein Quantification**

Soluble protein concentration was measured following the method described by Bradford (1976). For the determination of protein content, 10 µL of cell extract/standard were added to 280 µL of Bradford reagent in a 96°C well microplate. The assay was based on the binding of the dye Coomassie Blue G250 to protein, forming a stable dye–albumin complex, which can be quantified spectrophotometrically at 595 nm. Bovine serum albumin (BSA) was used as standard. Results were expressed as mg protein per g dry tissue ($mg.g^{-1}$ d.w.)

**Glutathione peroxidase (GPx)**

GPX activity was determined by the Paglia and Valentine (1987) method. In this assay, oxidized glutathione was immediately recycled back to the reduced form, thereby maintaining a constant concentration of substrate and allowing accurate kinetic studies to be performed.
For the determination of GPX activity, GPx reduces cumene hydroperoxide by oxidation of GSH with GSSG formation in the first reaction. In the second reaction GSSG is reduced again to GSH by GR, consuming NADPH. To the reaction mixture, containing 10 µL of cell extract, 112.5 µL of dilution buffer (Tris-HCl, pH 7.6; 5 mM EDTA), 45 µL of cumene hydroperoxide (2 mM), 60 µL of the GSH (5 mM) and 3 µL of GR (25 U/ml), 22.5 µL of 2 mM NADPH were added to initiate the reaction. The mixture was stirred for a few seconds and the decrease in absorbance at 340 nm was read every 15 seconds for 5 min (21 readings). Enzyme activity was determined using the molar extinction coefficient of 0.00622 $\mu M^{-1}$ $cm^{-1}$ for NADPH and expressed in units per g of dry tissue (U $g^{-1}$ d.w.).

**Glutathione S-transferase (GSTs)**

GSTs activity was determined spectrophotometrically using CDNB (2,4-Dinitrochlorobenzene) as substrate by the method of Habig and Jakobi (1981) in samples. The activity towards CDNB was determined at 340 nm by adding 165 µl of 0.1 M phosphate buffer (pH 6.5), 30 µl of 10 mM GSH, 100 µl of cell extract and finally 5 µl of 60 mM CDNB to start the reaction in a of well microplate. GSTs activity was obtained based on the extinction coefficient for CDNB (9.6 mM. $cm^{-1}$). The assay was performed at 25 °C. Results were expressed as nmol.$min^{-1}g^{-1}$ ($Ug^{-1}$) of dry tissue (mU $g^{-1}$ d.w.).

**Dehydroascorbate reductase (DHAR)**

The activity of DHAR was determined by monitoring the glutathione dependent reduction of dehydroascorbate (Ma and Cheng 2004). The reaction mixture containing 10 µl cell extracts and 185 µl of buffer reaction (50 mM Hepes buffer (pH 7.0), 0.1 mol EDTA and 2.5 mM GSH) was started by the addition of 5 µl of DHA to a final concentration of 0.2 mM into all the wells. The activity was determined by measuring the increase in the reaction rate at 265 nm for 5 min. Activity was calculated from the extinction coefficients the 14 $mM^{-1}cm^{-1}$. Results were expressed as nmol $min^{-1}$ $g^{-1}$ of dry tissue (mU $g^{-1}$ d.w.).

### 2.4.3 Electron transport activity

The electron transport activity was quantified according to King & Packard (1975) method modified by De Coen *et al.* (1997). In this method, the measurement of dehydrogenase activity is based on the reduction, during electron flow, of the tetrazolium dye INT (2-(4-iodophenyl)-3-(4-nitrophenyl)-5-phenyltetrazolium chloride) that turns purple upon reduction. Sample pH was brought to 8.5 with Tris-Hcl buffer (0.1 M Tris-HCl pH 10, 15% (w/v) PVP), 153 mM MgSO4 and 0.2% (v/v) Triton X-100). The reaction mixture containing cell extracts (pH 8.5), 82,7 µL of Tris- HCl pH 5.5 buffer and 35.7 µL of NAD(P)H, was started by adding 71.4 µL of 8 mM *p*-Iodo Nitro Tetrazolium (INT). The absorbance was read at 490 nm, during 10 min, with intervals of 25 seconds. The amount of formazan formed was calculated using the extinction coefficient for formazan (ε=15900 $M^{-1}cm^{-1}$) and the results expressed in nmol $min^{-1}$ $g^{-1}$ of dry tissue (nmol $m^{-1}g^{-1}$ d.w.).

### 2.4.4 Content of chlorophyll a, b and carotenoids content

To 0.01g of lyophilized leaf tissue 1 ml of 80% of acetone were added in the dark and sonicated in ice for 20 seconds, after centrifugation at 4000 g for 4 min at 4°C, the supernatant (300ul) was read spectrophotometrically at 663, 646 and 470 nm. Pigment content was expressed as µg $g^{-1}$ of dry weight using the equations of Lichtenthaler (1987):

$$\textbf{Chla}=12{,}21*A_{663}-2{,}81*A_{646}\ \mu g\ mL^{-1}$$

$$\textbf{Chlb}=20{,}13*A_{646}-5{,}03*A_{663}\ \mu g\ mL^{-1}$$

$$\textbf{Carotenoids}=(1000*A_{470}-3{,}27Chla-104Chlb)/198\ \mu g\ mL^{-1}$$

### 2.4.5 Data Analysis

Biochemical descriptors were, independently, submitted to hypothesis testing using permutational multivariate analysis of variance with the PERMANOVA+ add-on in PRIMER v6 (Anderson et al., 2008). Thus, for each descriptor, a two-way hierarchical design was followed with sites nested in areas and these as the main fixed factor. The t-statistic of the pair-wise comparisons for each descriptor were evaluated in terms of significance among different areas. Values lower than 0.05 ($p<0.05$) were considered as significantly different. The null hypotheses tested were: (a) for each organ: no significant differences existed among plants from different areas (s1 or s2); (b) for each biochemical parameter and for each organ: no significant differences existed among plants from different areas (s1 or s2); (c) for each biochemical

parameter and for each area (s1 or s2): no significant differences existed among organs. For each condition, significant differences (P≤0.05) among organs for the same site are represented with letters lower case (a-b) for s1 and capital (A-C) for s2 and significant differences (P≤0.05) between sites for each organ are represented with an asterisk (*).

The biochemical parameters matrix responses were used to calculate the Euclidean distance similarity matrix. The data used to calculate the matrix was previously normalized and transformed (square root). The matrix was then simplified through the calculation of the distance among centroid based on the condition and then submitted to ordination analysis, performed by Principal Coordinates (PCO). Spearman correlation vectors (r> 0.5) of biochemical responses of *H. portulacoides* and *J. maritimus* organs were applied to PCO graph.

## 2.5 Lipid extraction and LC-MS

Samples were previously lyophilized with the same procedure for mercury determination in plants.

The extraction of metabolites was carried out by dispersing 10 mg of lyophilized tissue in 1 mL of MTBE:MeOH (3:1) (Methyl tert-butyl ether:methanol) + 0.01% BHT (butylated hydroxytoluene). This mixture was fortified with 200 pmol of different internal lipids standards (C18 (plasmalogen)- 18:1 phosphatidylcholine, C18 (plasmalogen)-18:1 phosphatidylethanolamine, C16 (plasmalogen) lysophosphatidylcholine, 1,2,3-17:0 triacylglycerol, 1,3-17:0 D5 diacylglycerol, 17:0 monoacylglycerol, 17:0 cholesteryl ester, 16:0 D31-18:1 phosphatidic acid, 16:0 D31-18:1 phosphatidylcholine, 16:0 D31-18:1 phosphatidylethanolamine, 16:0 D31-18:1 phosphatidylserine, 16:0 D31-18:1 phosphatidylglycerol, 16:0 D31-18:1 phosphatidylinositol, 17:1 lysophosphatidylcholine, 17:1 lysophosphatidylglycerol, 17:1 lysophosphatidylserine, 17:1 lysophosphatidic acid, 17:1 lysophosphatidylcholine, 17:1 lysophosphatidylinositol) (Merrill et al., 2005).

The mixture was vortexed for 1 min and sonicated for 10 min. After this step, 500 µL of H2O:MeOH (3:1) (water:methanol) was added and vortexed for another minute. After centrifugation (10min at 13000 rpm), a 600 µL aliquot of the supernatant was transferred to a 1.5 mL microtube, evaporated to dryness under nitrogen gas and reconstituted with 150 µL de MeOH. Then the microtubes were centrifuged during 10 min at 13000rpm and 130 µL aliquot was transferred to UPLC vials for injection. Also, 200 pmol of internal standards sphingolipids (N-dodecanoylsphingosine, N-dodecanoylglucosyl-sphingosine and N-

dodecanoylsphingosylphosphorylcholine) were added in order to normalize the instrumental injections to the LC-MS equipment ((Merrill et al., 2005).

The LC/MS analysis consisted of a Waters Acquity UPLC system connected to a Waters LCT Premier orthogonal accelerated time of flight mass spectrometer (Waters), operated both positive and negative electrospray ionization modes. Full scan spectra from 50 to 1500 Da were acquired, and individual spectra were summed to produce data points each of 0.2s. Mass accuracy and reproducibility were maintained by using an independent reference spray via the LockSpray interference.

The analytical column was a 100 x 2.1 mm inner diameter, 1.7 mm C8 Acquity UPLC bridged ethylene hybrid (Waters). The two mobile phases were phase A:MeOH 1 mM ammonium formate and phase B:$H_2O_2$ mM ammonium formate. The flow rate was 0.3 ml min-1 and the gradient of A/B solvents started remained at 90:10; changed to 99:1 (from de minute 6 to 15); remained 99:1 (from 15 to 18); and finally returned to the initial conditions (until minute 20). The columm was held at 30°C.

## 2.6 Chemometric data analysis of LC-MS data

Each UPLC-MS chromatographic run recorded for every sample resulted in a raw chromatographic data files (*.raw* format), which was converted to the standard CDF format by Databridge program of the MassLynx TM v 4.1 software (Waters, USA).

Two different methodologies, XCMS and Regions of interest (ROI) + Multivariate curve resolution by alternating least squares (MCR-ALS) were used for the untargeted lipidomic study carried out. The aim of these two methodologies is to retrieve the important features in the dataset and to resolve their chromatographic profile, in order to calculate the areas. The two procedures were used to extract relevant information of samples for calculation of chromatographic areas in order to complement each one and to ascertain the effect of the contamination with mercury.

### 2.6.1 XCMS

XCMS approach is an open online platform that allows an automatic processing of data for feature detection and calculation of chromatographic peak areas (Smith et al., 2006). The XCMS analysis starts with the data processing algorithm, which basically consists in two main steps. The first step is to identify regions of interest (ROIs) by dominant spectra features. These identified ROIs are characterized with the presence of a chromatographic peak which at a

particular m/z value has intensity over a particular preselected threshold value. The second step is the identification and modeling of chromatographic peaks by means of a wavelet transformation and a Gaussian shape curve fitting approach. This approach only considers chromatographic peaks that are present in more than a percentage of all samples (commonly 50%), the rest of features are dismissed. Finally, chromatographic peaks of the same component in different samples are aligned by means. In this work, XCMS platform online has been used to import and pre-process raw chromatographic data in CDF format. The data imported were submitted in parwise job for each organ with the respective conditions (reference site and contaminated site) with defined UPLC parameters – High Res Pos (Waters). The final output is a data table that contains the selected features (identified by their exact m/z values) in the rows, and the area of these features for each sample in the columns.

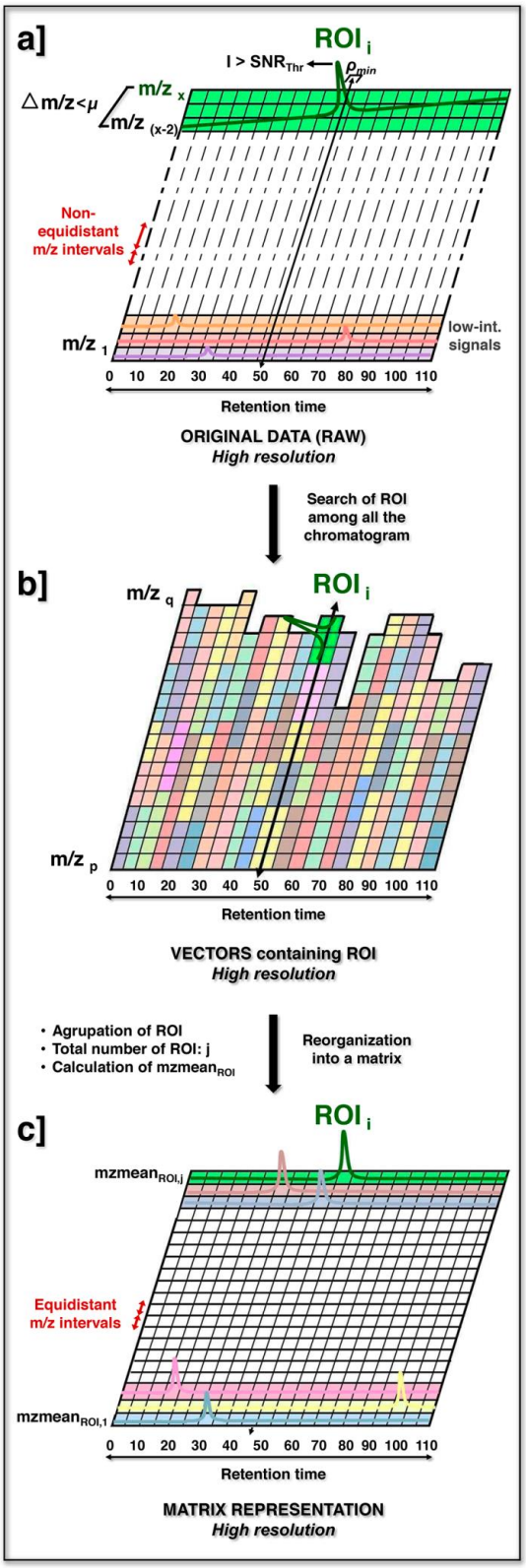


**Figure 2.2:** Scheme of the steps involved in the compression of data by the search of ROI: a] original data with non-equidistant m/z intervals where a significant mass trace is represented as ROIi (green) and distinguished from low-intensity signals (orange, pink and violet), b] vectors containing the distinct ROI (represented by sequences of squares of the same color) obtained at different regions of the chromatogram, including the previous ROIi (green) and c] matrix constructed from the reorganization of ROI vectors, again containing the same ROIi (in green). (SNRThr: signal-to-noise ratio threshold, mzmean: mean of all the m/z values from the series of data points grouped within the same ROI) (Gorrochategui et al., 2016).

### 2.6.2 Regions of Interest (ROI)

The method ROI (regions of interest), created by Stolt et al. (2006), is based on the concept of considering analytes as a region of data points with a high density ranked by a specific “data void”. Since MS-ROI individual data matrices have different number ROI m/z values (common and not

common), a preliminary step of ROI rearrangement to consider all those ROI m/z values with significant traces. When determinate individual matrix have a particular not significant trace at this ROI m/z, significant intensity higher than a fixed signal-to-noise ratio threshold, low random intensity values at the noise level is not assigned to the final matrix. See more details about MS-ROI augmented matrix building (Gorrochategui et al., 2016) and figure 2.2.

The MS-ROI augmented data matrix is built with three less contaminated samples (s1) and three more contaminated samples (s2) for each organ of H. *portulacoides* and *J. maritimus*. In addition, the final dimensions of this augmented matrix are the total number of retention times considered in the six chromatographic runs times in the rows and the number of finally considered m/z ROI values in the columns.

### 2.6.3 Multivariate curve resolution by alternating least squares (MCR-ALS)

MCR-ALS is a chemometric method developed for the resolution of pure contributions in unresolved mixtures (Tauler 1995). This method has been already described in literature with the application in different research fields like chromatographic systems, -omics data, process analysis, spectroscopy images and environmental data tables (De Juan et al., 2014; Ruckebusch e Blanchet, 2013).

In this work, MCR-ALS has been used to resolve the elution and mass spectra profiles of the metabolites obtained in the full-scan untargeted UPLC-MS analysis of the two wetland species sample extracts from a Hg contaminated salt marsh. MCR-ALS decomposes every individual experiment dataset arranged in a data matrix according to the following bilinear model:

$$D = CS^T + E$$

D contains the information (intensity values) of less and most contamination samples of each plant part, in which the rows are the chromatographic retention times and the columns the mass values. As a result of the MCR-ALS decomposition we obtained, the C matrix, that contains the chromatographic profile of each component and the S matrix, which gives the mass spectrometry information of each resolved component. For all the resolved components, we obtained the areas in each sample were obtained. These area values were further normalized by the internal standards added and fold changes were calculated from the arithmetic mean

values of each group. Also, a p-value was calculated to observe which compounds were statistically different between the two conditions.

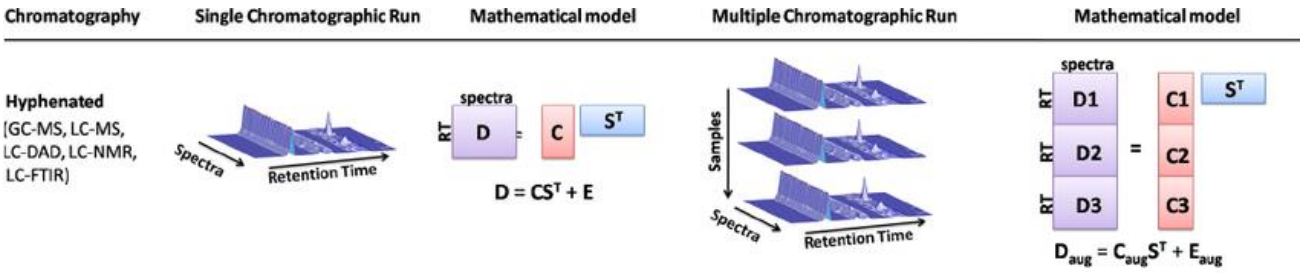


**Figure 2.3** Example of and application of MCR-ALS to the simultaneous analysis (Parastar & Tauler, 2014)

### 2.6.3 Evaluation of Hg effects on samples by chemometric analysis of metabolite concentration (peak areas) changes and identification

Once relative concentration changes for each metabolite were estimated by XCMS and MCR-ALS, other method was used to evaluate them and to discriminate samples according the Hg contamination. PCA was one of the methods used to explore the behavior of tissue sample depending on the condition.

The identification of metabolites was only performed for m/z values with statistically significant differences in their areas by the p-value (p-value <0.05) already calculated. Human Metabolome Database (HMDB) and LipidMaps (Sud et al., 2007) were used for the identification of lipid species. The assigned compound corresponded to the lipids molecule with the minimum mass error value with respect to the measured m/z, considering all the possible adducts in the positive and negative ionization. The annotated lipid also had to fulfil an adequate retention type regarding its polarity and literature.

Finally, only identified compounds with a mass error less than 10 ppm were selected for further interpretation of lipidomic results.

Tables where the compounds are sorted by their chromatographic retention time, includes the annotation of lipids like is described in the material and methods chapter. The correct mass of the candidate metabolites components whose profile peak areas were changing was compared with the exact mass values included in public databases such HMDB and Lipid Maps and only the are present in the tables the lipids with a mass error less than 10 ppm and shows a significant change ($p<0.05$).

### 2.6.4 Software

The software used in this work includes MassLynx V 4.1 (Waters) for raw UPLC-TOF data analysis. For matrix data processing and statistical analyses, the PLS Toolbox (The Mathworks Inc.) and MCR-ALS Toolbox and ROI were used in the MATLAB 8.3.0 – R2015b (The Mathworks Inc.) environment. XCMS was performed using an interactive platform online (xcmsonline.scripps.edu). The heatmaps were built using Metaboanalyst 3.0 (Xia et al., 2015).

## 2.7 Mass spectrometry imaging (MSI)

Initially, samples (roots, rhizome and stem) of both plants were flash frozen with nitrogen and sliced at 20 µm thickness with cryostat (Leica CM 3050S) at low temperature (-20°C) to obtain tissues sections. Then, the application of the matrix 2,5-dihydroxybenzoic acid (DHB) into indium titanium oxide (ITO) slides was performed by sublimation. In the case of leaves, they were imprinted directly onto the glass slide previous to sublimation (Ly et al. 2015).

Spectra were obtained using an Autoflex III MALDI-TOF/TOF instrument (Bruker Daltonik GmbH) equipped with a Smartbeam laser operated at 200-Hz laser repetition rate at the "large focus" setting. Spectra were acquired in positive reflector ion mode in the 400 to 2000 m/z range. Laser raster was set to 150 µm along both x-axis and y-axis, giving a final size of 33 by 30 pixels. External calibration was performed using Bruker Peptide Calibration Standard (Bruker Daltonik GmbH). The figure 2.4 represents a diagram of a typical MALDI-MS imaging technique (Jorge et al., 2015).

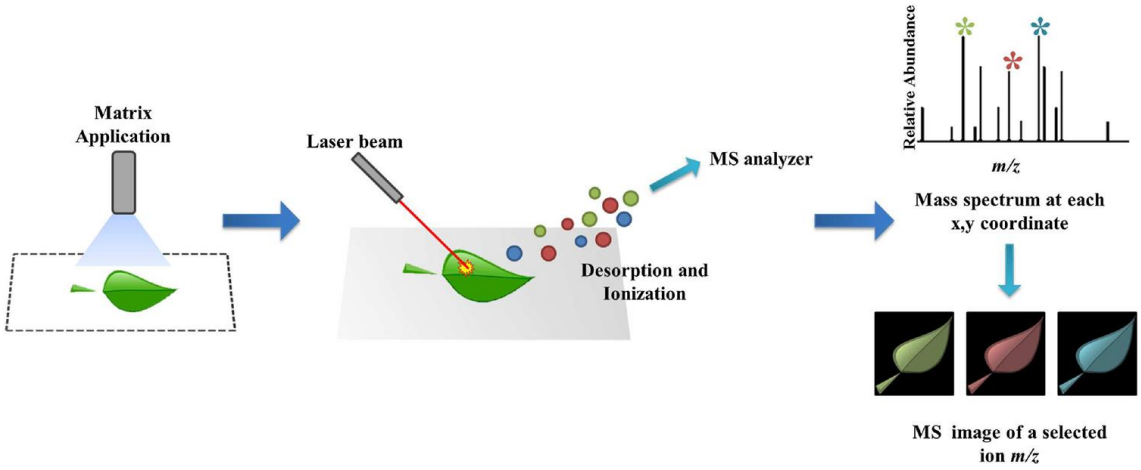


**Figure 2.4:** Representative diagram of a typical MALDI-MS imaging technique (Jorge et al. 2015).

# Chapter 3 – Results of *H. Portulacoides*

## 3.1 Mercury in sediments and plants

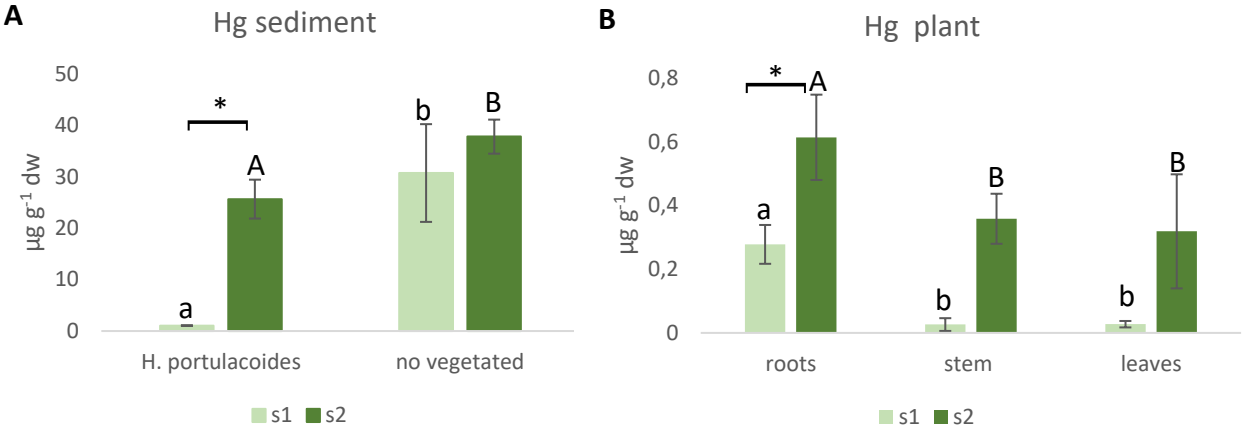


**Figure 3.1**: Total concentration of Hg. (A) Hg concentration in sediments vegetated by *Halimione portulacoides* or in non-vegetated sediment (µg $g^{-1}$ dw) in the two sampling sites: low contamination (s1) and high contamination (s2). (B) Hg concentration (µg $g^{-1}$ dw) in different plant organs (root, stem and leaves) of *Halimione portulacoides* colonizing the two sample sites (s1 e s2). Values are the mean of 3 replicates ± standard deviation**.** For each condition, significant differences (P≤0.05) among organs for the same site are represented with lower case (a-b) for s1 and capital letters (A-B) for s2 and for each organ significant differences (P≤0.05) between sites are represented with an asterisk (*).

The site and *H. portulacoides* cover contributed to the differences in Hg concentration observed in sediments. For the same (site s1 or s2) the presence of *H. portulacoides* decreased significantly ($p<0.05$) Hg in sediments. Hg concentration between sites is evidence lower levels in s1, but this difference is only significant when sediments are covered by *H. portulacoides* (figure 3.1A).

The distribution of Hg in the plant shows that most of the metal is allocated to roots. Differences in metal allocation are observed. In the less contaminated site (s1), roots accumulated most (87.7%) of the Hg uptaken by plant, whereas in s2, less than half (47%) of Hg is in roots, and stem and leaves accumulated similar (24 and 29% respectively) Hg levels (figure 3.1B).

## 3.2 Bioaccumulation and translocation of mercury

**Table 3.1** Bioaccumulation and translocation factors of the salt marsh plant, *Halimione portulacoides*, colonizing two sampling sites differing in Hg contamination (low s1 and high 2). Bioaccumulation factor(BAF): Hg concentration ratio between root and sediment (R/sediment). Translocation factors (TF): Hg concentration ratio between stem and root (S/R); leaves and root (L/R). Values are means ± standard deviation of 3 replicates. For each factors significant differences (P≤0.05) between sites are represented with an asterisk (*).

| | **Locations** | **Bioaccumulation factor (BAF)** | **Translocation factor (TF)** | |
|---|---|---|---|---|
| | | R/sediment | S/R | L/R |
| ***Halimione portulacoides*** | S1 | 0,228 ± 0,067 | 0,843 ± 0,108 | 0,105 ± 0,053 |
| | S2 | 0,036 ± 0,010* | 0,624 ± 0,071 | 0,519 ± 0,204 |

Differences in Hg accumulation and distribution are reflected in bioaccumulation and translocation factors. For both sites, BAFs were lower than 1, however the BAF in s2 is much lower, evidencing a higher restriction of Hg uptake in the mores contaminated sites. In contrast plants colonizing s2 were not able to restrict so efficiently acroptal movement of Hg, as evidenced by the higher TF for leaves in s2 compared to s1.

## 3.3 Biochemical parameters

### 3.3.1 Cell damage

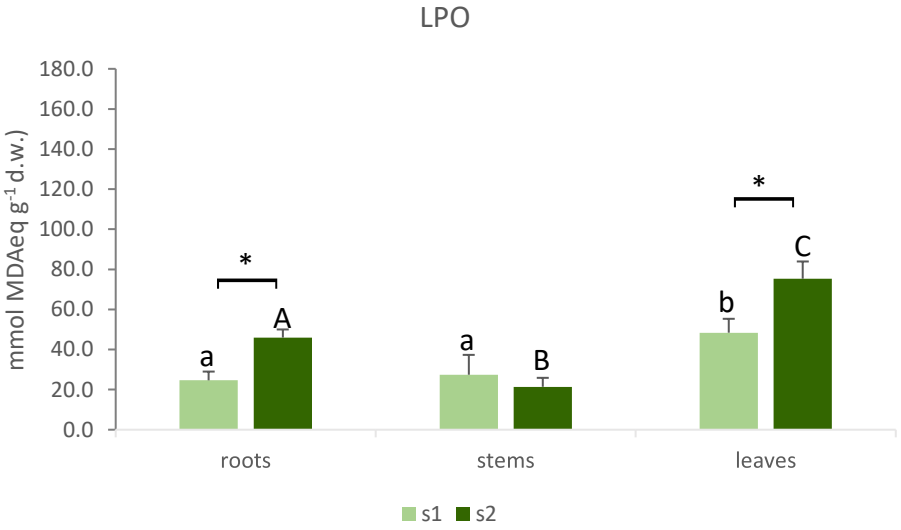


**Figure 1.2**: Lipid peroxidation (MDA nmol $g^{-1}$ dry weight) in organs (roots, stems and leaves) of *H. portulacoides* in two sampling sites: low contamination (s1) and high contamination (s2). Values are the mean of 3 replicates ± standard deviation**.** For each condition, significant differences (P≤0.05) among organs for the same site are represented with lower case (a-b) for s1 and capital letters (A-C) for s2 and for each organ significant differences (P≤0.05) between sites for each organ are represented with an asterisk (*).

Lipid peroxidation (LPO) varies between organs in plants from the same site and between sites in the same organ (figure 3.2). Leaves present higher LPO concentrations (both in s1 and s2). Stem and roots present identical LPO levels in s1, but in s2 significantly higher LPO levels are found in roots compared to stems. Comparing sites, roots and leaves from s2 have significance higher LPO concentrations than s1. In stems, LPO levels are similar in both sites (c.f. figure 3.2).

### 3.3.2 Soluble proteins

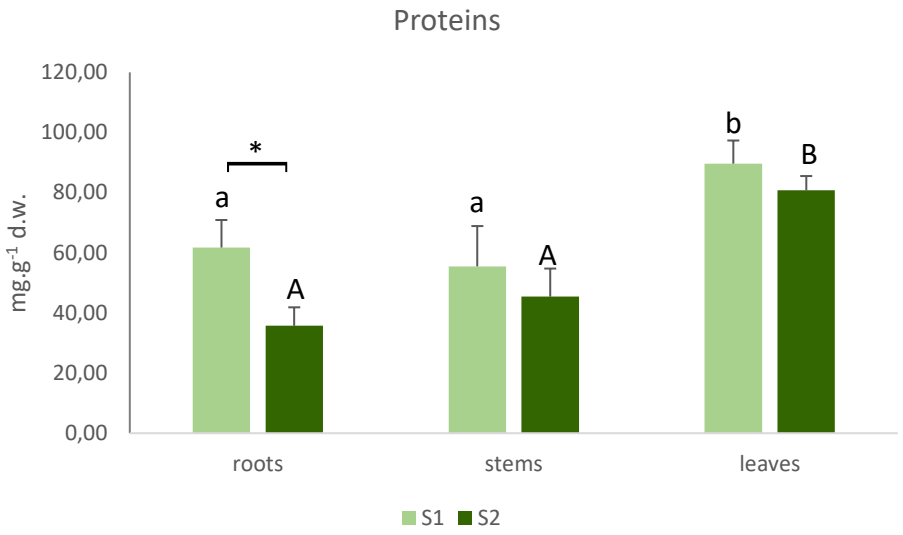


**Figure 3.3**: Soluble proteins (mg $g^{-1}$ dry weight) in organs (roots, stems and leaves) of *H. portulacoides* in two sampling sites: low contamination (s1) and high contamination (s2). Values are the mean of 3 replicates ± standard deviation**.** For each condition, significant differences (P≤0.05) among organs for the same site are represented with lower case (a-b) for s1 and capital letters (A-B) for s2 and for each organ significant differences (P≤0.05) between sites for each organ are represented with an asterisk (*).

Root and stem have identical protein levels both at s1 and s2 (figure 3.3). The comparison between sites shows that only roots present significant differences between sites with roots from s2 having 20% less proteins than s1. Protein concentration in leaves are higher that roots and stems, and no significant differences were observed between s1 and s2 (c.f. figure 3.3).

### 3.3.3 Antioxidant enzymes

**Glutathione peroxidase (GPx)**

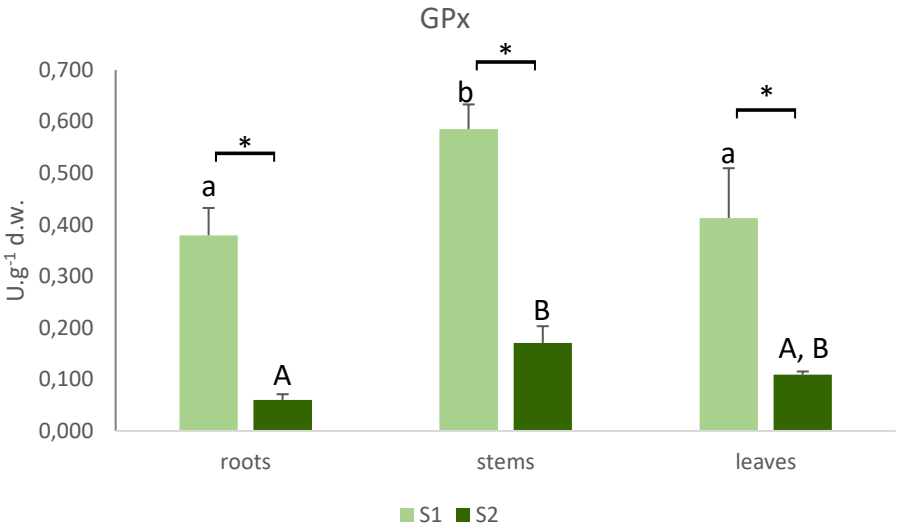


**Figure 3.4**: Activity of GPx (U $g^{-1}$ dry weight) in organs (roots, stems and leaves) of *H. portulacoides* in two sampling sites: low contamination (s1) and high contamination (s2). Values are the mean of 3 replicates ± standard deviation**.** For each condition, significant differences (P≤0.05) among organs for the same site are represented with lower case (a-b) for s1 and capital letters (A-B) for s2 and for each organ significant differences (P≤0.05) between sites for each organ are represented with an asterisk (*).

GPx activity evidences a strong inhibition in s2 compared to s1 in all organs analyzed (figure 3.4). The comparison of GPx activity among organs shows that stems present higher activity (s1 and s2) compared to roots (s1 and s2) and leaves (s1) (c.f. figure 3.4).

**Dehydroascorbate reductase(DHAR)**

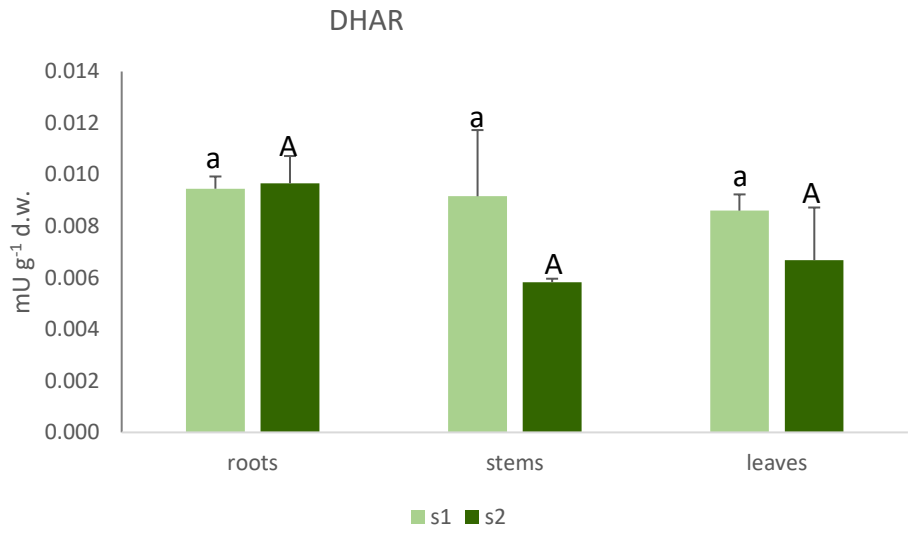


**Figure 3.5**: Dehydroascorbate reductase (nmol $min^{-1}$ $g^{-1}$ dry weight) in organs (roots, stems and leaves) of *H. portulacoides* in two sampling sites: low contamination (s1) and high contamination (s2). Values are the mean of 3 replicates ± standard deviation**.** For each condition, significant differences (P≤0.05) among organs for the same site are represented with lower case (a-b) for s1 and capital letters (A-B) for s2 and for each organ significant differences (P≤0.05) between sites for each organ are represented with an asterisk (*).

DHAR did not show significant differences between sampling sites or among organs (figure 3.5).

### 3.3.4 Biotransformation enzymes - Glutathione-S-transferases

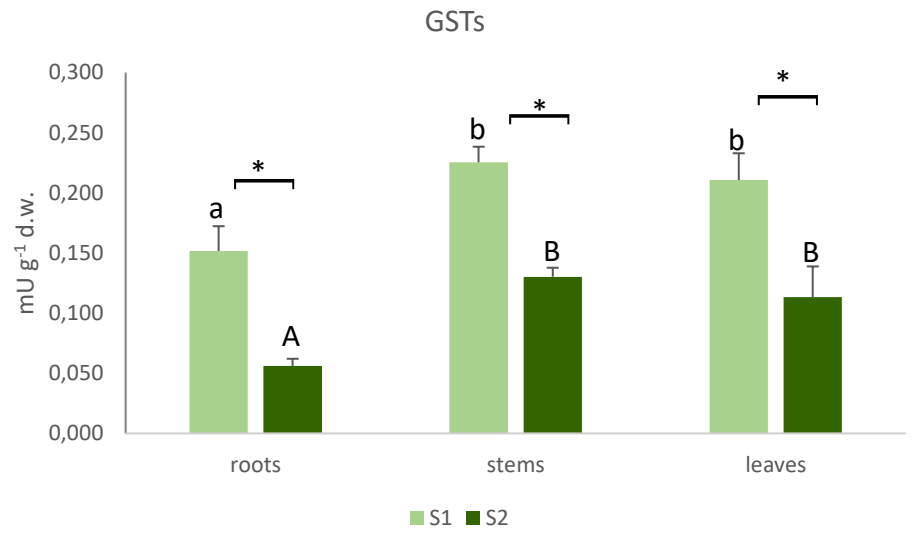


**Figure 3.6**: Activity of GSTs ($\mu g^{-1}$ dry weight) in organs (roots, stems and leaves) of *H. portulacoides* in two sampling sites: low contamination (s1) and high contamination (s2). Values are the mean of 3 replicates ± standard deviation**.** For each condition, significant differences (P≤0.05) among organs for the same site are represented with lower case (a-b) for s1 and capital letters (A-B) for s2 and for each organ significant differences (P≤0.05) between sites for each organ are represented with an asterisk (*).

GSTs activity is similar between aboveground organs (stem and leaves) and lower in roots both for s1 and s2 (figure 3.6). The sampling site also influenced significantly GSTs activity, with plant organs from s1 presenting significant higher activity than s2 (c.f. figure 3.6).

### 3.3.5 Electron Transport System Activity

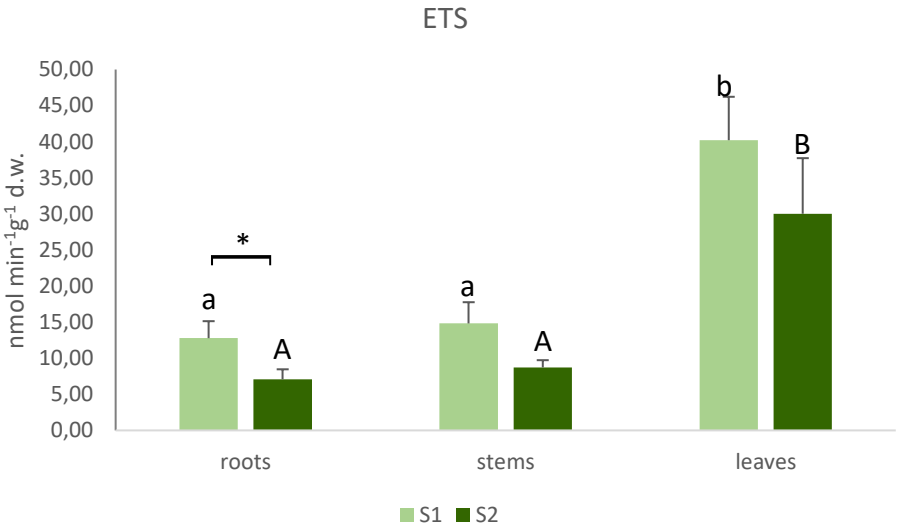


**Figure 3.7**: Activity of ETS (nmol $min^{-1}g^{-1}$ dry weight) in organs (roots, stems and leaves) of *H. portulacoides* in two sampling sites: low contamination (s1) and high contamination (s2). Values are the mean of 3 replicates ± standard deviation**.** For each condition, significant differences (P≤0.05) among organs for the same site are represented with lower case (a-b) for s1 and capital letters (A-B) for s2 and for each organ significant differences (P≤0.05) between sites for each organ are represented with an asterisk (*).

The activity of the electron transport system (ETS) is similar between roots and stems and lower compared to leaves (figure 3.7). The three organs presented high ETS in s1, but significant differences were only noticed in roots (c.f. figure 3.7).

### 3.4.5 Photosynthetic pigments

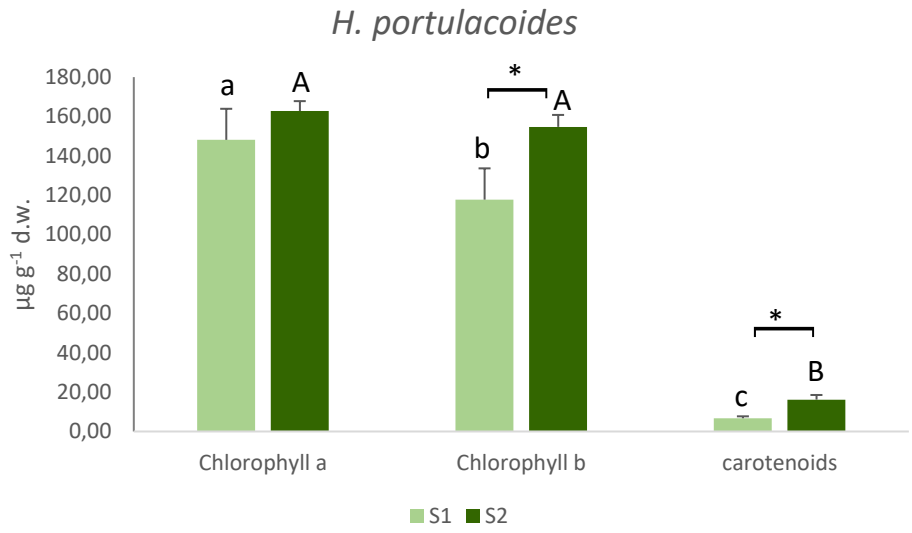


**Figure 3.8:** Chlorophyll *a*, *b* and carotenoids content ( $\mu g^{-1} g^{-1}$ dry weight) in leaves of *H. portulacoides* in two sampling sites: low contamination (s1) and high contamination (s2). Values are the mean of 3 replicates ± standard deviation**.** For each condition, significant differences (P≤0.05) among organs for the same site are represented with lower case (a-b) for s1 and capital letters (A-B) for s2 and for each organ significant differences (P≤0.05) between sites for each organ are represented with an asterisk (*).

In s2 *H. portulacoides* leaves have identical concentrations of chlorophyll a and b and lower 40% concentrations of carotenoids. In s1, chlorophyll a concentration is higher than carotenoids but also than chlorophyll b (figure 3.8). The concentration of photosynthetic pigments is higher in s2 than s1, showing significant differences for chlorophyll b and carotenoids (c.f. figure 3.8).

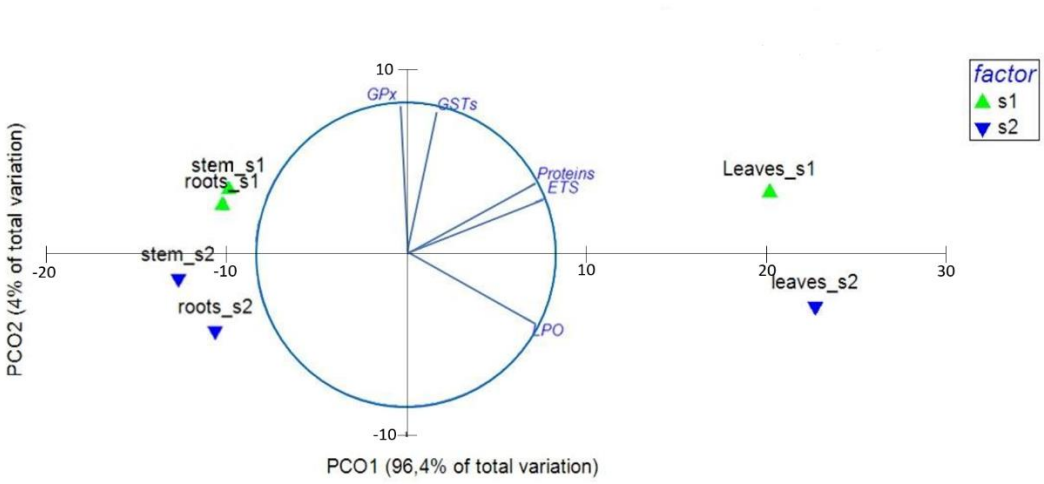


**Figure 3.9:** Biochemical responses of *H. portulacoides* exposed to two Hg concentrations, plotted on axes 1 and 2 of Principal Coordinates (PCO) graph. Biochemical data are superimposed on the PCO. The low (s1) and high (s2) contaminated sites are indicated for each organ of *H. Portulacoides* (leaves, stems and roots). The biomarkers presented are: GPx, glutathione peroxidase; GTSs, Glutathione-S-transferases; Proteins; ETS, electron transport system; LPO, lipid peroxidation.

Figure 3.9 shows the centroids PCO ordination graph resulting from applying a multivariate analysis to the biochemical parameters of *H. portulacoides* organs from two sites differing in Hg concentration. The PCO 1 axis explained 96.4% of the total variation of the data, clearly separating leaves on the positive side from roots and stems (on the negative side of the axis). The PCO 2 axis explained 4% of the total variation. The three organs from s1 are on the positive side while the same organs from s2 are on the negative side. From the PCO analysis it is possible to observe that: a) roots and stems from s1 are correlated with GPX and GSTs activity; b) leaves from s1 are strongly correlated with proteins content and ETS activity while leaves from s2 is strongly correlated with LPO levels.

## 3.5 Lipidomic analysis

Lipidomic profiles of *Halimione portulacoides* organs from s1 and s2 were compared. Significant differences between sites were put at evidence by a complete bioinformatics analysis of the data (section 2.5).

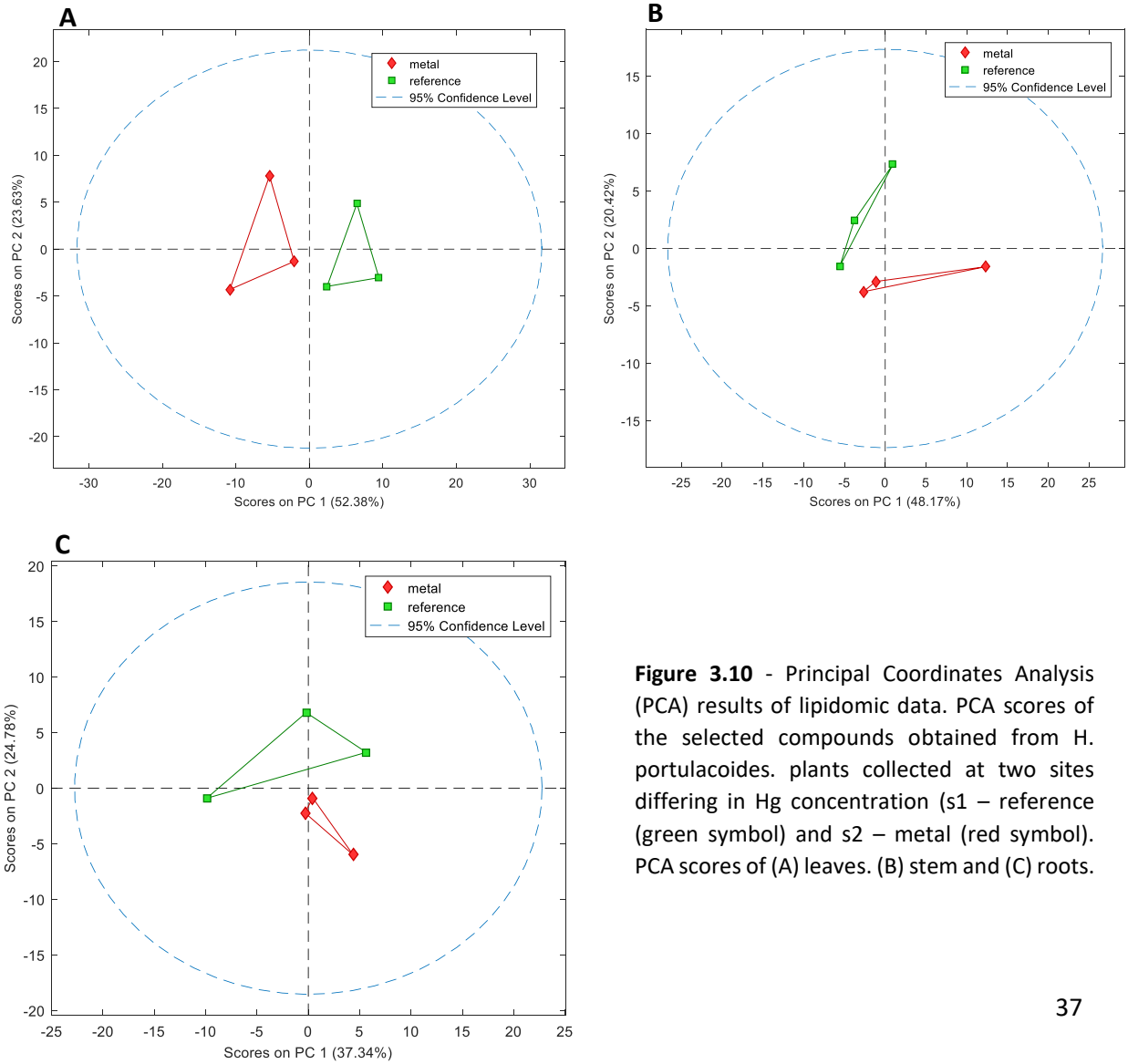


**Figure 3.10** - Principal Coordinates Analysis (PCA) results of lipidomic data. PCA scores of the selected compounds obtained from H. portulacoides. plants collected at two sites differing in Hg concentration (s1 – reference (green symbol) and s2 – metal (red symbol). PCA scores of (A) leaves. (B) stem and (C) roots.

Principal coordinate Analysis (PCA) of lipidomic data clearly separate organs (roots, leaves and stems) from s1 and s2 (figures 3.10A; 3.10B and 3.10C).

For leaves, PCA axis 1 (PC1) explained 52.38% and PCA axis 2 (PC2) explained 23.63% of total variance significantly separating ($p<0.05$) s1 from s2 (figure 3.10A). In the case of stems, PCA axis 1 (PC1) explained 48.17% and PCA axis 2 (PC2) explained 20.42% of total variance significantly separating ($p<0.05$) s1 from s2 (figure 3.10B). For roots, the PCA axis 1 (PCA1) explained 37.34% and PCA axis 2 (PC2) explained 24.78% of total variance significantly separating (s1 from s2 (figure 3.10C).

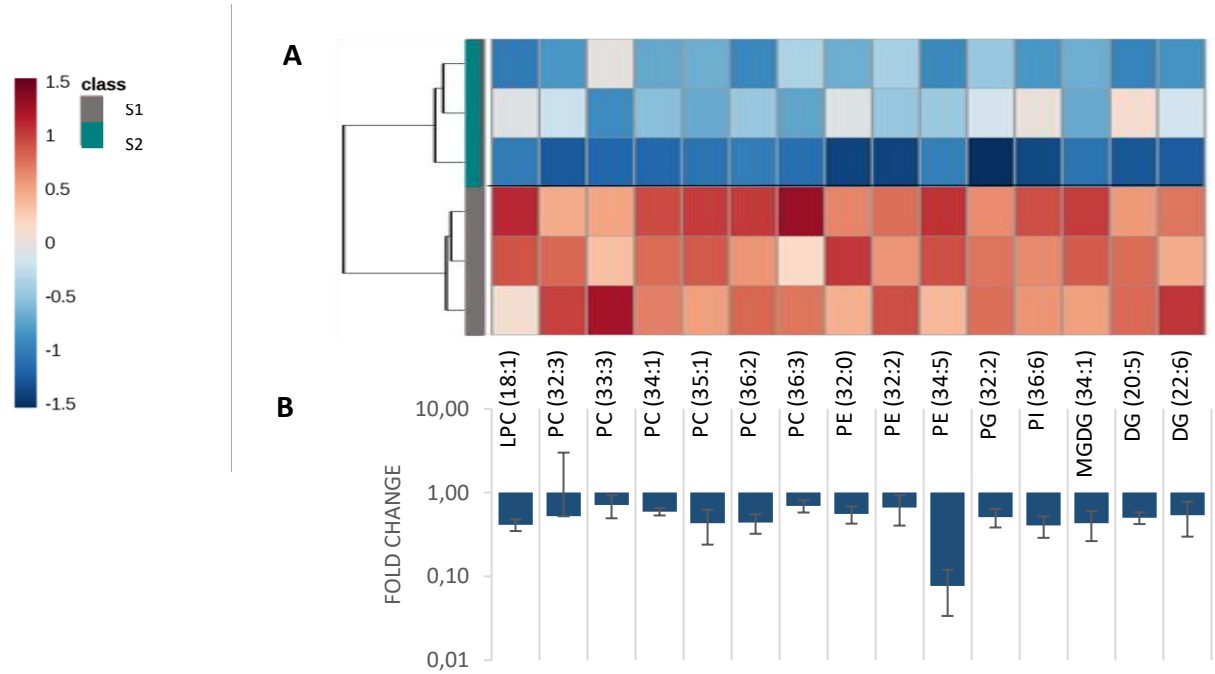


**Figure 3.11:** Lipids of *H. portulacoides* roots from two sites differing in Hg contamination: low contamination (s1) and high contamination (s2). A) Heatmap of the lipids selected from XCMS and MCR-ALS. B) Bar graphs of lipids variation at s2 compared to s1 (mean ± SD, n=3). LPC: lysophosphatidyl-choline; PC: Phosphatidyl-Choline; PE: Phosphatidyl-Ethanolamine; PG: Phosphatidyl-Glycerol; PI: Phosphatidyl-Inositol; MGDG: Mono-Galactosyl-Diacyl-Glycerol; DG: Diacylglycerol. Decreases are represented by blue bars and increases by red bars.

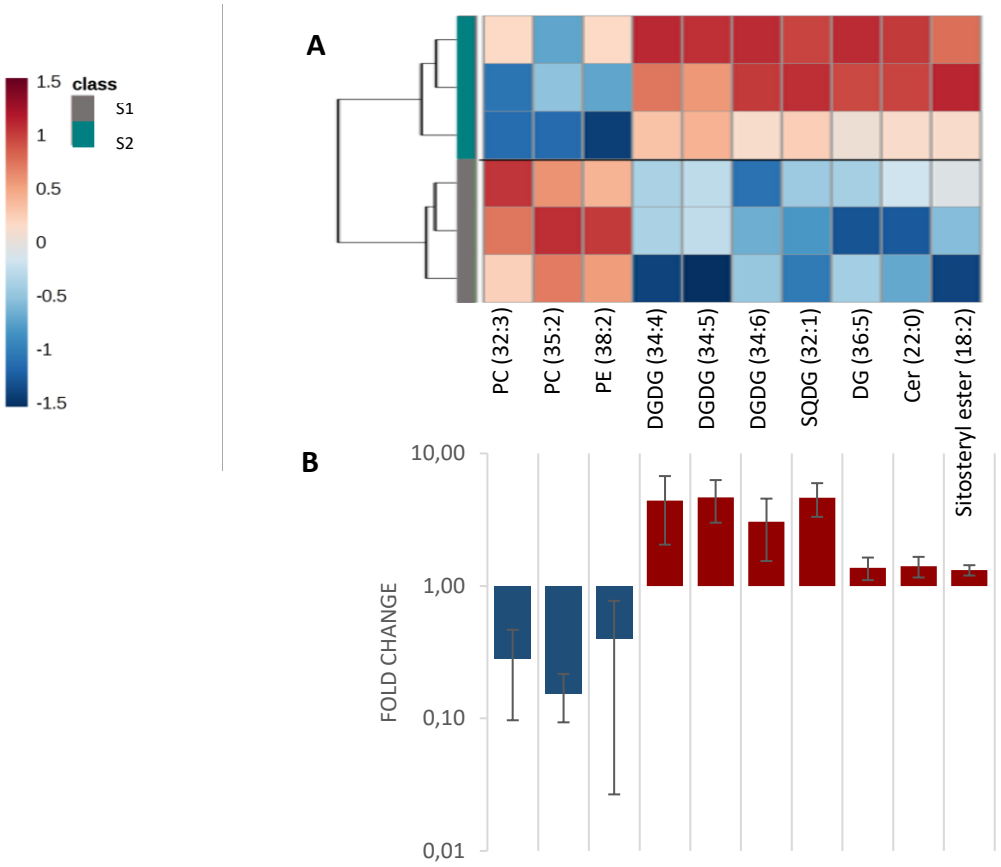


**Figure 3.12:** Lipids of *H. portulacoides* stem from two sites differing in Hg contamination: low contamination (s1) and high contamination (s2). A) Heatmap of the lipids selected from XCMS and MCR-ALS. B) Bar graphs of lipids variation at s2 compared to s1 (mean ± SD, n=3). SQDG: Sulfoquinovosyl-Diacyl-Glycerol; PC: Phosphatidyl-Choline; PE: Phosphatidyl-Ethanolamine; DGDG: Di-Galactosyl-Diacyl-Glycerol; DG: Diacylglycerol; Cer: Ceramide. Decreases are represented by blue bars and increases by red bars.

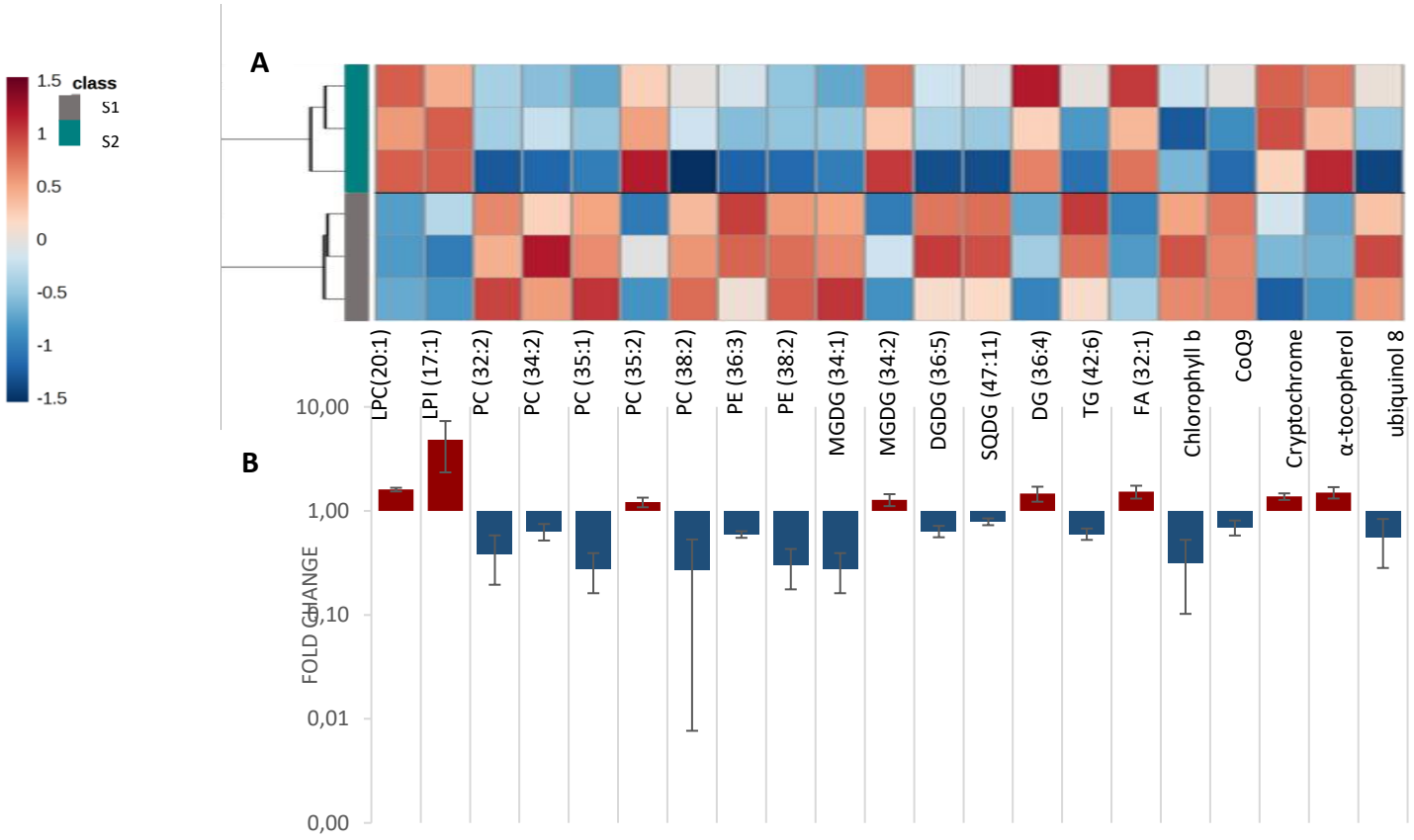


**Figure 3.13:** Lipids of *H. portulacoides* leaves from two sites differing in Hg contamination: low contamination (s1) and high contamination (s2). A) Heatmap of the lipids selected from XCMS and MCR-ALS. B) Bar graphs of lipids variation at s2 compared to s1 (mean ± SD, n=3). LPC: lysophosphatidyl-choline; LysoPI: Lysophosphatidyl-inositol; FA: fatty-acid; SDQG: Sulfoquinovosyl-Diacyl-Glycerol; PC: Phosphatidyl-Choline; PE: Phosphatidyl-Ethanolamine; MGDG: Mono-Galactosyl-Diacyl-Glycerol; DGDG: Di-Galactosyl-Diacyl-Glycerol; DG: Diacylglycerol; TG: Triacylglycerol and CoQ9: Ubiquinone. Decreases are represented by blue bars and increases by red bars.

Tables 8.1, 8.2 and 8.3 include the complete detailed list of m/z values of lipid metabolites from leaves, stem and roots, showing alterations between s1 and s2 sites.

In roots, from the 15 lipids presenting alterations, all decreased in s2 compared to s1. Most of the present lipids (80%) are phospholipids and the remaining are galactolipids and glycerolipids. A specific phospholipid, PE (34: 1), stood out by presenting the largest decrease in s2 relative to s1. In stems 30% of the lipids presented strong decreases in s2 compared to s1, being all phospholipids. The others increased, in particular galactolipids, which increased between 2 and 5 fold in s2 relatively to s1. Leaves showed differences in 21 lipids between s1 and s2. These lipids are phospholipids (42%), galatolipids (19%), glycerolipids (10%) and the remaining belongs to different families. The two phospholipids with small size (17 and 20 carbons) and higher degree of unsaturation (1 double bond) increased in s2 compared to s1. The remaining phospholipids (high size 32-34 carbons) and with high degree of unsaturation (2 or 3

double bonds) evidenced a slight increase and (PC 35: 2) decreased. Most of the galactolipids evidencing differences decreased in s2. MGDG (34: 2) showed a slight increase in s2 compared to s1. The two storage lipids (glycerolipids) that changed between s1 and s2 show different trends, with DG (36: 4) increasing and TG (42: 6) decreasing. The fatty acid (32: 1) also increased. Other molecules such as chlorophyll b, CoQ9 and ubiquinol decreased. On the contrary, α-tocopherol and cryptochrome increased.

## 3.6 Mass spectrometry Imaging (MSI)

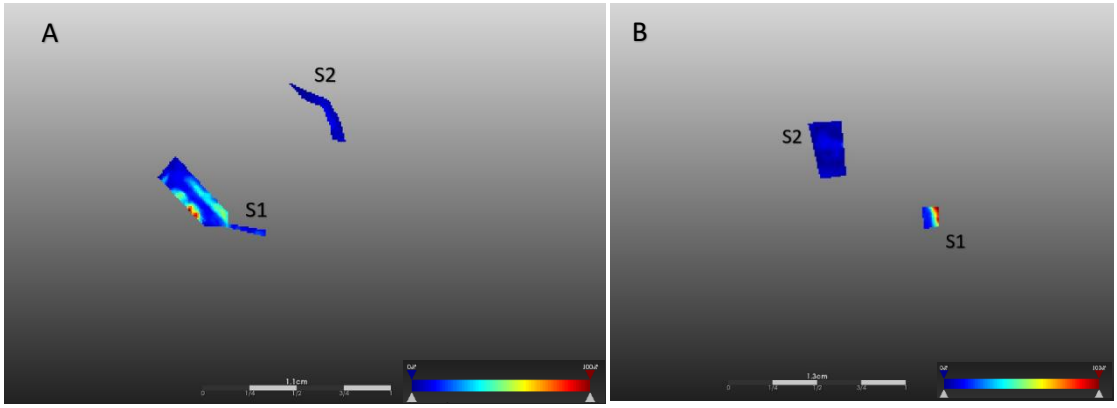


**Figure 3.14-** MALDI-MS images of *H. portulacoides* in the two sampling areas: low contamination (s1) and high contamination (s2). (A) Longitudinal sections of roots. (B) Longitudinal sections of stem.

Mass spectrometry imaging (MSI) techniques provides information at spatial level allowing to localize the distribution of different molecules in the image. Besides chemical/structural information from the mass spectrometry, for each m/z found, it is possible a obtain a distribution map, which provides morphological information about the tissue studied (Bedia et al., 2016).

The longitudinal sections overall of roots and stem, respectively, of *H. Portulacoides*. In both organs, we can observe that there was a decrease of some compounds. Since the red color that represent high intensity (as represented in label of figures), which means a great level of some m/z compounds in less contaminated area (s1) and with Hg concentrations increasing in area s2 these compounds decreased (represented by the dark blue color). In fact, there was a general decreased once the sections of s2 area are all dark blue. From the matrix compound by *m/z*, we can search for compounds already identified by LC-MS and verify that follow the same trend and see its distribution. Some of the lipids detected, we supposed that are DG (20:5), MGDG (34:1) and PI (36:6) in roots and Cer (22:0) in stem due to the same *m/z* detected and showing the same trend observed in LC-MS methodology.

This technique can be as a complement for our study that shows alterations in lipids composition with different levels of Hg contamination since allows to locate the areas of the organs in which the changes occur. Moreover, this technique allows to localize the areas by organ where the alterations in lipid content occur but results obtained o not clarify if changes occur preferentially in some parts of the organs.

# Chapter 4: Results of *J. maritimus*

## 4.1 Metal in sediments and plants

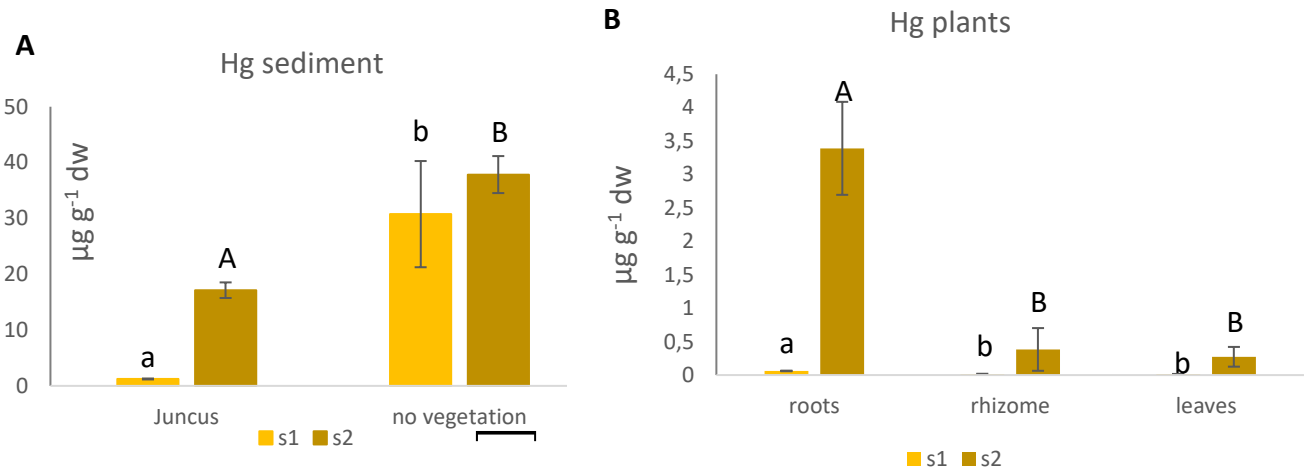


**Figure 4.1**: Total concentration of Hg. (A) Hg concentration in sediments vegetated by *J. maritimus* or in non-vegetated sediment (µg $g^{-1}$ dw) in the two sampling sites: low contamination (s1) and high contamination (s2). (B) Hg concentration (µg $g^{-1}$ dw) in different organs (root, stem and photosynthetic organs) of *Juncus maritimus* colonizing the two sample areas (s1 e s2). Values are the mean of 3 replicates ± standard deviation**.** For each condition, significant differences (P≤0.05) among organs for the same site are represented with lower case (a-b) for s1 and capital letters (A-B) for s2 and for each organ significant differences (P≤0.05) between sites are represented with an asterisk (*).

The sediments of the two sites show differences in Hg concentration. Significant differences were observed in sediments covered with *J. maritimus* but in non-vegetated sediments differences between sites were not significant (figure 4.1A). The presence of *J. maritimus* decreased significantly Hg in the sediment, with non-vegetated sediments, having 29.5 and 20.7 fold more Hg that *J. maritimus* occupied sediments for s1 and s2, respectively, c.f. figure 4.1A.

The accumulation of Hg in the plants of *J. maritimus* plants from s1 and s2 evidences higher Hg concentrations in three organs at s2 compared to s1 (figure 4.1B). However, Hg is differently distributed in plants from the two sites. In the less contaminated site (s1) 59% of Hg is allocated in roots, 25% in stems and 15% leaves. In s2, most of the Hg is allocated in the roots (85%) and the rest distributed between the rhizomes (9%) and leaves (6%) (figure 4.1B). These differences are reflected in the bioaccumulation (BF) and translocation (TF).

## 4.2 Bioaccumulation and translocation of mercury

**Table 4.1** Bioaccumulation and translocation factors of the salt marsh plant, *Juncus maritimus*, colonizing two sampling sites differing in Hg contamination (low s1 and high 2). Bioaccumulation factor (BAF): Hg concentration ratio between root and sediment (R/sediment). Translocation factors (TF): Hg concentration ratio between rhizome and root (Rz/R); leaves and root (L/R). Values are means ± standard deviation of 3 replicates, significant differences (P≤0.05) between sites for each organ are represented with an asterisk (*).

| | **Locations** | **Bioaccumulation factor (BAF)** | **Translocation factor (TF)** | |
|---|---|---|---|---|
| | | R/sediment | Rz/R | L/R |
| *Juncus maritimus* | S1 | 0,058 ± 0,006[a] | 0,101 ± 0,087[a] | 0,257 ± 0,003[a] |
| | S2 | 0,137 ± 0,048[a] | 0,616 ± 0,254[a] | 0,077 ± 0,029[a] |

In both sites, plants accumulate Hg at concentrations for below sediment concentrations (BF<1). The higher BF for s2 compared to s1, evidence the inability of *J. maritimus* to restrict the entrance of Hg at higher contamination levels.

Hg translocation from the roots to the rhizome is less efficient in plants colonizing s2; however, the translocation to leaves is 2,3-fold lower in s2 than in s1 plants, showing the high effort to restrict Hg from photosynthetic organs (table 4.1).

## 4.3 Biochemical parameters

### 4.3.1 Cell damage

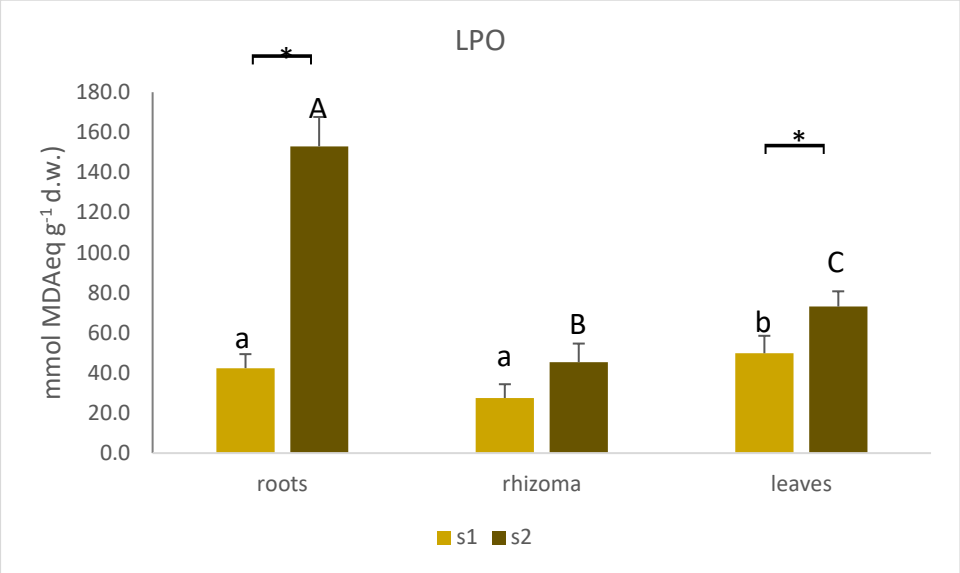


**Figure 4.2**: Lipid peroxidation MDA (nmol $g^{-1}$ dry weight) in organs (roots, rhizomes and leaves) of *J. maritimus* in the sampling sites: low contamination (s1) and high contamination (s2). Values are the mean of 3 replicates ± standard deviation**.** For each condition, significant differences (P≤0.05) among organs for the same site are represented with lower case (a-b) for s1 and capital letters (A-C) for s2 and for each organ significant differences (P≤0.05) between sites for each organ are represented with an asterisk (*).

In s1 lipid peroxidation is similar between roots and rhizomes and significantly lower than leaves between plant. (figure 4.2). In s2 roots displayed LPO levels significantly higher than rhizomes (3-fold) and leaves (2-fold), with rhizomes presenting the lowest concentrations (c. f. figure 4.2). The three plant organs from s2 presented higher LPO levels than the same organ from s1, but differences were significant for roots and leaves (c.f. figure 4.2).

### 4.3.2 Soluble proteins

For both sites roots and rhizomes presented significant higher protein levels than leaves (figure 4.3). Belowground organs (roots and rhizomes) from s2 has 2 to 3-fold more proteins compared to s1. However, leaves from the two sites presented similar protein concentrations (c.f. figure 4.3).

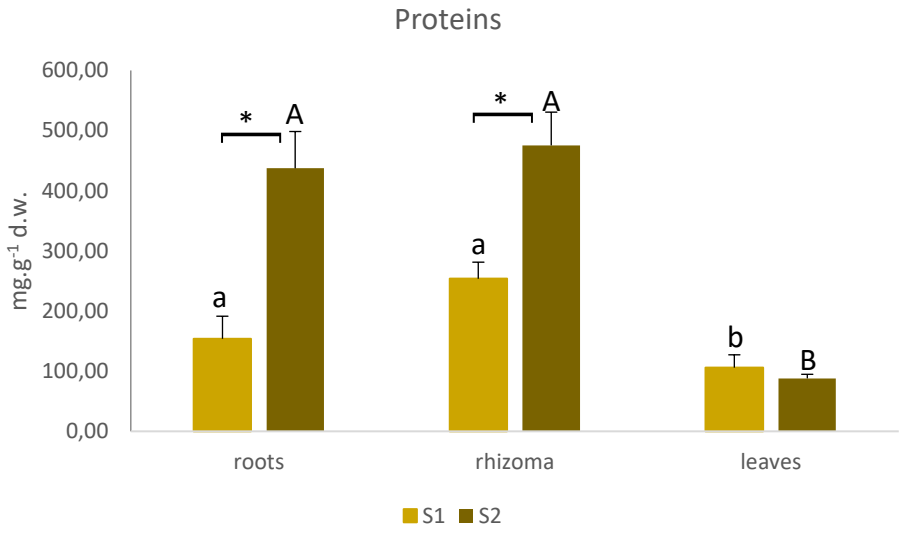


**Figure 4.3**: Soluble proteins (mg.g$^{-1}$ dry weight) in organs (roots, rhizomes and leaves) of *J. maritimus* in the sampling sites: low contamination (s1) and high contamination (s2). Values are the mean of 3 replicates ± standard deviation**.** For each condition, significant differences (P≤0.05) among organs for the same site are represented with lower case (a-b) for s1 and capital letters (A-B) for s2 and for each organ significant differences (P≤0.05) between sites for each organ are represented with an asterisk (*).

### 4.3.3 Antioxidant enzymes

**Glutathione peroxidase (GPx)**

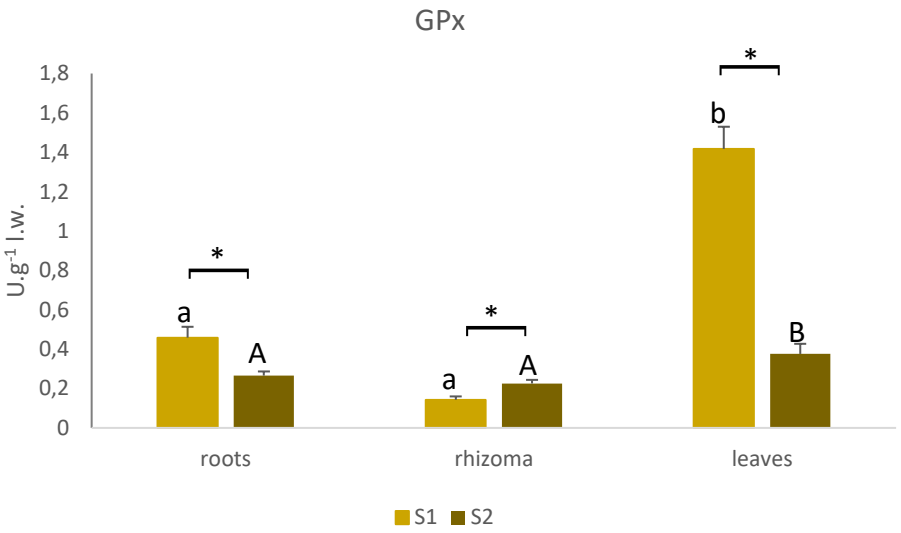


**Figure 4.4**: Activity of GPx (U $g^{-1}$ dry weight) in organs (roots, rhizomes and leaves) of *J. maritimus* in the sampling sites: low contamination (s1) and high contamination (s2). Values are the mean of 3 replicates ± standard deviation**.** For each condition, significant differences (P≤0.05) among organs for the same site are represented with lower case (a-b) for s1 and capital letters (A-B) for s2 and for each organ significant differences (P≤0.05) between sites for each organ are represented with an asterisk (*).

For both sites, GPx activity is similar between roots and rhizomes and significantly higher in leaves (figure 4.4). Roots and leaves have significantly higher GPx activity at s1 compared to s2, especially in leaves, where GPx is 3-fold higher in s1 than in s2. An opposite trend is observed in rhizome with significantly higher activity in s2 compared to s1 (c.f. figure 4.4).

**Dehydroascorbate reductase (DHAR)**

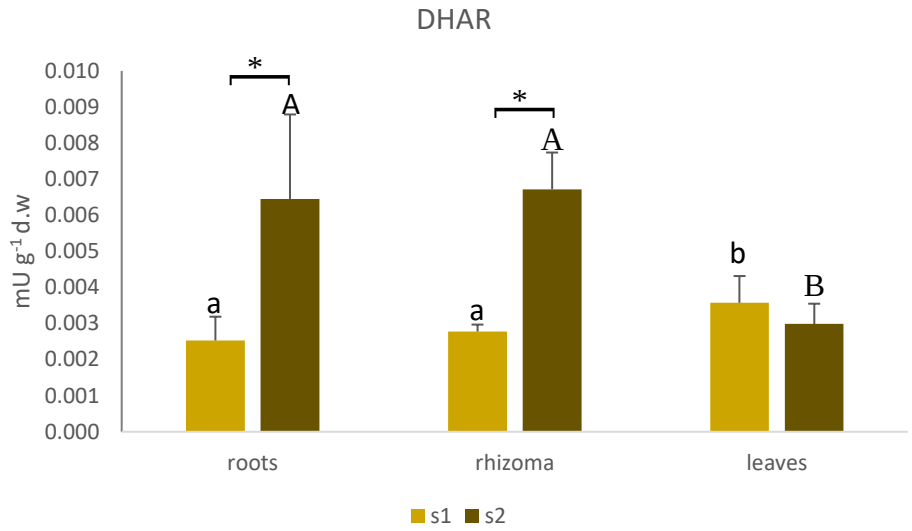


**Figure 4.5**: Dehydroascorbate reductase (mU $g^{-1}$ dry weight) in organs (roots, rhizomes and leaves) of *J. maritimus* in the sampling sites: low contamination (s1) and high contamination (s2). Values are the mean of 3 replicates ± standard deviation**.** For each condition, significant differences (P≤0.05) among organs for the same site are represented with lower case (a-b) for s1 and capital letters (A-B) for s2 and for each organ significant differences (P≤0.05) between sites for each organ are represented with an asterisk (*).

The activity of dehydroascorbate redutase (DHAR) in roots and rhizomes shows significant high activity in s2 compared to s1 but in leaves the activity is similar (p>0.05) between the two sites (figure 4.5). The analysis of plants from s1, shows that roots and rhizomes have similar activities (p>0.05), but these are lower (p<0.05) than the DHAR activity in leaves (figure 4.5). In plants from s2 roots and rhizomes have similar DHAR activity, which are significantly higher than the activity in leaves (c.f. figure 4.5).

### 4.3.4 Biotransformation enzymes – Gluthatione-S-transferases

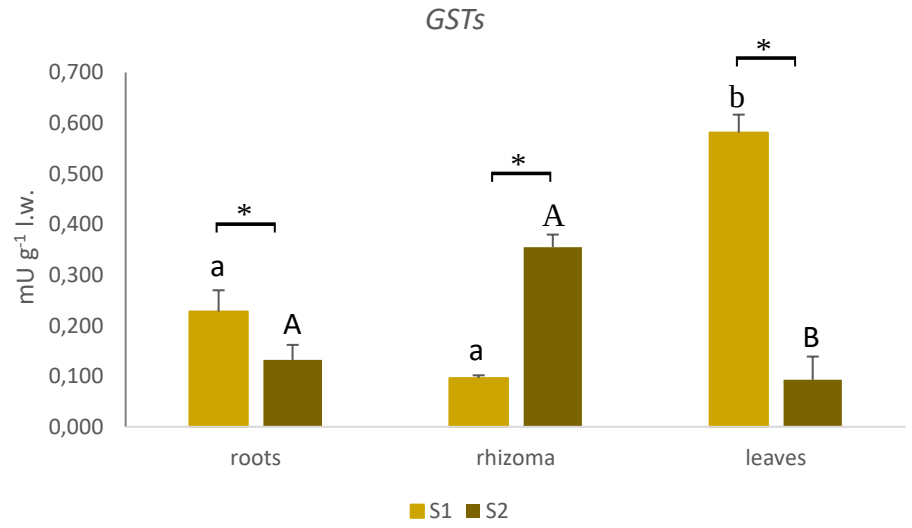

**Figure 4.6**: Activity of GSTs ($\mu g^{-1}$ dry weight) in organs (roots, rhizomes and leaves) of *J. maritimus* in the sampling sites: low contamination (s1) and high contamination (s2). Values are the mean of 3 replicates ± standard deviation**.** For each condition, significant differences (P≤0.05) among organs for the same site are represented with lower case (a-b) for s1 and capital letters (A-B) for s2 and for each organ significant differences (P≤0.05) between sites for each organ are represented with an asterisk (*).

GSTs activity differs among organs at each site and between sites for each same organ. For s1 the activity is significantly different among the three organs, with leaves displaying the highest activity and rhizome the lowest. For s2 rhizomes have the highest activity, with leaves and roots presenting similar activities (figure 4.6). For each plant organ GSTs activity is always significantly different between sites. In leaves and roots the activity is higher in s1 and in rhizome in s2 (c.f. figure 4.6).

### 4.4.5 Electron Transport System Activity

The activity of ETS (electron transport system) is identical between roots and rhizomes in s1. In leaves ETS activity is significantly higher than roots and rhizomes. For each organ, significant differences ($p<0.05$) were regarded for roots and leaves with lower activity in s2 for both organs. Rhizomes values were also lower in s2 compared to s1 but the difference is not significant ($p>0.05$) (c.f. figure 4.7).

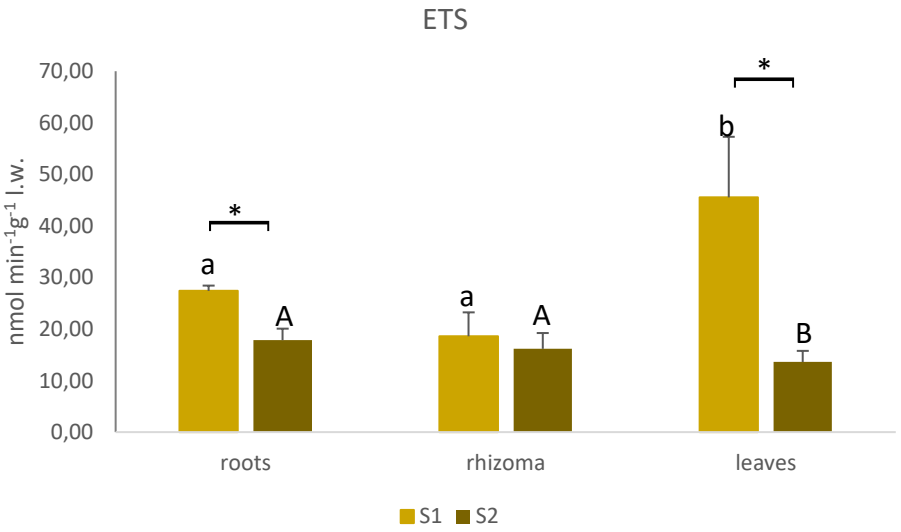


**Figure 4.7**: Activity of GSTs ($\mu g^{-1}$ dry weight) in organs (roots, rhizomes and leaves) of *J. maritimus* in the sampling sites: low contamination (s1) and high contamination (s2). Values are the mean of 3 replicates ± standard deviation**.** For each condition, significant differences (P≤0.05) among organs for the same site are represented with lower case (a-b) for s1 and capital letters (A-B) for s2 and for each organ significant differences (P≤0.05) between sites for each organ are represented with an asterisk (*).

### 4.4.6 Photosynthetic pigments

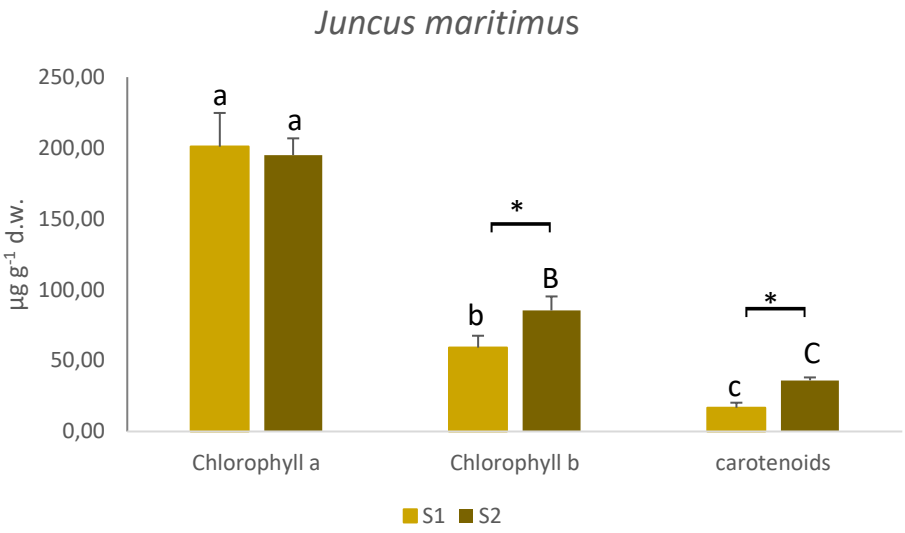


**Figure 4.8**: Chlorophyll *a*, *b* and carotenoids content ($\mu g^{-1} g^{-1}$ dry weight) in leaves of *J. maritimus* in the sampling sites: low contamination (s1) and high contamination (s2). Values are the mean of 3 replicates ± standard deviation**.** For each condition, significant differences (P≤0.05) among organs for the same site are represented with lower case (a-c) for s1 and capital letters (A-C) for s2 and for each organ significant differences (P≤0.05) between sites for each organ are represented with an asterisk (*).

Chlorophyll a is the dominant photosynthetic pigment of *J. maritimus* (figure 4.8). Leaves present 2.3 to 3.2 – fold less chlorophyll b and 5 to 11 fold less carotenoids compared to chlorophyll a for s1 and s2, respectively. For each pigment, significant high concentrations were observed in chlorophyll b and carotenoids for s2 compared to s1. However similar concentrations of chlorophyll a were observed between sites (c.f. figure 4.8).

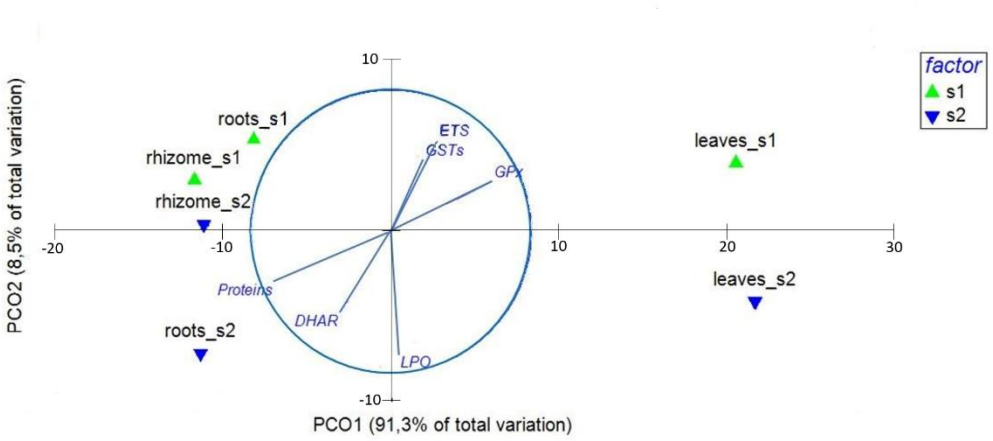


**Figura 2.9:** Biochemical responses of *J. maritimus* exposed to different Hg concentrations, plotted on axes 1 and 2 of Principal Coordinates (PCO) graph. Biochemical are superimposed on the PCO (r>0.5). The less (s1) and more (s2) contamination are indicated for each organ of *J. maritimus* (leaves, rhizome, roots). The biomarkers presented are: GPx, glutathione peroxidase; GTSs, Glutathione-S-transferases; Proteins; ETS, electron transport system; LPO, lipid peroxidation; DHAR, dehydroascorbate reductase.

Figure 4.9 shows the centroids PCO ordination graph resulting from applying a multivariate analysis to the biochemical parameters of *J. maritimus* organs from two sites differing in Hg concentration. The PCO 1 axis explained 91.3% of the total variation of the data, clearly separating leaves on the opposite site from roots and rhizome (in the negative side of axis). The PCO 2 axis explained 8.5% of the total variation. Roots and leaves of s1 are at the positive side while roots and leaves from s2 are on negative side. Rhizomes from both s1 and s2 are very close and appear near the origin of the axis but on the positive side. From the PCO analysis it is possible to observe that: a) roots and rhizomes from both sites are strongly correlated with protein concentrations and DHAR activity; b) roots and leaves from s2 show a strong correlation with LPO levels; and c) ETS, GSTs and GPx are strongly correlated with leaves from s1.

## 4.5 Lipidomic analysis

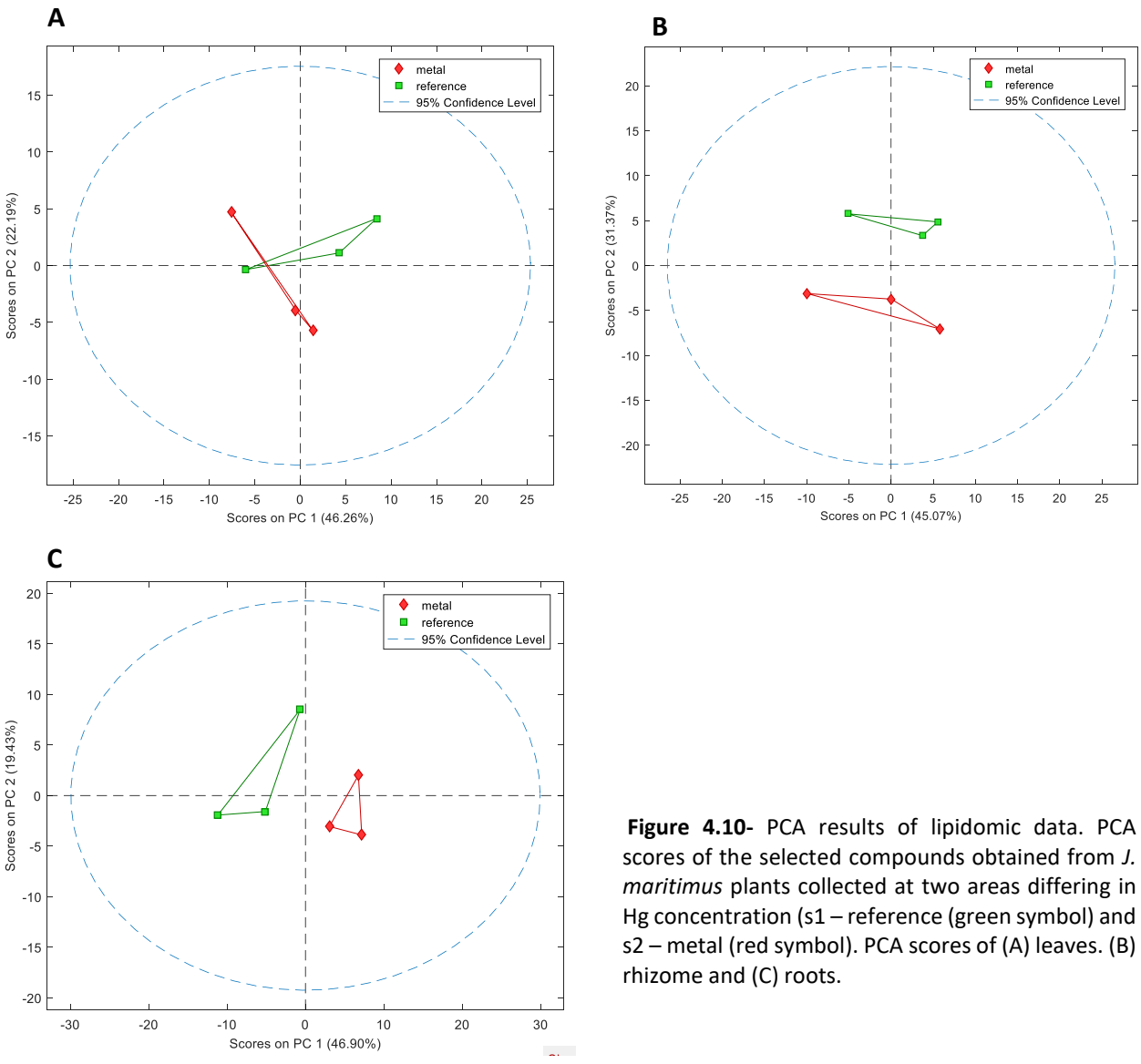


**Figure 4.10**- PCA results of lipidomic data. PCA scores of the selected compounds obtained from *J. maritimus* plants collected at two areas differing in Hg concentration (s1 – reference (green symbol) and s2 – metal (red symbol). PCA scores of (A) leaves. (B) rhizome and (C) roots.

Principal Component Analysis (PCA) graphs obtained for *J. maritimus* leaves, rhizome and roots are represented in figures 4.10A, 4.10B and 4.10C. For leaves, PCA axis 1 (PC1) explained 46.26% and PCA axis 2 (PC2) explained 22.19% of total variance, significantly separating ($p<0.05$) s1 from s2 (figure 4.10A). However, there is no a clear distinction between the two conditions (s1 and s2). In rhizomes, PCA axis 1 (PC1) explained 45.07% and PCA axis 2 (PC2) explained 31.37% of total variance, significantly separating ($p<0.05$) s1 from s2 (figure 4.10B). Finally, in roots, 46.90% is explained by PCA axis 1 (PCA1) and PCA axis 2 (PC2) explained 19.43% of total variance, significantly separating s1 from s2 (figure 4.10C).

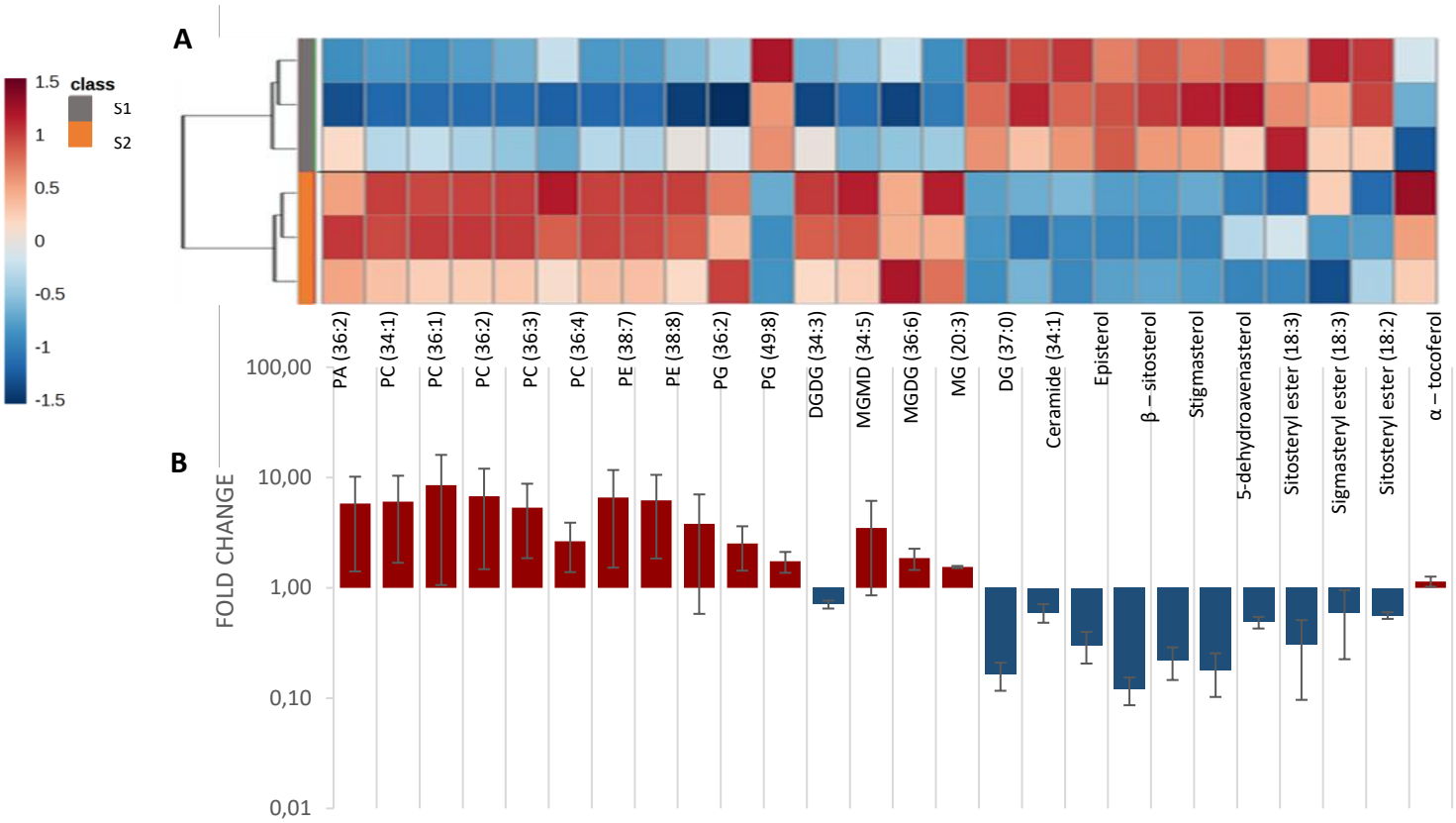


**Figure 4.11-** Lipids of *J. maritimus* roots from two sites differing in Hg contamination: low contamination (s1) and high contamination (s2). A) Heatmap of the lipid selected from XCMS and MCR-ALS. B) Bar graphs of lipids variation at s2 compared to s1 (mean ± SD, n=3). PA: Phosphatidic Acid; PC: Phosphatidyl-Choline; PE: Phosphatidyl-Ethanolamine; PG: Phosphatidyl-Glycerol; DGDG: Di-Galactosyl-Diacyl-Glycerol; MGDG: Mono-Galactosyl-Diacyl-Glycerol; DG: Diacylglycerol. Decreases are represented by blue bars and increases by red bars.

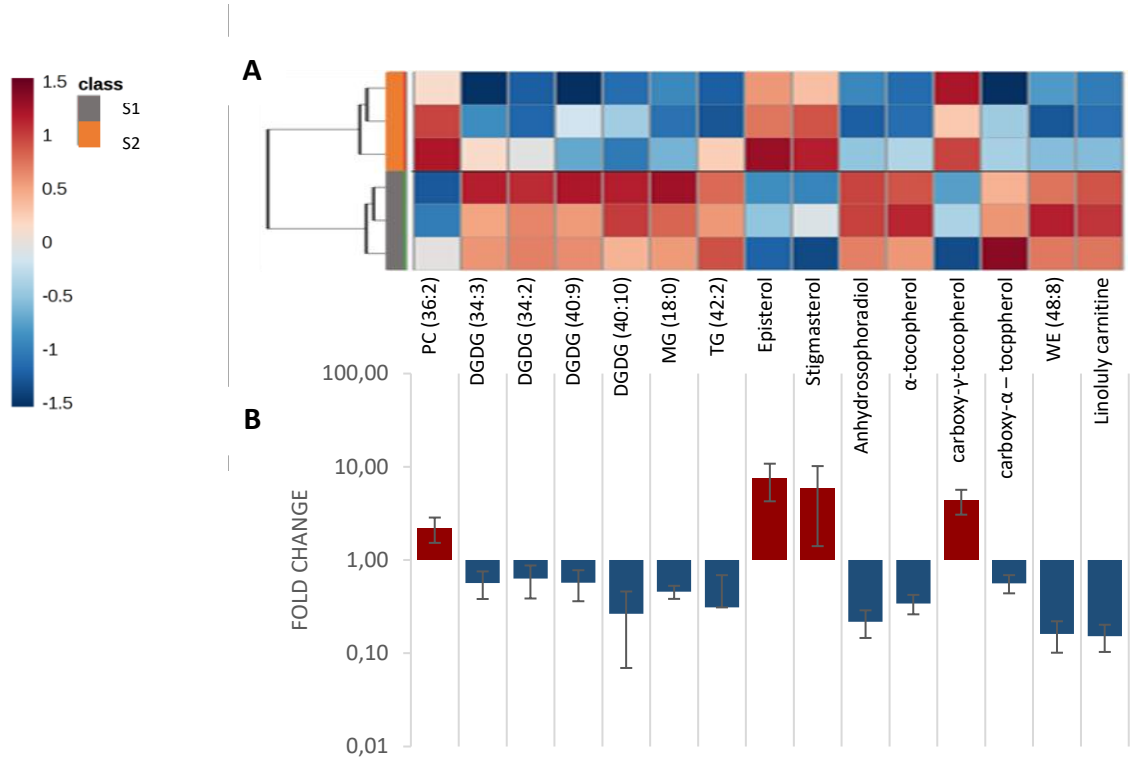


**Figure 4.12-** Lipids of *J. maritimus* rhizome from two sites differing in Hg contamination: low contamination (s1) and high contamination (s2). A) Heatmap of the lipid selected from XCMS and MCR-ALS. B) Bar graphs of lipids variation at s2 compared to s1 (mean ± SD, n=3). MG: monoacylglycerol; PC: Phosphatidyl-Choline; DGDG: Di-Galactosyl-Diacyl-Glycerol; TG: Triacylglycerol and WE: Decreases are represented by blue bars and increases by red bars.

Lipidomic profiles of *J. maritimus* organs from s1 and s2 were compared. Significant differences between sites were put at evidence by a complete analysis of data (section 2.4). Tables 8.4 and 8.5 include the complete detailed list of m/z values of rhizome and roots respectively of metabolites corresponding to the lipids that showed alterations between s1 and s2 sites.

Roots of *J. maritimus* from s1 and s2 differed in 25 identified lipids. The main families of lipids are phospholipids (40%), galactolipids (12%) and sterols (28%). All the phospholipids detected showed a significant increase (between 2 to 6 fold) in s2 compared to s1. In addition, all the phospholipids presented were mono or polyunsaturated, presenting from 1 to 8 double bonds (figure 4.11). With the exception of DGDG (34:3), galactolipids also showed a trend to increase in s2 compared to s1. Reserve lipids (MG and DG) also increased in s2 compared to s1. Other lipidic compounds, including sterols and α-tocopherol, decreased in s2 compared to s1 (figure 4.10). In the rhizomes (figure 4.12) were identified changes in 15 lipids between s1 and s2. All the galactolipids (26%), and glycerolipids (13.3%) decreased in s2 compared to s1. The

same trend was observed in lipid molecules including α-tocopherol and carboxy- α-tocopherol but carboxy-γ-tocopherol increased. Sterols and the only phospholipid (PC (36:2)) detected increased in s2 relatively to s1 (figure 4.11). In leaves it were not detected changes in lipid metabolites between s1 and s2 indicating that lipid profiles did not present significant alterations in peak areas.

## 4.6 Mass spectrometry Imaging (MSI)

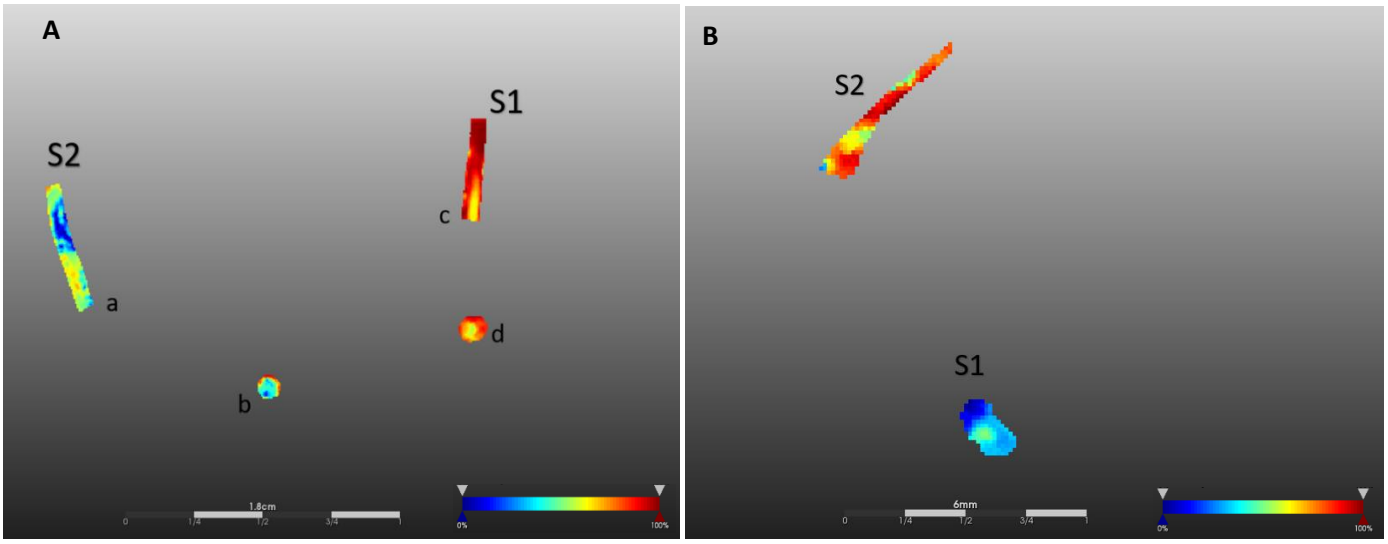


**Figure 4.13-** MALDI-MS images of *J. maritimus* in the two sampling areas: low contamination (s1) and high contamination (s2). (A) Several sections of rhizome: a and c - Longitudinal sections; b and d – transversal sections. (B) Longitudinal sections of roots.

In *J. maritimus*, Figures 4.13.A are images overall of rhizome where a and c are longitudinal sections and b and d are transversal sections of rhizome. Figure 4.13.B represents images of longitudinal sections overall of roots.

In rhizomes, general decrease of the pixels detected is observed in s2 compared to s1 (figure 4.13A). In less contaminated area, peripheral areas of both sections have the highest intensities of the detected compounds (represented by red color). Some of the lipids detected from the matrix compound *m/z*, stigmasterol and carboxy-γ-tocopherol can be the lipids that changed due to Hg toxicity.

Concerning with roots of *J. maritimus*, were observed the opposite relatively to rhizome. The image 4.13.B showed an increase of the *m/z* compounds in more contaminated area (s2) in a heterogeneous way throughout the section compared with the less contaminated area (s1). In fact, we supposed that some of the lipids detected were stigmasterol, α-tocopherol, glycerolipids (DG (36:5) and TG (54:7)) and phospholipids (PC (36:2) and PG (36:2)) whose showed the same trend observed in LC-MS analysis.

# Chapter 5: Discussion

This work intends to clarify the effects that Hg impose on salt marsh vegetation by comparing the response investigating of two plant species (belonging to distinct taxonomic groups - monocotyledonous and dicotyledonous) colonizing two sites differing in Hg concentrations, and for that three hypotheses were formulated.

## 5.1 *H. portulacoides*

For the dicotyledonous species, *our first hypothesis* that Hg distribution in plants would avoid high Hg concentrations in the most vulnerable organs (the leaves) in order to decrease the interference with metabolic processes sensitives to metals like photosynthesis and respiration was supported by the data.

In *H. portulacoides*, Hg concentration increased from the less contaminated to the most contaminated site in all the organs, especially in aboveground tissues.

In *Phragmites australis* and *Juncus maritimus* (Anjum et al., 2012; Figueira et al., 2012), Hg accumulation and distributions showed a similar pattern to *H. portulacoides*, the one described in our study. In fact, the highest concentration of Hg was found in the roots, but the restriction of acropetal Hg transport lost efficiency at the most contaminated site, increasing the concentration in aboveground organs and leaving plants more vulnerable to Hg toxicity. In a study from the same area (Laranjo Basin – Ria de Aveiro), bioaccumulation and translocation of Hg in *H. portulacoides* were similar between locations with different levels of Hg contamination (Castro et al., 2009) and the pattern of Hg distribution in plants was similar between location, with Hg concentrations in roots being much higher (7 -30 fold) than in stems and leaves. The results reported by Castro et al. (2009) are in agreement with those in our study for the low contamination site, since for s1 Hg concentrations in roots were 10 to 11-fold higher compared to stems and leaves respectively. However, at the high contaminated site, Hg concentration in roots was less than 2-fold higher that in leaves and stems. This difference in Hg allocation may evidence the inability of plants to restrict the acropetal movement of Hg at higher levels of sediment contamination.

However relatively high Hg concentrations in leaves can be compatible with cellular activities to metals such as photosynthesis or respiration since *H. portulacoides* possesses anatomical adaptations to salinity, such epidermal trichomes on leaves diverting salt ions to the epidermal tissue and protecting photosynthetic tissues from salt toxicity (Hagemeyer and

Waisel, 1988; MacFarlane and Burchett, 2000; Neumann et al., 1995). These trichomes also can accumulate metals (Hagemeyer and Waisel, 1988; MacFarlane and Burchett, 2000; Neumann et al., 1995), this way, the increase of Hg from roots to leaves from s1 to s2, may have a lower impact than initially expected, and may justify the similar chlorophyll and protein levels and the non-significant differences in ETS activity in leaves from both sites.

This Hg allocation patterns with relatively high concentration in aboveground organs (stems and leaves), at sites with higher Hg contamination, may explain the lower Hg concentrations in vegetated compared to non-vegetated sediments. Indeed, our results evidenced that colonization by *H. portulacoides* showed to be a determining factor in the concentration of Hg in the sediments, significantly reducing Hg contamination in vegetated sites and contributing for sediment decontamination and restoration of a Hg contaminated environment.

Our *second hypothesis* that plants would counteract Hg toxicity by triggering antioxidant responses, especially in tissues accumulating high Hg concentrations (roots) or in tissues more vulnerable to Hg toxicity (photosynthetic tissue) was also supported by our data. Indeed, most of the biochemical parameters determined put at evidence differences related to the level of Hg were plants growth.

Mercury is extremely toxic to plants, it interferes with the photosynthetic process, by decreasing photosynthetic pigments affecting the photosynthetic electron transport chain and originating ROS (Singh et al., 2012). Hg also binds to sulfhydryl groups in proteins resulting in protein inactivation (Hameed et al. 2016).

In order to counteract Hg toxicity plant cells possess several to mechanism, GPx and GSTs activity is signifincantly inibithed by Hg in all *H. portulacoides* organs, since these two enzymes are involved in ROS scavenging and biotransformation of toxic xenobiotics, like endogenous aldehydes formed from lipid hydroperoxides (Møller 2001). The decrease in the activity of these two enzymes will result in the magnification of oxidative stress, due to the less efficient removal of ROS and higher toxicity due to the less efficient biotransformation of toxic aldehydes (Ingle et al., 2005). Anjum et al. (2014) also reported a decrease in GSTs activity in response to Hg in roots and leaves of the *H. portulacoides* (Santos et al., 2015; Bankaji et al., 2016) reported a decrease of GPx activity in roots and leaves of salt marsh plants, *Suaeda fruticosa* and *Juncus acutus* seedlings with Zn and Pb exposure and Cd, respectively.

The activity of dehydroascorbate reductase which plays a critical role in the ascorbate-glutathione recycling in higher plants (Gangwar et al., 2014), does not show a

significant variation between the two Hg levels, indicating that high Hg levels did not induce ascorbate regeneration. Since ascorbate reduces oxidized tocopheryl radicals, regenerating tocopherol (which plays an important role in restricting lipid peroxidation) (Munné-Bosch 2005), results indicate that ascorbate is not providing an increased protection to oxidative stress. Anjum *et al.*, (2014) and Baccouch et al. (2001) also reported no changes in DHAR activity in *H. portulacoides* exposed to Hg and *Zea mays* seedling exposed to Ni, respectively.

Energy used in basal metabolism, growth and reproduction may vary in response to environmental conditions, and exposure to a pollutant may disturb this use (McKenney, 1998; De Coen, 1999). Rapid measurements of the energy status of an organism, such as the electron transport activity, may deliver important information on the effects of a specific condition, like exposure to Hg (Widdows and Donkin, 1992; De Coen and Janssen, 1997). In our study, Hg decreased significantly the activity of ETS in roots and leaves. It was also observed that metals like Cu, Cr and Pb also decreased ETS activity (Tewari et al., 2006; Prasad *et al.*, 1991). According to Hameed et al. (2016 and Patra et al. (2000) Hg ions bind to mitochondrial membranes, inhibiting the electron transport system as was observed in our study. This decrease will negatively impact the energy status of cells, and will decrease the energy available for anabolic process such as proteins and metabolites synthesis. Indeed, our results evidence a decrease in protein content. The decrease in proteins is particularly important since most responses towards metal toxicity is achieved by enhancing the activity of specific enzymes (which are entirely or mostly proteins) and in our study the activity of these enzymes analyzed they decreased or did not change at higher Hg concentration. This result provide evidence that antioxidant defenses were not triggered and *H. portulacoides* plants can not rely on antioxidant response to counteract the oxidative stress generated by Hg.

When ROS are not effectively eliminated damage overcomes. Membranes are especially vulnerable to ROS attack, generating a peroxidation cascade (Pamplona 2008; Sharma et al., 2012). For this reason, in our work, the organs with higher concentration of Hg (roots), or more vulnerable metal toxicity (leaves) showed a significant higher damage at the most contaminated area as shown by LPO levels (Elloumi et al., 2007; Choudhary et al., 2012; Zengin and Munzuroglu, 2006). Antioxidant lipophilic molecules such carotenoids and tocopherol interrupt the progression of the peroxidation cascade (Sharma et al., 2012). Enzymes such as GPx, GSTs and DHAR, on the other hand are involved in the conversion of lipid peroxide products, such aldehydes which are toxic to cells (Pizzimenti et al., 2013), into less toxic and more soluble products, but the activity of these enzymes did not increase at the higher Hg concentration. The combined effect of ROS burst and accumulating toxic lipid peroxide products

potentiates the toxicity of Hg. Anjum *et al.* (2014) also showed that Hg accumulated in *H. portulacoides*, can be correlated to the membrane disruption and cell metabolism impairment.

Perceive the alterations that membranes undergo in the presence of Hg would bring important information to understand process such photosynthesis, respiration, transport or signaling which are highly dependent on membrane integrity and fluidity (Sharma et al., 2012).

Our *third hypothesis* that *H. portulacoides* would evidence different lipid profiles in membranes due to Hg toxicity and to mechanisms counteracting this toxicity are also supported by data.

Most lipids detected in *H. portulacoides* has a high degree of unsaturation, due to the number of double bonds (in average 3) making them susceptible to lipid peroxidation, which is in agreement with the LPO levels determined. The organs with higher Hg concentration (roots at s2) and leaves at s2 was more susceptible to peroxidation for having a higher membrane density (photosynthetic tissues at s2) evidence higher increases in LPO levels 1.8 and 1.5 – fold, respectively compared s1. On the contrary, stems have similar levels of LPO in the two sites

Among lipid compounds displaying changes due to Hg, the most significant were the concentrations in some galactolipids. These compounds are the most abundant lipids in all photosynthetic tissues, especially in thylakoid membranes, allowing the efficient packing of thylakoid membranes (Dörmann and Benning 2002; Marques et al., 2016). It was also reported that composition of galactolipids affects the lipid bilayer of membranes, which is crucial for maintaining membrane stability and the activity of membrane proteins (Hölzl and Dörmann 2007). Moreover, a specific galactolipid (Sulphoquinovosyldiacylglycerol - SQDG) was reported to can decrease the size and the number of chloroplasts when plants are exposed to metals (Elloumi et al., 2014). In our work, the observed decrease of SQDG may reflect the oxidative stress experienced by *H. portulacoides* leaves at the highest Hg concentration. Kumar et al. (2012), also reported a decrease in SQDG concentration in *Talinum triangulare* exposed to Pb and concluded that SQDG concentrations are affected by ROS (Kumar et al., 2012). Thus, a decrease in SQDG may have implications in photosynthesis described by Elloumi et al. (2014). The decrease in galactolipids of leaves from s2 can indicate that light depend reactions may be affected and that Hg can negatively affect photosynthesis, by disturbing the architecture of thylakoid membranes.

Our study also showed a significant decrease chlorophyll b (determined by LC-MS) in leaves from s2. Several studies reported chlorophyll decreases in different plant species exposed to several metals such as *Picea abies* and *Zea mays*, *Quercus palustris* and *Acer rubrum* exposed

to cadmium and iron (Siedlecka and Krupa, 1996; Elloumi et al., 2007; Choudhary et al., 2012; Zengin and Munzuroglu, 2006).

In our study the determination of chlorophyll b by LC-MS and spectrophotometry resulted in contradicting results, since spectrophotometric determination evidenced an increase in these pigments and point out differences resulting by using different methodologies. Silva (2010) also reported an overall increase of chlorophyll a, chlorophyll b and total carotenoids content in *H. portulacoides* exposed to Zn.

As antioxidants, carotenoids, play a key role as ROS scavengers to protect the chloroplasts against photo-oxidative damage, by quenching singlet state of chlorophyll an ROS and inhibiting lipid peroxidation under stress conditions (Hameed et al., 2016; Hou et al., 2007). ROS detoxification is an essential function of carotenoids that contributes towards the protection of enzymes and electron transport in thylakoids membranes in plants under metal stress (Sengar et al., 2008). In our study, carotenoids increased in the leaves of *H. portulacoides* but was not sufficient effectively reduce ROS and to protect leaf membranes from peroxidation induced by the high Hg concentrations.

α-tocopherol (α-Toc), which is the most active form of vitamin E and is produced in the thylakoid membranes of chloroplasts and other plastids (Lushchak and Semchuk 2012; Munné-Bosch 2005) is a lipophilic antioxidant that stabilizes the membrane structure and protects polyunsaturated fatty acyl from peroxidation, consequently protecting the photosynthetic apparatus from oxidative damage (Hasanuzzaman et al., 2014; Singh et al., 2016). In our study, the leaves of *H. portulacoides*, also showed a significant increase of α-toc in plants from s2 compared to s1, thus providing protection to thylakoid membranes and to the photosynthetic apparatus and the photosynthetic activity. Several studies also reported that increased levels of α-toc can prevent cell membrane from damage under stress by metals. Artetxe et al. (2002) reported an increase of α-toc in *Lemna minor* exposed to cadmium and Zn. Gajewska e Skłodowska, (2007) showed that levels increased in shoots of *Triticum aestivum* seedlings when exposed to Ni. In *Arabidopsis thaliana* exposed to Cu and Cd, α-toc also increased (Colin et al., 2008).

Plants depend on cryptochromes and other photoreceptors to sense environmental cues, such as irradiance, day-night transition and photoperiods (Li and Yang 2007; Liu et al., 2012). In addition, regulation of the circadian clock and plants growth is also influenced by these compounds (Liu et al., 2012). In a previous study, it was shown that overexpression of cryptochrome genes resulted in overproduction of anthocyanins in *A. thaliana* leaves (Li and

Yang 2007). The increase of cryptochromes in our study suggests that anthocyanins synthesis might also be enhanced by high Hg concentrations. Given the antioxidant role of anthocyanins, Kovinich et al. (2015), a high concentration of these compounds may contribute to increase the tolerance of *H. portulacoides* plants to Hg.

Hg decreased Ubiquinol 8 and ubiquinone (CoQ9) in the leaves of *H. portulacoides.* Ubiquinol is a reduced form of ubiquinone (or Coenzyme Q) and is involved in electron transport in mitochondrial membranes (Ingle et al., 2005). Both compounds were reported as lipid-soluble antioxidants that protect membrane lipids from peroxidation (Turunen et al., 2004). Ubiquinol and ubiquinone participate in the mitochondrial electron transport chain and their oxidation will produce ubisemiquinone which can result in the production of $O_2^-$ a very reactive ROS (Blokhina and Fagerstedt 2010). Thus, the decrease of ubiquinol may reflect the oxidative status in mitochondria. In our study, the decrease of these two compounds can explain the higher levels of lipid peroxidation measured in the leaves at s2 and the significant decrease in ETS activity observed in roots.

Lysophospholipids (LP) can be hydrolyzed from the membrane associated lipids and released into the extracellular space where they can be recognized by extracellular receptors and trigger signaling cascades (Hou et al., 2016). In our study, two LP compounds increased in the leaves of *H. portulacoides* plants exposed to high Hg concentration. This increase may suggest that there was an increase in membrane lipid hydrolysates that may serve as signals that being recognized by extracellular receptors, may initiate signaling pathways, which may trigger a response to Hg.

In general, in all the three organs analyzed a significant decrease in phospholipids was observed, especially roots. This decrease can be associated with loss of membrane integrity, since phospholipids are important constituents of cell membranes (Ruelland et al. 2014). Hölzl and Dörmann (2007) reported that in leaves phosphatidylcholine (PC) molecules reported to decreased in the outer amounts in the outer chloroplast envelope, which was related with alterations in photosynthesis. According to Elloumi *et al.* (2014), alterations in lipid composition may affect membrane permeability, energy transduction capacity and the activities of membrane bound enzymes. Sharmila et al. (2014) reported that Hg can decrease membrane fluidity by interacting with phospholipids. Hg can bind to the head groups of phosphatidylethanolamine (PE) and PC (Sharmila et al., 2014), phospholipid subclasses that in our study decreased in the tree organs of *H. portulacoides* at s2. Thus in the cells of all the *H.*

*portulacoides* organs exposed to high Hg concentration, all these activities may also have been affected.

In our study, a phosphoinositide (PI (36:6)) decreased in roots. PIs are signaling lipids derived from phosphatidylinositol (Hou et al., 2016; Ruelland et al., 2014). These signaling molecules are involved in several cellular process including stress responses (Hou et al., 2016). Moreover, PIs can act as specific ligands in proteins and can also affect biophysical properties of lipid bilayers (Hou et al., 2016). Thus, the decrease of these lipids caused by Hg, can induce instability in lipid bilayers and make membranes less permeable to ions (Dowhan et al., 2015), preventing the entrance of Hg into *H. portulacoides* roots. In fact, the bioaccumulation factor in plants from s2 is 6-fold lower compared to plants from s1.

The LC-MS separation and bioinformatic identification used in our study were able to discriminate the lipid profiles in the organs of *H. portulacoides* plants exposed at two Hg concentrations.

Results put at evidence of suitability of this methodology to evidence the alteration induced by Hg in membrane lipid profiles of *H. portulacoides*, evidencing simultaneously the toxic effects and the mechanism counteracting their toxicity.

## 5.2 *J. maritimus*

For the monocotyledonous species, we also expected that Hg distribution in plants would avoid high Hg concentration in the most vulnerable organs (the leaves) as our *first hypothesis*.

The colonization of sediments *J. maritimus* shows to be a determining factor in the concentration of mercury in the sediments, reducing the concentration of Hg especially in less contaminated site. In previous studies (Castro et al. 2009; Figueira et al. 2012) it was reported also for *J. maritimus similar* Hg concentrations in the less contaminated site.

In *J. maritimus*, Hg concentration increased from the less contaminated to the most contaminated site in all the organs, especially in roots. Indeed, roots at s2 accumulated most of the Hg uptaken by plants, (approximately 85%). Metal retention in roots protect the more sensitive aboveground organs from Hg toxicity (Singh et al., 2016).

In our study, it's the high percentage of Hg content retained in roots shows the efficient restriction of Hg uptaken movement, especially in the most contaminated site.

The high retention of Hg in roots is in accordance with the low translocation factors in our work for *J. maritimus,* especially for s2. These results are in agreement with which it was demonstrated that, in general, many plants exclude mercury, retaining it primarily, Patra and Sharma (2000) who reported that exclusion of metals, including Hg from abovegrounds organs amount retention primarily in roots is a general pattern of metal distribution in plants. It seems that roots acts as a barrier in order to avoid the translocation of the metal to the aerial parts of the plant. In J. maritimus their mechanism constitutes an efficient way to protect leaves from Hg toxicity and is in accordance with the similar chlorophyll a and protein content and the non-significant differences in DHAR activities in leaves from both sites. The higher concentrations of Hg accumulated by plants at both sites, may explain the lower Hg concentrations in vegetated compared to non-vegetated sediments. Indeed, colonization by *J. maritimus* showed to be a determining factor in the concentration of Hg in the sediments, significantly reducing Hg contamination in vegetated sites.

Our *second hypothesis* that plants would counteract Hg toxicity by triggering antioxidant responses, especially in tissues accumulating high Hg concentrations (roots) or in tissues more vulnerable to Hg toxicity was also supported by our data. Indeed, most of biochemical parameters determined show differences between plants exposed to different contamination. These differences were mainly observed in roots and leaves with both organs from s2 presenting lower GPx, GSTs and ETS activity.

GPx and GSTs are involved in ROS scavenge and biotransformation of aldehydes formed from lipid hydroperoxides (Møller 2001). Although, the decrease in the activity of both enzymes at s2 evidence the inability of roots and leaves to mitigate the oxidative stress generated by Hg (Santos et al., 2015; Bankaji et al., 2016) also reported a decrease in GSTs activity for *H. portulacoi*des exposed to Hg. However, in other plant species, such as *Pisum sativum* and *Oryza sativa* exposed to Cd (Dixit et al., 2001; Moons 2003) and *Posidonia oceanica* exposed to Hg (Ranvier et al., 2000; Ferrat 2002 a, c). GPx activity also decreased in the halophyte *Sueda fruticose* exposed to Cd and Cu (Bankaji et al., 2016).

The activity of ETS, which gives the respiration activity (McKenney, 1998; De Coen, 1999) is found in our study. This decrease in ETS has a negative impact the energy status of cells leaving less energy available to face stress conditions. It was also observed that metals like Cu, Cr and Pb also decreased ETS activity (Tewari et al., 2006; Prasad et al., 1991).

The activity of dehydroascorbate reductase (DHAR) increased in roots and rhizomes of *J. maritimus* at high Hg concentration. These results suggest that to tolerate Hg toxicity, *J.*

*maritimus* is increased the reduction of dehydroascorbate to ascorbate using DHAR in order to decrease Hg toxicity. Regeneration of ascorbate from an oxidize regulates the cellular ascorbate (AsA) redox state increasing plant responsiveness and tolerance to metal stress (Gangwar et al., 2014; Zhang 2013). AsA has an important antioxidant role in plants limiting ROS-induced damage to macromolecules (Noctor and Foyer 1998). Huang *et al.*, (2010) reported the increase of ascorbate levels Kan*delia candel* and *Bruguiera gymnorrhiza* exposed to Hg. DHAR activity also increased in *Sorghum bicolor* exposed to Cr (VI) (Shanker and Pathmanabhan 2004) and in *Glycine max* seedligs at a lower Cd concentrations (Balestrasse et al., 2001). Moreover, Martret et al (2011) concluded that overexpression of DHAR and GSTs can provide protection to plants against oxidative stress caused by metals. The significantly higher activity of the enzymes (GSTs, GPx and DHAR) in rhizomes from s2, certainly contributed to mitigate oxidative stress and to lipid peroxidation levels high significantly different from s1.

Membranes are cell structures more vulnerable to ROS attack. In our study, the plant organ with the highest LPO levels was the roots at s2. Also, rhizomes and leaves did not show a significant difference between in two sites. This result may be related to the concentration of Hg (2 to 6 fold higher than other organs) accumulated in the roots in s2 area functioning as main sink, protecting the aboveground tissues from membrane damage.

Chlorophylls and carotenoids are often measured in order to evaluate the impact of an environmental stress in photosynthesis, as changes in pigment content are linked to photosynthetic productivity (Kalaikandhan, 2014). Our results showed a significant increase of chlorophyll b and carotenoids from the less to the most contaminated site.

Carotenoids, play a key role as ROS scavengers, protect of chloroplasts against photo-oxidative damage and metal shoots (Hou et al., 2007). In our study, carotenoids increased in leaves of *J. maritimus* at s2 and thus evidencing the strategy of leaves to protect the activities from metal toxicity. However, it was not enough to prevent higher levels of lipid peroxidation at s2.

Our *third hypothesis* that *J. maritimus* would evidence different lipid profiles in membranes due to Hg toxicity and to mechanisms counteracting their toxicity are also supported by data.

In the rhizome of *J. maritimus*, high Hg concentration induced a significant decrease in galactolipids content, specifically, Di-Galactosyl-Diacyl-Glycerol (DGDG). The decrease in DGDG can will lead to membrane disorganization affecting membrane permeability and the activiy of membranes bound enzymes and light reaction processes (Elloumi et al., 2014). The same

galactolipids also detected in non-photosynthetic organs of *Arabidopsis* , like roots (Shimojima and Ohta 2011).

Thus, tocopherol related compounds, a potent antioxidant, were detected with significant changes in rhizome and roots of *J. maritimus*. In both organs, α-tocopherol, decreased at Hg toxicity. Changes of α-tocopherol content during plant responses to environmental stresses, such metals, are characterized by two phases. In the first one, occur the increases of synthesis of tocopherol which reduces ROS and protect membranes from oxidative damage. The second phase happens when the stress is too severe and tocopherol degradation exceeds its synthesis and levels decrease (Munné-Bosch 2005). Consequently, lipid peroxidation increase as was observed in roots and rhizomes of *J. maritimus*. γ-tocopherol showed a different trend increasing at high that increased with Hg toxicity. γ-tocopherol is the last intermediate in the α-tocopherol pathway catalyzed by γ – tocopherol methyl transferase (γ-TMT) (Hasanuzzaman et al., 2014). This enzyme is overexpressed in plants exposed to metals resulting in an increase of α-tocopherol of *J. maritimus.* However in our study γ-TMT may be inhibited by high Hg concentrations, resulting in lower α-tocopherol and higher γ – tocopherol (Munné-Bosch 2005). Yusuf et al. (2010) also reported the same increase of γ – tocopherol in *Brassica juncea* when exposure to CdCl2.

Triacyclglycerols (TAGs) decreased at high Hg concentration at s2. TAGs play a key role in intracellular lipid homeostasis and cell survival ((Xu and Shanklin 2016). This class of lipids are involved with energy storage and their decrease may have related to the higher be a mobilization or energy consumption for other organ in stress conditions.

Linoleyl carnitine is an acylcarnitines and was already detected in plants species such *A. thaliana*, *Brassica juncea*, *Linum usitatissimum* and *Nicotiana tabacum* (Bourdin et al., 2007). The main role of acylcarnitines is the activation of fatty acids transport though organelles membranes. Linoleyl carnitine decreased in rhizome of *J. maritimus* at higher Hg concentration. Thus, the reduction of linolelyl carnitine can result in a lower availability of fatty acids for Beta-oxidation and for energy available to mitigate Hg stress. *Pistia stratiotes* exposed to cooper and zinc nanoparticles also showed a decrease in linoleyl carnitine (Olkhovych et al., 2016).

Changes in phyto plant sterols, were detected in the rhizome and roots of *J. maritimus* at high Hg concentrations. Distinct alterations were recorded with decreases in roots and increases in rhizomes. Stigmasterol and episterol are abundant constituents of the plasma membrane, the tonoplast and the endoplasmic reticulum (Wewer et al., 2011). Phyto sterols are involved in membrane fluidity and permeability. Bassuany et al. (2014) and Santos et al. (2014)

reported a decrease in LPO of *Linum usitatissimum* plants and showed that these treated with stigmasterol. In salt tolerant genotypes of *Oryza sativa* and *Saccharum officinarum* lower lipid peroxidation and higher membrane stability was observed after treatment with stigmasterol (Bassuany et al., 2014). In our study, the increase of stigmasterol may help restraining lipid peroxidation due as was verified in rhizome at high Hg concentration since no significant changes were detected in rhizome from the two sites.

Episterol increased in rhizomes at s2. This lipid is a precursor for the biosynthetic pathway for brassinosteroids (BRs) (Vardhini 2015). Brassinosteroids are phytohormones and counteracting the negative effect induced by stress plants and confering resistance to plants against abiotic stress (Vardhini 2015). The supplementation of BRs in *Raphanus sativus* exposed to Hg with the aim to minimize oxidative stress resulted in the increase of protein content and GSTs activity (Vardhini 2015). Kapoor et al. (2014) also studied the application of BRs in *Raphanus raphanistrum* exposed to cadmium and mercury as a result the activity of enzymes GPX and DHAR and in protein content increased, and may explain at least in part the increase with DHAR, GSTs, GPx activity and protein content observed in rhizomes from s2, thus, increasing plant tolerance to Hg stress.

On the other hand, these two sterols plus beta-sitosterol and 5-dehydroavenasterol were reduced in roots. Sitosterol is other sterol abundant in plant tissues and considered the more efficient than stigmasterol (Piironen et al., 2000; Santos et al., 2014), and it was reported to reduce membrane permeability in *Glycine max* (Schuler et al., 1991). Thus, a reduction of sitosterol may lead to increased membrane permeability.

In addition free sterols, plants also contain considerable amounts of esters sterols which are localized in cytosolic oil bodies (Wewer et al. 2011). The roles of steryl esters include storage and transportation as a transport form of sterols (Piironen et al., 2000; Sixty-fifth 1993). These results may indicate a reduction in storage and immobilization of lipid reserves in roots facing higher Hg concentrations compromising the ETS activity. Indeed our results show a significant decrease in ETS activity in roots at s2, most delivering enough energy to fight efficient Hg stress.

High Hg concentrations increased phospholipids was had significant changes, especially in roots. According to literature, PCs and PEs are abundant constituents of plasma membrane, tonoplast and endoplasmic reticulum (Wewer et al., 2011; Ruelland et al., 2014). The increase of these lipids in belowground organs may be the response of J. maritimus plants to high Hg concentration, since phospholipids were reported to increase membrane permeability and strength (Ruelland et al., 2014). Phosphatidic acid (PA), was identified as a cellular signaling

molecule. It being involved regulation of plant responses to hormones and reprogramming lipid metabolism and binds to protein and is involved in recruitment to membranes (Hou et al., 2016). This lipid is rapidly generated in response to abiotic stress and is involved in osmotic stress, salt and pathogen attack response (Ruelland et al., 2014). Diacylglycerol (DG) is one of the precursors of phosphatidic acid (PA) (Hou et al., 2016; Ruelland et al., 2014) and in our work a decrease in DG (37:0) was noticed, probably related with a higher PA (Ruelland et al., 2014). On the other hand, PA can originate abscisic acid (ABA), which is a phytohormone that is linked with tolerance to adverse environmental conditions and its signaling pathway is a central regulator of abiotic stress in plants (Bücker-neto et al., 2017; Hou et al., 2016). In literature, there are several studies that demonstrating an increase of ABA concentration in plants tissues after metal exposure. Munzurro et al. (2008) reported an increase of ABA levels in *Triticum* seeds exposed to Hg. Moreover, it was shown that Cd exposure lead to increased ABA levels in the roots of *Typha latifolia* and *Phragmites australis* (Fediuc et al., 2005) and also in *Oryza sativa* (Kim et al., 2014). So, the increase of phosphatidic acid in the roots of J. maritimus exposed to high Hg concentration can lead to abscisic acid production and in this way an induction of protective mechanism against Hg toxicity.

Regarding to leaves, lipid profiles did not change with high Hg concentrations. This result can be explained by the efficient Hg restriction to aboveground organs of *J. maritimus*.

# Chapter 6 – Final conclusions

Colonization of sediments by different plant species induced differences in Hg in sediments at the more contaminated site, where colonization lead to lower Hg concentration in *H. portulacoides* than *J. maritimus*. These results evidence not only the ability of plants to alter its concentrations in the surrounding sediments but also act their effect differs between species and is influenced by the concentration.

The colonization in the same site, concentration of Hg at each species differed considerably. The Hg concentration in *J. maritimus* roots from s2 has 5.5 fold higher than *H. portulacoides* roots, evidencing the different ability of the two species to bioaccumulate Hg. *H. portulacoides* has higher BAF and lower Hg concentrations, restrict efficiently the abortion of Hg at high concentrations whereas *J. maritimus* protects from Hg contamination increasing TF at higher sediment Hg concentration and accumulating higher levels of Hg than *H. portulacoides*. The two plant species also show different translocation patterns. *J. maritimus* translocate less Hg from roots to other organs than *H. portulacoides*, Otte et al. (1991) and Fitzgerald et al. (2003) reported that dicotyledonous species tend to accumulate similar concentrations of metals. Since *J. maritimus* accumulated higher levels of Hg at high Hg concentrations, the more efficient restriction of upward movement distributed in similar concentrations between the two species in stem and leaves. Thus, species have different allocation strategies to cope with Hg stress. *H. portulacoides* restrict the entry of Hg into the plant more efficiently, accumulating less Hg. *J. maritimus* accumulate high levels of Hg, but restricts more efficiently the translocation from roots to different organs. Both strategies resulting in similar concentrations for stems and leaves, although 1.2 to 16% lower for J. *maritimus*.

In this work, several biochemical parameters were analyzed to evaluate the mechanisms plant responses to mitigate Hg toxicity.

The levels of lipid peroxidation, the main of oxidative damage, are similar in stems and leaves of both species, evidencing of every biochemical exposed to identical oxidative stress levels induced resulting from identical Hg concentrations. Soluble proteins content may evidence the effect of tissues to counteract toxicity, by triggering new responses or enhancing the antioxidant response. *J. maritimus* showed responses as evidenced by the increase of DHAR and GSTs activity for roots and rhizomes. In leaves the antioxidant enzymes were inhibited in the mitigation of oxidative stress, however carotenoids and chlorophyll b increased to protect the photosynthetic apparatus from oxidative damage. These protection mechanism metals have been efficient since no changes the lipid profiles were detected in leaves submitted to different

Hg levels. On the contrary, *H. portulacoides* did not trigger any of the mechanism analyzed to soluble proteins, which are mainly soluble enzymes, were not increased (stems and leaves) or decreased in roots. The activity of GPx and GSTs decreased and DHAR activity did not change in the three organs. As in *J. maritimus*, chlorophyll b and carotenoids were increased but was not enough to counteract de Hg toxicity in leaves since LPO increased significantly and the lipid profile was changed.

The lipidome study shows that Hg contamination induced differences in the lipid profiles and *H. portulacoides* and *J. maritimus* displayed different alterations. These results show that each plant group is affected in different way and they have different strategies to cope with Hg.

In *H. portulacoides*, the phospholipids decrease in all organs analyzed, can be related with alteration in membrane permeability (Dowhan et al., 2015). In addition, galactolipids which are abundant in thylakoid membranes and decrease at high Hg and may indicate interfere with photosynthesis process. On the other hand, α-tocopherol, a potent lipidic antioxidant, increased in leaves, thus providing a better protection to chloroplast membranes and the maintenance the photosynthetic activity.

In *J. maritimus*, the changes were detected in lipidome of roots and rhizomes. This result suggested that lipids of leaves are not affected by Hg and evidence the efficiency of Hg translocation restriction and carotenoids and chlorophyll b increased in order to protect leaves from Hg toxicity. Moreover, the increase of phosphatidic acid in roots can lead to production of abscisic acid that may help in alleviate the oxidative stress. In roots, all the phospholipids species detected decreased evidencing an opposite trend of *H. portulacoides*. Phyto sterols decrease in roots of J. maritimus but not in H. portulacoides leading to alterations of membrane permeability and may explain the high ability of J. maritimus to accumulate Hg. α-tocopherol decreased in roots and rhizome evidencing a decrease of protection of membranes from peroxidation. On the other hand, in H. portulacoides levels of α-tocopherol increased evidencing an increase of protection involved in leaves membranes.

This study used some analytical tools that collectively provide a more comprehensive understanding how Hg affect salt marsh plants, namely alterations induced at physiological, biochemical and lipidomic levels. Such an integrated approach will provide information that can be used as an “early-warming” system to detect the impact of Hg and possible other metals, impact on salt marshes communities.

# Chapter 7: References


Adam, P. Saltmarshes in times of change. Environmental Conservation. 2002. 29: 39-61.

Adam, P. Saltmarsh ecology. Cambridge University Press. 1993. 461 p.

Anderson JM, Gorley RN, Clarke KR. PERMANOVA+ for PRIMER: Guide to software and statistical methods. PRIMER-E, Plymouth, UK. 2008. 214 p.

Anjum NA, Ahmad I, Válega M, Pacheco M, Figueira E, Duarte AC, et al. Salt marsh macrophyte *Phragmites australis* strategies assessment for its dominance in mercury-contaminated coastal lagoon (Ria de Aveiro, Portugal). Environ Sci Pollut Res. 2012. 19(7):2879–2888.

Anjum NA, Gill SS, Gill R, Hasanuzzaman M, Duarte AC, Pereira E, Ahmad I, Tuteja R, Tuteja N. Metal/metalloid stress tolerance in plants: role of ascorbate, its redox couple, and associated enzymes. Protoplasma. 2014. 251(6):1265–1283.

Anjum NA, Duarte AC, Pereira E, Ahmad I. Oxidative stress status, antioxidant metabolism and polypeptide patterns in *Juncus maritimus* shoots exhibiting differential mercury burdens in Ria de Aveiro coastal lagoon (Portugal). Environ Sci Pollut Res. 2014;21(10):6652–61.

Anjum NA, Israr M, Duarte AC, Pereira ME, Ahmad I. *Halimione portulacoides* (L.) physiological/biochemical characterization for its adaptive responses to environmental mercury exposure. Environ Res. 2014. 131:39–49.

Armstrong W, Justin SHFW, Beckett PM, Lythe S. Root adaptation to soil waterlogging. Aquat. Bot. 1991. 39:57–73.

Artetxe U, García-Plazaola JI, Hernandez A, Becerril JM. Low Light Grown Duckweed Plants Are More Protected against the Toxicity Induced by Zn and Cd. Plant Physiology and Biochemistry. 2002. 40(10):859–63.

ATSDR. Priority List of Hazardous Substances. 2015.

Baccouch S, Chaoui A, El Ferjani E. Nickel toxicity induces oxidative damage in *Zea mays* roots. Journal of Plant Nutrition. 2001. 24:1085–1097.

Baker AJM. Accumulators and excluders -strategies in the response of plants to heavy metals. J Plant Nutr [Internet]. 1981. 3(1–4):643–654.

Balestrasse KB, Gardey L, Gallego SM, Tomaro M.L. Response of antioxidant defence system in soybean nodules and roots subjected to cadmium stress. Aust. J. Plant Physiol. 2001. 28:497-504.

Bankaji I, Caçador I, Sleimi N. Assessing of tolerance to metallic and saline stresses in the halophyte *Suaeda fruticosa*: The indicator role of antioxidative enzymes. Ecol Indic. 2016. 64:297–308.

Barh D, Khan MS, Davies E. PlantOmics: The omics of plant science. PlantOmics Omi Plant Sci. 2015;1–825.

Bassuany FM, Hassanein R a, Baraka DM, Khalil RR. Role of stigmasterol treatment in alleviating the adverse effects of salt stress in flax plant. 2014. 10(4):1001–1020.

Bedia C, Tauler R, Jaumot J. Compression strategies for the chemometric analysis of mass spectrometry imaging data. J Chemom. 2016. 30(10):575–588.

Birben E, Sahiner UM, Sackesen C, Erzurum S, Kalayci O. Oxidative Stress and Antioxidant Defense. World Allergy Organ J. 2012. 5(1):9–19.

Blokhina O, Fagerstedt K V. Reactive oxygen species and nitric oxide in plant mitochondria: Origin and redundant regulatory systems. Physiol Plant. 2010. 138(4):447–462.

Bourdin B, Adenier H, Perrin Y. Carnitine is associated with fatty acid metabolism in plants. Plant Physiol Biochem. 2007;45(12):926–931.

Bradford MM. A rapid and Sensitive Method for the Quantitation of Microgram Quantities of Protein Utilizing the Principle of Protein-Dye Binding. Anal Biochem. 1976. 72:248-254.

Bücker-neto L, Luiza A, Paiva S, Machado RD, Arenhart RA, Margis-pinheiro M. Interactions between plant hormones and heavy metals responses. Genetics and Molecular Biology. 2017. 40(1 Suppl 1): 373–386

Cargnelutti D, Tabaldi LA, Spanevello RM, de Oliveira Jucoski G, Battisti V, Redin M, Linares CE, Dressler VL, de Moraes Flores EM, Nicoloso FT, Morsch VM, Schetinger MR. Mercury toxicity induces oxidative stress in growing cucumber seedlings. Chemosphere. 2006. 65(6):999-1006.

Carvalho AR. Mecanismos de Resposta a Mercúrio Em Plantas de Sapal [master's thesis on internet]. Aveiro (Portugal). 2009

Castro R, Pereira S, Lima A, Corticeiro S, Válega M, Pereira E, et al. Accumulation, distribution and cellular partitioning of mercury in several halophytes of a contaminated salt marsh. Chemosphere. 2009. 76(10):1348–55.

Choudhary S, Ansari MYK, Aslam R. Sequential effects of cadmium on plant growth, biochemical and cytophysiological aspects, antioxidant activity, and molecular screening of protein by SDS–PAGE in *Trigonella*. Toxicol. Environ. Chem. 2012. 94(8):1557–1570.

Clarkson TW. The three modern faces of mercury. Environ Health Perspect. 2002. 110(1):11-23.

Collin, VC, Eymery F, Genty B, Rey P, Havaux M. Vitamin E is essential for the tolerance of *Arabidopsis thaliana* to metal-induced oxidative stress. Plant Cell Environ. 2008. 31:244–257.

Coquery M, Welbourn PM. Mercury uptake from contaminated water and sediment by the rooted and submerged aquatic macrophyte *Eriocaulon septangulare*. Arch Environ Cont Toxicol. 1994. 26: 335-341

Crowder A. Acidification, metals and macrophytes. Environmental Pollution. 1991. 71, 171–203 p.

De Coen W.M., Janssen C.R. The use of biomarkers in *Daphnia magna* toxicity testing: IV. Cellular energy allocation: a new methodology to assess the energy budget of toxicant-stressed Daphnia populations. J. Aquat. Ecosyst. Stress Recovery. 1997. 6: 43 – 55.

De Coen, W.M. Energy metabolism, DNA damage and population dynamics of the waterflea *Daphnia magna* Straus under toxic stress. PhD thesis, Ghent University, Belgium. 1999. p. 545.

De Juan A, Jaumot J, Tauler R. Multivariate Curve Resolution (MCR). Solving the mixture analysis problem. Anal Methods. 2014. 6:4964-4976.

Dixit V, Pandey V, Shyam R. Differential antioxidative responses to cadmium in roots and leaves of pea (*Pisum sativum* L. cv. Azad). Journal of Experimental Botany. 2001. 52:1101–1109.

Dörmann P, Benning C. Galactolipids rule in seed plants. Trends Plant Sci. 2002. 7(3):112–118.

Dowhan W, Bogdanov M, Mileykovskaya E. Functional Roles of Lipids in Membranes. Sixth Edit. Biochemistry of Lipids, Lipoproteins and Membranes: Sixth Edition. Elsevier; 2015. 1-40 p.

Doyle MO, Otte ML. Organism – induced accumulation of iron, zinc and arsenic in wetland soils. Environmental Pollution. 1997. 96(1): 1-11.

Edwards R, Dixon DP, Walbot V. Plant glutathione S -transferases: enzymes with multiple functions in sickness and in health. Trends Biotechnol. 2000. 5(5):193–198.

Elloumi N, Ben F., Rhouma A, Ben B, Mezghani I, Boukhris M. Cadmium induced growth inhibition and alteration of biochemical parameters in almond seedlings grown in solution culture. Acta Physiol. Plant. 2007. 29:57–62.

Elloumi N, Zouari M, Chaari L, Jomni C, Marzouk B, Ben Abdallah F. Effects of cadmium on lipids of almond seedlings (*Prunus dulcis*). Bot Stud. 2014. 55(1):1–9.

Fediuc E, Lips SH, Erdei L. O-acetylserine (thiol) lyase activity in Phragmites and Typha plants under cadmium and NaCl stress conditions and the involvement of ABA in the stress response. J Plant Physiol. 2005. 162(8):865–72.

Figueira E, Freitas R, Pereira E, Duarte A. Mercury uptake and allocation in *Juncus maritimus*: implications for phytoremediation and restoration of a mercury contaminated salt marsh. J Environ Monit. 2014.14(8):2181.

Ferrat L, Bingert A, Roméo M, Gnassia-Barelli M, Pergent-Martini C. Mercury uptake and enzymatic response of *Posidonia oceanica* after an exposure to organic and inorganic forms. Environ. Toxicol. Chem. 2002a. 21(11):2365-2371.

Ferrat L, Pergent-Martini C, Romeo M, Fernandez C. Is glutathione transferase (GST) activity in *Posidonia oceanica* a stress response to mercury exposure? Bull. Mar. Sci. 2002c. 71 (3):1103-1190.

Fitzgerald EJ, Caffrey JM, Nesaratnam ST, McLoughlin P. Copper and lead concentrations in salt marsh plants on the Suir Estuary, Ireland. Environ Pollut. 2003. 123(1):67–74

Fouillen L, Colsch B, Lessire R. The lipid world concept of plant lipidomics. 1st ed. Vol. 67, Advances in Botanical Research. Elsevier Ltd.; 2013. 331-376 p.

Gajewska E, Skłodowska M. Relations between tocopherol, chlorophyll and lipid peroxides contents in shoots of Ni-treated wheat. J Plant Physiol. 2007. 164(3):364–366.

Gangwar S, Singh VP, Tripathi DK, Chauhan DK, Prasad SM, Maurya JN. Plant Responses to Metal Stress. Second Edi. Vol. 2, Emerging Technologies and Management of Crop Stress Tolerance. Elsevier Inc.; 2014. 215-248 p.

Godbold DL, Hiittermann A. Inhibition of photosynthesis and transpiration - mercury-induced root damage in spruce seedling. Physiologia Plantarum. 1988. 74:270–275.

Gorrochategui E, Jaumot J, Lacorte S, Tauler R. Data analysis strategies for targeted and untargeted LC-MS metabolomic studies: Overview and workflow. TrAC - Trends Anal Chem. 2016. 82:425–442.

Grigore, M.; Ivanescu, L.; Toma, C. Halophytes: An Integrative Anatomical Study. 1ed. Switzerland. Springer International Publishing. 2014

Habig WH, Pabst MJ, Jakoby WB. Glutathione S-transferases the first enzymatic step in mercapturic acid formation. Journal of Biological Chemistry. 1974. 249:7130-7139.

Halliwell, B.; Gutteridge, J. Free Radicals in Biology and Medicine, 4th ed.; Oxford University Press: Oxford, UK, 2007.

Hameed A, Rasool S, Azooz MM, Hossain MA, Ahanger MA, Ahmad P. Heavy Metal Stress. Plant Metal Interaction. Elsevier Inc.; 2016. 557-583 p.

Hasanuzzaman M, Nahar K, Fujita M. Role of Tocopherol (Vitamin E) in Plants: Abiotic Stress Tolerance and Beyond. Second Edi. Vol. 2, Emerging Technologies and Management of Crop Stress Tolerance. Elsevier Inc.; 2014. 267-289 p.

Hölzl G, Dörmann P. Structure and function of glycoglycerolipids in plants and bacteria. Prog Lipid Res. 2007. 46(5):225–243

Hou Q, Ufer G, Bartels D. Lipid signalling in plant responses to abiotic stress. Plant, Cell Environ. 2016. 39(5):1029–48.

Hou W, Chen X, Song G, Wang Q, Chi Chang C. Effects of copper and cadmium on heavy metal polluted waterbody restoration by duckweed (*Lemna minor*). Plant Physiol Biochem. 2007. 45(1):62–69.

Huang G-Y, Wang Y-S, Sun C-C, Dong J-D, Sun Z-X. The effect of multiple heavy metals on ascorbate, glutathione and related enzymes in two mangrove plant seedlings (*Kandelia candel* and *Bruguiera gymnorrhiza*). Oceanol Hydrobiol Stud. 2010. 39(1):11–25.

Hughes R.G. Biological and Physical Processes That Affect Saltmarsh Erosion and Saltmarsh Restoration: Development of Hypotheses. In: Reise K. (eds) Ecological Comparisons of Sedimentary Shores. Ecological Studies (Analysis and Synthesis. Springer, Berlin, Heidelberg, 2001. 151:173–192.

Hummel J, Segu S, Li Y, Irgang S, Jueppner J, Giavalisco P. Ultra Performance Liquid Chromatography and High Resolution Mass Spectrometry for the Analysis of Plant Lipids. Front Plant Sci. 2011. 2:1–17.

Ingle RA, Smith JAC, Sweetlove LJ. Responses to nickel in the proteome of the hyperaccumulator plant *Alyssum lesbiacum*. BioMetals. 2005. 18(6):627–641.

Jorge TF, Rodrigues A, Caldana C, Schmidt R, Dongen JT Van, Thomas-oates J, António C. Mass spectrometry-based plant metabolomics: metabolite responses to abiotic stress. Mass Spectrom Rev. 2016. 35(5):620-49.

Kalaikandhan R, Vijayarengan P, Sivasankar R, Mathivanan S. The pigment content of *Sesuvium portulacastrum* L. under copper and zinc stress. Department of Botany, Annamalai University, Annamalainagar. Int.J.Curr.Microbiol.App.Sci. 2014. 3(3):1056-1066.

Kapoor D, Rattan A, Gautam V, Kapoor N, Bharadwaj R. 24-Epibrassinolide mediated photosynthetic pigments and antioxidative defense systems of radish seedling under cadmium and mercury stress. J. Stress Physiol. Biochem. 2014. 10:110–121.

Kiekens, L. Zinc. In: Alloway, B.J., Ed., Heavy Metals in Soils, 2nd Edition, Blackie Academic and Professional, London. 1995. 284-305 p.

Kim YH, Khan AL, Kim DH, Lee SY, Kim KM, Waqas M, Jung HY, Shin JH, Kim JG, Lee IJ. Silicon mitigates heavy metal stress by regulating P-type heavy metal ATPases, *Oryza sativa* low silicon genes, and endogenous phytohormones. BMC Plant Biol. 2014. 14:13.

King FD, Packard TT. Respiration and the activity of the respiratory electron transport system in marine zooplankton. Limnol Oceanogr. 1975. 20:849–854

Kovinich N, Kayanja G, Chanoca A, Otegui MS, Grotewold E. Abiotic stresses induce different localizations of anthocyanins in Arabidopsis. Plant Signal Behav. 2015. 10(7):e1027850.

Kumar A, Prasad MN V, Sytar O. Lead toxicity, defense strategies and associated indicative biomarkers in *Talinum triangulare* grown hydroponically. Chemosphere. 2012. 89(9):1056-1065.

Lagoons, 2013. Results of the problem based science analysis: The Ria de Aveiro Lagoon. LAGOONS Report D3.2.1. 50 p.

Lasat M. Phytoextraction of toxic metals: a review of biological mechanisms. JEnviron Qual. 2002. 31(1):109-120.

Leita L, De Nobili M, Cesco S, Mondini C. Analysis of intercellular cadmium forms in roots and leaves of bush bean. J Plant Nutr. 1996. 19(3–4):527-533.

Lenka M, Panda KK, Panda BB. Monitoring and assessment of mercury pollution in the vicinity of a chloralkali plant. IV. Bioconcentration of mercury in in situ aquatic and terrestrial plants at Ganjam, India. Arch Environ Cont Toxicol. 1992. 22(2):195-202.

Li Q-H, Yang H-Q. Cryptochrome Signaling in Plants†. Photochem Photobiol. 2007. 83(1):94–101.

Lichtenthaler HK. Chlorophylls Carotenoids. Chlorophylls Carotenoids Pigment Photosynth Biomembr. 1987. 148:350–82.

Lillebø A, Sousa A, Queiroga H, Soares J, Aleixo A. Results of the problem based science analysis: The Ria de Aveiro Lagoon. 2013.

Liu H, Liu B, Zhao C, Pepper M, Lin C. The action mechanisms of plant cryptochromes. Trends Plant Sci. 2012. 16(12):684–691.

Lodenius M. Mercury. in terrestrial ecosystems: A Review; in Watras, C.J., and Huckabee, J.W., eds., Mercury pollution: integration and synthesis. Lewis, Ann Arbor, MI, 1995. 343-354 p.

Lozano-Rodriguez E, Luguera M, Lucena JJ, Carpena-Ruiz R.O. Evaluation of two different acid digestion methods in closed systems of trace element determinations in plant. Quim Anal. 1995. 14:27-30.

Lushchak VI, Semchuk NM. Tocopherol biosynthesis: Chemistry, regulation and effects of environmental factors. Acta Physiol Plant. 2012. 34(5):1607–1628.

Ly A, Schöne C, Becker M, Rattke J, Meding S, Aichler M, et al. High-resolution MALDI mass spectrometric imaging of lipids in the mammalian retina. Histochem Cell Biol. 2015. 143(5):453–462

Ma F, Cheng L. Exposure of the shaded side of apple fruit to full sun leads to up-regulation of both the xanthophyll cycle and the ascorbate-glutathione cycle. Plant Sci. 2004. 166(6):1479–1486.

Maciel E, Leal MC, Lillebø AI, Domingues P, Domingues MR, Calado R. Bioprospecting of marine macrophytes using MS-based lipidomics as a new approach. Mar Drugs. 2016. 14(3):1–28.

Marques AS, Bedia C, Lima KMG, Tauler R. Assessment of the effects of As(III) treatment on cyanobacteria lipidomic profiles by LC-MS and MCR-ALS. Anal Bioanal Chem. 2016. 408(21):5829–5841.

Marrs KA. The Functions and Regulation of Glutathione S-Transferases in Plants. Annu Rev Plant Physiol Plant Mol Biol. 1996;47(1):127–158.

Marschner, H. Mineral nutrition of higher plants, 2nd edition. New York. Academic Press. 1995.

Martret BL, Poage M, Shiel K, Nugent GD, Dix PJ. Tobacco chloroplast transformants expressing genes encoding dehydroascorbate reductase, glutathione reductase, and glutathione-S-transferase, exhibit altered anti-oxidant metabolism and improved abiotic stress tolerance. Plant Biotechnol. 2001. 9:661-673.

Mason RP, Fitzgerald WF. The distribution and biogeochemical cycling of mercury in the ecuatorial Pacific Ocean. Deep Sea Res Part I. 1993. 40(40):1897–924.

Matthews DJ, Moran BM, McCabe PF, Otte ML. Zinc tolerance, uptake, accumulation and distribution in plants and protoplasts of five European populations of the wetland grass *Glyceria fluitans*. Aquat Bot. 2004. 80(1):39–52.

McKenney Jr., C.L.; (1998); Physiological dysfunction in estuarine mysids and larval decapods with chronic pesticide exposure. In: Wells, P.G., Blaise, C. (Eds.), Microscale Testing in Aquatic Toxicology: Advances, Techniques, and Practice. CRC Press, Boca Raton, FL. 1998. 465 – 476 p.

Meharg AA, Wood M, Ripton A. Integrated tolerance mechanisms: constitutive and adaptive plant responses to elevated metal concentrations in the environment. Plant, Cell Environ. 1990. 17(9):989–993.

Merrill AH, Sullards MC, Allegood JC, Kelly S, Wang E. Sphingolipidomics: High-throughput, structure-specific, and quantitative analysis of sphingolipids by liquid chromatography tandem mass spectrometry. Methods. 2005. 36(2):207-224

Mitsch, W. J. & J. G. Gosselink, 2000. Wetlands. Wiley, New York

Møller IM. Plant mitochondria and oxidative stress: Electron Transport, NADPH Turnover, and Metabolism of Reactive Oxygen Species. Annual Review of Plant Physiology and Plant Molecular Biology. 2001. 52(1):561–591

Moons A. Osgstu3 and osgstu4, encoding tau class glutathione S-transferase, are heavy metal- and hypoxic stress-induced and differentially salt stress-responsive in rice roots. FEBS Letters. 2003. 553:427–432.

Moons A. Regulatory and Functional Interactions of Plant Growth Regulators and Plant Glutathione S-Transferases (GSTs). Vitam Horm. 2005. 72(5):155–202.

Moreno FN, Anderson CWN, Stewart RB, Robinson BH. Phytofiltration of mercury-contaminated water: Volatilisation and plant-accumulation aspects. Environmental and Experimental Botany. 2008. 62:78-85.

Munné-Bosch S. The role of α-tocopherol in plant stress tolerance. J Plant Physiol. 2005. 162(7):743–748.

Munzuro Ö, Fikriye KZ and Yahyagil Z. The abscisic acid levels of wheat (*Triticum aestivum* L. cv. Çakmak 79) seeds that were germinated under heavy metal ($Hg^{++}$,$Cd^{++}$,$Cu^{++}$) stress. GUJSci. 2008. 21:1-7.

Noctor G, Foyer CH. Ascorbate and Glutathione: Keeping Active Oxygen Under Control. Annu Rev Plant Physiol Plant Mol Biol. 1998. 49(1):249–279.

Olkhovych O, Volkogon M, Taran N, Batsmanova L, Kravchenko I. The Effect of Copper And Zinc Nanoparticles on the Growth Parameters, Contents of Ascorbic Acid, and Qualitative Composition of Amino Acids and Acylcarnitines in *Pistia stratiotes* L. (Araceae). Nanoscale Res Lett. 2016. 11(1):218.

Otte M. L. Contamination of coastal wetlands with heavy metals: factors affecting uptake of heavy metals by salt marsh plants. Cap 12. In: Rozema L.; Verkleij J.A. (eds). Ecological Responses to Environmental Stress; Kluwer Academic Publishers. 1991. 126-133p.

Paglia DE, Valentine WN. Studies on the quantitative and qualitative characterization of glutathion proxidase. J Lab Med. 1987. 70:158-165

Pamplona R. Membrane phospholipids, lipoxidative damage and molecular integrity: A causal role in aging and longevity. Biochim Biophys Acta - Bioenerg. 2008. 1777(10):1249-1262.

Parastar H, Tauler R. Multivariate curve resolution of hyphenated and multidimensional chromatographic measurements: A new insight to address current chromatographic challenges. Anal Chem. 2014;86(1):286–97.

Patra M. and Sharma A. Mercury toxicity in plants. Bot Rev. 2000. 66: 379–422.

Pedro, JG. O papel da vegetação na formação dos sistemas lagunares da Ria Formosa. *Os Sistemas Lagunares do Algarve* – Textos e resumos do seminário comemorativo do dia mundial do ambiente, 5- 7 de Junho de 1985. Faro: Universidade do Algarve. 1986. 61-68 p.

Piironen V, Lindsay DG, Miettinen TA, Toivo J, Lampi AM. Plant sterols: Biosynthesis, biological function and their importance to human nutrition. J Sci Food Agric. 2000. 80(7):939–966.

Pizzimenti S, Ciamporcero E, Daga M, Pettazzoni P, Arcaro A, Cetrangolo G, Minelli R, Dianzani C, Lepore A, Gentile F, Barrera G. Interaction of aldehydes derived from lipid peroxidation and membrane proteins. Front Physiol. 2013. 4;4:242

Prasad SM, Singh J.B, Rai LC, Kumar HD. Metal-Induced Inhibition of Photosynthetic Electron Transport Chain of the Cyanobacterium Nostoc Muscorum. FEMS Microbiol Lett. 1991. 82:95–100.

Prasad M.N. and Hagemeyer J.Heavy metal stress in plants (eds M.N. Prasad & J. Hagemeyer). Springer, Berlin, Germany. 1999.

Ranvier S, Gnassia-Barelli M, Pergent G, Capiomont A, Roméo M. The effect of mercury on glutathione S-transferase in the marine phanerogam *Posidonia oceanica*. Bot. Mar. 2000. 43:161-168.

Raskin, I. Plant genetic engineering may help with environmental cleanup. Proc. Natl. Acad. Sci. USA. 1996. 93: 3164-3166 p.

Rauser WE. Structure and function of metal chelators produced by plants. Cell Biochem Biophys. 1999. 31(1):19–48.

Reboreda R, Caçador I. Halophyte vegetation influences in salt marsh retention capacity for heavy metals. Environmental Pollution. 2007. 146:147–154.

Regoli F, Giuliani ME. Oxidative pathways of chemical toxicity and oxidative stress biomarkers in marine organisms. Vol. 93, Marine Environmental Research. Elsevier Ltd; 2014. 106-117 p.

Ribeyre F, Boudou A. Experimental study of inorganic and methylmercury bioaccumulation by four species of freshwater rooted macrophytes from water and sediment contamination sources. Ecotoxicol Environ Saf. 1994. 28:270-286.

Rose, F. Colour Identification Guide to the Grasses, Sedges, Rushes and Ferns of the British Isles and North Western Europe. London. Viking. 1989.

Rozema J, Otte ML, Broekman RA, Kamber G, Punte H. The response of *Spartina anglica* to heavy metal pollution. In: Gray AJ (ed.), *Spartina anglica*. HMSO, London. 1990. 39-47 p.

Ruckebusch C, Blanchet L. Multivariate curve resolution: A review of advanced and tailored applications and challenges. Anal Chim Acta. 2013. 765:28–36.

Ruelland E, Kravets V, Derevyanchuk M, Martinec J, Zachowski A, Pokotylo I. Role of phospholipid signalling in plant environmental responses. Environ Exp Bot. 2014. 114:129–143.

Santos MAZ dos, Miguel, Roehrs CMP de P, Freitag RA, De and AV, Bairros. Analysis of Phytosterols in Plants and Derived Products by Gas Chromatography – A Short Critical Review. Austin Publ Gr. 2014. 1(5):1–4.

Santos D, Duarte B, Caçador I. Biochemical and photochemical feedbacks of acute Cd toxicity in *Juncus acutus* seedlings: The role of non-functional Cd-chlorophylls. Estuar Coast Shelf Sci. 2015. 167:228–239.

Schuler I, Milon A, Nakatani Y, Ourisson G, Albrecht AM, Benveniste P, Hartman MA. Differential effects of plant sterols on water permeability and on acyl chain ordering of soybean phosphatidylcholine bilayers. Proc Natl Acad Sci U S A. 1991. 88:6926–6930.

Sengar RK, Gautam M, Grag SK, Sengar K, Chaudhary R. Lead stress effects on physiobiochemical activities of higher plants. Rev Environ Contam Toxicol. 2008. 196: 73–93.

Sethi S, Brietzke E. Recent advances in lipidomics: Analytical and clinical perspectives. Prostaglandins Other Lipid Mediat. 2017. 128–129:8–16.

Shanker AK, Djanaguiraman M, Sudhagar R, Chandrashekar CN, Pathmanabhan G. 2004. Differential antioxidative response of ascorbate glutathione pathway enzymes and metabolites in chromium speciation stress in green gram roots. Plant Sci. 2004. 166:1035-1043.

Sharma P, Jha AB, Dubey RS, Pessarakli M. Reactive Oxygen Species, Oxidative Damage, and Antioxidative Defense Mechanism in Plants under Stressful Conditions. J Bot. 2012. 2012:1–26.

Shimojima M, Ohta H. Critical regulation of galactolipid synthesis controls membrane differentiation and remodeling in distinct plant organs and following environmental changes. Prog Lipid Res. 2011. 50(3):258–266.

Siedlecka A, Krupa Z. Interaction between cadmium and iron and its effects on photosynthetic capacity of primary leaves of Phaseolus vulgaris. Plant Physiol. Biochem. 1996. 34:833–841.

Silva, M. G. Vegetação do Sapal – Parque Natural da Ria Formosa (3ª Edição). Eurosite – Programa de Germinação dos Sítios Naturais Europeus. 1993.

Silva M.H.A. Aspectos morfológicos e ecofisiológicos de algumas halófitas do sapal da Ria de Aveiro. Universidade de Aveiro. 2000. 191 p.

Silva V.F. Response of salt marsh plants to heavy metals in the Tagus estuary [master's thesis on internet]. Aveiro (Portugal). 2010.

Singh BR, McLaughlin MJ. (1999); Cadmium in soils and plants: Summary and research perspectives. In: McLaughlin MJ, Singh BR (eds) Cadmium in soils and plants. Kluwer Academic Publ, Boston. 1999. 257-267 p.

Singh VP, Srivastava PK, Prasad SM. Impact of low and high fluence rates of UV-B radiation on growth and oxidative stress in *Phormidium foveolarum* and N*ostoc muscorum* under copper toxicity: Differential display of antioxidants system. Acta Physiol Plant. 2012. 34(6):2225–2239.

Singh R, Srivastava PK, Singh VP, Dubey G, Prasad SM. Light intensity determines the extent of mercury toxicity in the cyanobacterium *Nostoc muscorum*. Acta Physiol Plant. 2012. 34(3):1119–1131.

Singh S, Parihar P, Singh R, Singh VP, Prasad SM. Heavy Metal Tolerance in Plants: Role of Transcriptomics, Proteomics, Metabolomics, and Ionomics. Front Plant Sci. 2016. 8;6:1143

Sixty-fifth JHS. Review article number 81 steryl fatty acyl esters in plants. 1993. 34(1):17–29.

Smith CA, Want EJ, O'Maille G, Abagyan R, Siuzdak G, CA Smith, J Elizabeth, G O'Maille, Abagyan R, Siuzdak G. XCMS: processing mass spectrometry data for metabolite profiling using Nonlinear Peak Alignment,Matching,and Identification. ACS Publ. 2006. 78(3):779–787.

Stolt R1, Torgrip RJ, Lindberg J, Csenki L, Kolmert J, Schuppe-Koistinen I, Jacobsson SP. Second-order peak detection for multicomponent high-resolution LC/MS data. Anal Chem. 2006. 78(4):975–983.

Sud M, Fahy E, Cotter D, Brown A, Dennis EA, Glass CK, et al. LMSD: LIPID MAPS structure database. Nucleic Acids Res. 2007. 35(SUPPL. 1):527–532.

Tauler RR. Multivariate curve resolution applied to secon order data. Chemom Intell Lab Syst. 1995. 30(1):133–146.

Tenenboim H, Burgos A, Willmitzer L, Brotman Y. Using lipidomics for expanding the knowledge on lipid metabolism in plants. Biochimie. 2016a. 130:91–96.

Tenenboim H, Burgos A, Willmitzer L, Brotman Y. Using lipidomics for expanding the knowledge on lipid metabolism in plants. Biochimie. 2016b. 130:91–96.

Tewari RK, Kumar P, Sharma PN. Antioxidant responses to enhanced generation of superoxide anion radical and hydrogen peroxide in the copper-stressed mulberry plants. Planta. 2006. 223(6):1145–1153.

Turunen M, Olsson J, Dallner G. Metabolism and function of coenzyme Q. Biochim Biophys Acta - Biomembr. 2004. 1660(1–2):171–199.

United States Environmental Protection Agency (USEPA. Electrokinetic and phytoremediation in situ treatment of metal-contaminated soil: State-of-the-Practice. Draft for final review; EPA/542/R-00/XXX. US Environmental Protection Agency, Office of Solid Waste and Emergency Responce Technology Innovation Office, Washington DC. 2000.

Válega M, Lillebø AI, Pereira ME, Duarte AC, Pardal MA. Long-term effects of mercury in a salt marsh: Hysteresis in the distribution of vegetation following recovery from contamination. Chemosphere. 2008. 71(4):765–772.

Vardhini, Bojjam Vidya. 2015. "Brassinosteroids Are Potential Ameliorators of Heavy Metal Stresses in Plants." Plant Metal Interaction: Emerging Remediation Techniques (1970):209–37.

Verkleij JA, Schat H. Mechanisms of metal tolerance in higher plants. In: Shaw, AJ (ed.). Heavy Metal Tolerance in Plants: Evolutionary Aspects. 1989. 179-194 p.

Waisel AY, Liphschitz N, Kuller Z. Patterns of Water Movement in Trees and Shrubs. Ecological Society of America. 1972. 53 (3):520-523.

Wagner GJ. Accumulation of Cadmium in Crop Plants And Its Consequences to Human Health. Vol. 51, Advances in Agronomy. Elsevier Masson SAS; 1993. 173-212 p.

Wewer V, Dombrink I, vom Dorp K, Dormann P. Quantification of sterol lipids in plants by quadrupole time-of-flight mass spectrometry. J Lipid Res [Internet]. 2011. 52(5):1039–1054.

Widdows J, Donkin P. Mussels and environmental contaminants: bioaccumulation and physiological aspects. In: Gosling, E.M. (Ed.), The Mussel Mytilus. Elsevier, Amsterdam. 1992. 383 – 424 p.

Williams TP, Bubb JM, Lester JN. Metal Accumulation Within Salt Marsh Environments : A Review. Marine Pollution Bulletin. 1994. 28(5):277–290.

Windham L, Weis JS, Weis P. Uptake and distribution of metals in two dominant salt marsh macrophytes, *Spartina alterniflora* (cordgrass) and *Phragmites australis* (common reed). Estuar Coast Shelf Sci. 2003. 56(1):63–72.

Windham, L., J. S. Weis, and P. Weis. 2003. "Uptake and Distribution of Metals in Two Dominant Salt Marsh Macrophytes, Spartina Alterniflora (Cordgrass) and Phragmites Australis (Common Reed)." Estuarine, Coastal and Shelf Science 56(1):63–72.

Xia J, Sinelnikov IV, Han B, Wishart DS. MetaboAnalyst 3.0—making metabolomics more meaningful. Nucleic Acids Res. 2015. 1;43(W1):W251-7.

Xu C, Shanklin J. Triacylglycerol Metabolism, Function, and Accumulation in Plant Vegetative Tissues. Annu Rev Plant Biol. 2016. 67(1):179–206.

Yusuf MA, Kumar D, Rajwanshi R, Strasser RJ, Tsimilli-Michael M, Govindjee, Sarin NB. Overexpression of gamma-tocopherol methyl transferase gene in transgenic Brassica juncea plants alleviates abiotic stress: Physiological and chlorophyll a fluorescence measurements. Biochim Biophys Acta - Bioenerg. 2010. 1797(8):1428–1438.

Zhang W-H, Tyerman SD. Inhibition of Water Channels by $HgCl_2$ in Intact Wheat Root Cells. Plant Physiol. 1999. 120(3):849–58.

Zhang, Wen-Hao and Stephen D. Tyerman. 1999. "Inhibition of Water Channels by HgCl2 in Intact Wheat Root Cells." Plant Physiology 120(3):849–58.

Zhang, Y. Ascorbic Acid in Plants. Springer-Verlag. 1 ed. New York. 2013.

Zhao YY, Wu SP, Liu S, Zhang Y, Lin RC. Ultra-performance liquid chromatography-mass spectrometry as a sensitive and powerful technology in lipidomic applications. Chem Biol Interact [Internet]. 2014. 220:181–92.

Zhou ZS, Wang SJ, Yang ZM. Biological detection and analysis of mercury toxicity to alfalfa (*Medicago sativa*) plants; Chemosphere. 2008. 70:1500–1509.

Zornoza P, Vázquez S, Esteban E, Fernández-Pascual M, Carpena R. Cadmium-stress in nodulated white lupin: strategies to avoid toxicity. Plant Physiology and Biochemistry. 2002. 40. 1003–1009 p.

# Chapter 8: Annexes

## 8.1 *Halimione portulacoides*

**Table 8.1**- List of the *m/z* values that presented significant changes (p-value <0.05) between less contaminated and more contaminated sites by mercury in leaves of *Halimione portulacoides*. The absolute concentrations of lipids were calculated considering the area of the corresponding internal standards added to the extraction. The identified compound corresponds to the lipid molecule with the minimum mass error value with respect to the measured *m/z*, considering all the possible adducts in the positive and negative ionization mode. The list only contains the compounds with a Benjamini–Hochberg's corrected *p-value* <0.05. LPC: lysophosphatidyl-choline; LysoPI: Lysophosphatidyl-inositol; FA: fatty-acid; SDQG: Sulfoquinovosyl-Diacyl-Glycerol; PC: Phosphatidyl-Choline; PE: Phosphatidyl-Ethanolamine; MGDG: Mono-Galactosyl-Diacyl-Glycerol; DGDG: Di-Galactosyl-Diacyl-Glycerol; DG: Diacylglycerol; TG: Triacylglycerol and CoQ9: Ubiquinone.

| mzmed | rtmed | name | code | adduct | *m/z (adduct)* | *monoisotopic_mass* | delta | ppm error | fold change | p-value |
|---|---|---|---|---|---|---|---|---|---|---|
| 567.418 | 3.3 | LPC (20:1) | HMDB10391 | [M + NH4+]+ | 567.413263 | 549.379439663 | 0.01 | 9 | 1.60 | 0.004 |
| 607.291 | 3.2 | LPI(17:1) | lipidmaps | [M + Na+]+ | 607.2877 | | 0.01 | 10 | 4.06 | 0.006 |
| 584.421 | 3.5 | FA(32:1) | lipidmaps | [M + NH4+]+ | 584.4157 | | 0.00 | 8 | 1.52 | 0.006 |
| 981.579 | 5.1 | SQDG (47:11) | lipids maps | [M-H]- | 981.5767 | 980.5767 | 0.00 | 2 | 0.79 | 0.048 |
| 730.544 | 8.5 | PC (32:2) | HMDB08098 | [M + H+]+ | 730.538131 | 729.530854925 | 0.01 | 9 | 0.37 | 0.009 |
| 758.576 | 7.7 | PC (34:2) | HMDB08296 | [M + H+]+ | 758.569431 | 757.562155053 | 0.01 | 9 | 0.63 | 0.039 |
| 774.599 | 9.4 | PC (35:1) | HMDB07945 | [M + H+]+ | 774.600731 | 773.593455181 | 0.00 | 2 | 0.22 | 0.018 |
| 772.584 | 8.5 | PC (35:2) | HMDB07946 | [M + H+]+ | 772.585081 | 771.577805117 | 0.00 | 2 | 1.22 | 0.037 |
| 814.638 | 9.3 | PC (38:2) | HMDB09554 | [M+NH4+]+ | 815.627278 | 797.593455181 | 0.01 | 15 | 0.22 | 0.018 |
| 743.574 | 5.5 | PE (36:3) | HMDB11350 | [M + NH4+]+ | 743.569763 | 725.535940303 | 0.00 | 6 | 0.60 | 0.043 |
| 772.588 | 8.5 | PE (38:2) | HMDB09550 | [M + H+]+ | 772.585081 | 771.577805117 | 0.00 | 4 | 0.30 | 0.001 |
| 774.613 | 9.4 | MGDG 34:1 | lipid maps | [M + NH4+]+ | 774.6090 | | 0.00 | 5 | 0.22 | 0.018 |
| 772.599 | 8.5 | MGDG 34:2 | lipid maps | [M + NH4+]+ | 772.5933 | | 0.01 | 7 | 1.31 | 0.015 |
| 956.632 | 5.0 | DGDG 36:5 | lipid maps | [M + NH4+]+ | 956.6305 | | 0.00 | 2 | 0.61 | 0.042 |
| 634.542 | 9.3 | DG 36:4 | HMDB56210 | [M + NH4+]+ | 634.540498 | 616.506675286 | 0.00 | 2 | 1.54 | 0.031 |
| 1024.842 | 13.9 | TG (42:6) | HMDB50843 | [M + NH4+]+ | 1024.832764 | 1006.798941124 | 0.01 | 9 | 0.60 | 0.037 |
| 929.506 | 10.5 | Chlorophyll b | HMDB31146 | M+Na | 929..503796 | 906.51457789 | 0.00 | 2 | 0.38 | 0.006 |
| 812.657 | 15.5 | CoQ9 | HMDB06707 | [M + NH4+]+ | 812.655134 | 794.621311112 | 0.00 | 3 | 0.72 | 0.048 |

| | | | | | | | | | | |
|---|---|---|---|---|---|---|---|---|---|---|
| 585.427 | 4.2 | Cryptochrome | HMDB29857 | [M + H+]+ | 585.430222 | 584.422945658 | 0.00 | 5 | 1.37 | 0.025 |
| 448.416 | 5.3 | alpha-tocopherol | HMDB01893 | [M + NH4+]+ | 448.414904 | 430.381080844 | 0.00 | 2 | 1.57 | 0.024 |
| 748.617 | 13.3 | Ubiquinol 8 | HMDB01060 | [M+H+]+ | 748.623834 | 730.590010984 | 0.01 | 9 | 0.54 | 0.044 |

**Table 8.2:** List of the *m/z* values that presented significant changes (p-value <0.05) between less contaminated and more contaminated sites by mercury in stem of *Halimione portulacoides*. The absolute concentrations of lipids were calculated considering the area of the corresponding internal standards added to the extraction. The identified compound corresponds to the lipid molecule with the minimum mass error value with respect to the measured *m/z*, considering all the possible adducts in the positive and negative ionization mode. The list only contains the compounds with a Benjamini–Hochberg's corrected *p-value* <0.05. SDQG: Sulfoquinovosyl-Diacyl-Glycerol; PC: Phosphatidyl-Choline; PE: Phosphatidyl-Ethanolamine; DGDG: Di-Galactosyl-Diacyl-Glycerol; DG: Diacylglycerol; Cer: Ceramide.

| **mzmed** | **rtmed** | **name** | **code** | **adduct** | ***m/z (adduct)*** | ***monoisotopic_mass*** | **delta** | **ppm error** | **fold change** | **p-value** |
|---|---|---|---|---|---|---|---|---|---|---|
| 791.494 | 5.1 | SQDG (32:1) | Lipids maps | [M-H]- | 791.4985 | 790.49056 | 0.00 | 5 | 4.49 | 0.045 |
| 728.525 | 7.3 | PC (32:3) | HMDB08196 | [M + H+]+ | 728.522481 | 727.515204861 | 0.00 | 3 | 0.31 | 0.049 |
| 772.584 | 8.5 | PC (35:2) | HMDB07946 | [M + H+]+ | 772.585081 | 771.577805117 | 0.00 | 2 | 0.16 | 0.018 |
| 772.591 | 8.6 | PE (38:2) | HMDB09764 | [M + H+]+ | 772.585081 | 771.577805117 | 0.01 | 8 | 0.37 | 0.043 |
| 930.616 | 5.3 | DGDG 34:4 | LIPID MAPS | [M + NH4+]+ | 930.6148 | 912.58 | 0.00 | 1 | 3.53 | 0.032 |
| 928.600 | 4.3 | DGDG 34:5 | LIPID MAPS | [M + NH4+]+ | 928.5992 | 910.5644 | 0.00 | 1 | 5.03 | 0.045 |
| 926.585 | 4.3 | DGDG 34:6 | LIPID MAPS | [M + NH4+]+ | 926.5835 | 908.5487 | 0.00 | 2 | 3.71 | 0.037 |
| 615.500 | 9.8 | DG 36:5 | HMDB55974 | [M + H+]+ | 615.498301 | 614.491025222 | 0.00 | 2 | 1.35 | 0.037 |
| 622.614 | 12.1 | Cer (22:0) | HMDB11766 | [M + H+]+ | 622.613271 | 621.605995399 | 0.00 | 1 | 1.39 | 0.028 |
| 694.650 | 17.8 | Sitosteryl ester (18:2) | HMDB06734 | [M + NH4+]+ | 694.649655 | 676.615831804 | 0.00 | 0 | 1.31 | 0.046 |

**Table 8.3:** List of the *m/z* values that presented significant changes (p-value <0.05) between less contaminated and more contaminated sites by mercury in roots of *Halimione portulacoides*. The absolute concentrations of lipids were calculated considering the area of the corresponding internal standards added to the extraction. The identified compound corresponds to the lipid molecule with the minimum mass error value with respect to the measured *m/z*, considering all the possible adducts in the positive and negative ionization mode. The list only contains the compounds with a Benjamini–Hochberg's corrected *p-value* <0.05. LysoPC: lysophosphatidyl-choline; PC: Phosphatidyl-Choline; PE: Phosphatidyl-Ethanolamine; PG: Phosphatidyl-Glycerol; PI: Phosphatidyl-Inositol; MGDG: Mono-Galactosyl-Diacyl-Glycerol; DG: Diacylglycerol.

| mzmed | rtmed | name | code | adduct | *m/z (adduct)* | *monoisotopic_mass* | delta | ppm error | fold change | p-value |
|---|---|---|---|---|---|---|---|---|---|---|
| 522.356 | 2.3 | LPC (18:1) | HMDB02815 | [M + H+]+ | 522.355416 | 521.348139535 | 0.00 | 1.12 | 0.40 | 0.048 |
| 728.525 | 7.3 | PC (32:3) | HMDB08196 | [M + H+]+ | 728.522481 | 727.515204861 | 0.00 | 2.81 | 0.52 | 0.010 |
| 742.537 | 8.1 | PC (33:3) | HMDB08198 | [M + H+]+ | 742.538131 | 741.530854925 | 0.00 | 1.93 | 0.71 | 0.035 |
| 760.588 | 8.7 | PC (34:1) | HMDB07972 | [M + H+]+ | 760.585081 | 759.577805117 | 0.00 | 4.12 | 0.59 | 0.002 |
| 774.599 | 9.4 | PC (35:1) | HMD07945B | [M + H+]+ | 774.600731 | 773.593455181 | 0.00 | 2.11 | 0.43 | 0.004 |
| 786.603 | 9.2 | PC (36:2) | HMDB08590 | [M + H+]+ | 786.600731 | 785.593455181 | 0.00 | 3.27 | 0.43 | 0.002 |
| 784.589 | 8.2 | PC (36:3) | HMDB08591 | [M + H+]+ | 784.585081 | 783.577805117 | 0.00 | 4.78 | 0.68 | 0.038 |
| 692.525 | 8.1 | PE (32:0) | HMDB08986 | [M + H+]+ | 692.522481 | 691.515205345 | 0.00 | 4.00 | 0.56 | 0.024 |
| 688.494 | 6.1 | PE (32:2) | HMDB08829 | [M + H+]+ | 688.491181 | 687.483904733 | 0.00 | 3.94 | 0.67 | 0.019 |
| 710.471 | 7.6 | PE 34:5 | HMDB08964 | [M + H+]+ | 710.475531 | 709.468254669 | 0.00 | 6.38 | 0.07 | 0.047 |
| 719.483 | 8.0 | PG (32:2) | HMDB10586 | [M-H]- | 719.485761 | 718.478485484 | 0.00 | 4 | 0.51 | 0.04 |
| 855.503 | 6.3 | PI 36:6 | HMDB06736 | [M + H+]+ | 855.5018 | 854.4945 | 0.00 | 1.64 | 0.39 | 0.025 |
| 774.613 | 9.4 | MGDG 34:1 | LIPID MAPS | [M + NH4+]+ | 774.609 | 756.5742 | 0.00 | 4.52 | 0.43 | 0.004 |
| 704.526 | 7.9 | DG(20:5 | HMDB07585 | [M + NH4+]+ | 704.524848 | 686.491025222 | 0.00 | 1.80 | 0.51 | 0.049 |
| 730.540 | 8.5 | DG(22:6) | HMDB07788 | [M + NH4+]+ | 730.540498 | 712.506675286 | 0.00 | 0.07 | 0.53 | 0.012 |

### 8.2 *Juncus maritimus*

**Table 8.4**- List of the *m/z* values that presented significant changes (p-value <0.05) between less contaminated and more contaminated sites by mercury in rhizome of *Juncus maritimus*. The absolute concentrations of lipids were calculated considering the area of the corresponding internal standards added to the extraction. The identified compound corresponds to the lipid molecule with the minimum mass error value with respect to the measured *m/z*, considering all the possible adducts in the positive and negative ionization mode. The list only contains the compounds with a Benjamini–Hochberg's corrected *p-value* <0.05. MG: monoacylglycerol; PC: Phosphatidyl-Choline; DGDG: Di-Galactosyl-Diacyl-Glycerol; TG: Triacylglycerol and WE: was ester.

| mzmed | rtmed | name | code | adduct | *m/z (adduct)* | *monoisotopic_mass* | delta | ppm error | fold change | p-value |
|---|---|---|---|---|---|---|---|---|---|---|
| 376.335 | 3.16 | MG (18:0) | HMDB11131 | [M + NH4+]+ | 376.342133 | 358.308309832 | 0.01 | 18 | 0.45 | 0.013 |
| 814.600 | 7.64 | PC (36:2) | HMDB11244 | [M+FA-H] | 814.596742 | 769.598540559 | 0.00 | 4 | 2.08 | 0.040 |
| 932.632 | 5.54 | DGDG 34:3 | lipid maps | [M + NH4+]+ | 932.6305 | 914.5957 | 0.00 | 1 | 0.56 | 0.023 |
| 934.653 | 6.26 | DGDG 34:2 | HMDB41511 | [M + NH4+]+ | 934.646145 | 916.612322146 | 0.01 | 7 | 0.62 | 0.050 |
| 985.596 | 5.84 | DGDG (40:9) | LIPID MAPS | [M-H]- | 985.5894 | | 0.01 | 7 | 0.55 | 0.020 |
| 983.579 | 5.25 | DGDG (40:10) | LIPID MAPS | [M-H]- | 983.5737 | | 0.01 | 6 | 0.23 | 0.022 |
| 985.907 | 13.66 | TG(42:2) | HMDB43153 | [M + H+]+ | 985.915768 | 984.908491572 | 0.01 | 9 | 0.28 | 0.041 |
| 399.363 | 5.17 | Episterol | HMDB06847 | [M + H+]+ | 399.362142 | 398.354866094 | 0.00 | 1 | 6.64 | 0.037 |
| 413.378 | 5.63 | Stigmasterol | HMDB00937 | [M + H+]+ | 413.377792 | 412.370516166 | 0.00 | 1 | 4.06 | 0.027 |
| 706.652 | 15.98 | WE(48:8) | | M+NH4 | 706.6496 | 688.6157769 | 0.00 | 3 | 0.17 | 0.009 |
| 425.376 | 2.41 | Anhydrosophoradiol | | M+H | 425.377792 | 424.370516158 | 0.00 | 4 | 0.22 | 0.001 |
| 441.369 | 1.85 | Linoleyl carnitine | | M+NH4 | 441.368682 | 423.3348589 | 0.00 | 0 | 0.16 | 0.001 |
| 431.388 | 5.08 | a-tocopherol | HMDB01893 | [M + H+]+ | 431.388357 | 430.381080844 | 0.00 | 0 | 0.35 | 0.004 |
| 447.346 | 5.89 | Carboxy-g-tocopherol | HMDB12557 | [M + NH4+]+ | 447.346886 | 446.33960996 | 0.00 | 1 | 3.97 | 0.038 |
| 419.315 | 4.09 | Carboxy-a-chromanol | HMDB39317 | [M + H+]+ | 419.315586 | 418.308309832 | 0.00 | 2 | 0.56 | 0.029 |

**Table 8.5**- List of the *m/z* values that presented significant changes (p-value <0.05) between less contaminated and more contaminated sites by mercury in roots of *Juncus maritimus*. The absolute concentrations of lipids were calculated considering the area of the corresponding internal standards added to the extraction. The identified compound corresponds to the lipid molecule with the minimum mass error value with respect to the measured *m/z*, considering all the possible adducts in the positive and negative ionization mode. The list only contains the compounds with a Benjamini–Hochberg's corrected *p-value* <0.05. PA: Phosphatidic Acid; PC: Phosphatidyl-Choline; PE: Phosphatidyl-Ethanolamine; PG: Phosphatidyl-Glycerol; DGDG: Di-Galactosyl-Diacyl-Glycerol; MGDG: Mono-Galactosyl-Diacyl-Glycerol; DG: Diacylglycerol.

| mzmed | rtmed | name | code | adduct | *m/z (adduct)* | *monoisotopic_mass* | delta | ppm error | fold change | p-value |
|---|---|---|---|---|---|---|---|---|---|---|
| 718.544 | 8.0 | PA(36:2) | HMDB07862 | [M + H+]+ | 718.538131 | 717.530855409 | 0.01 | 8 | 2.87 | 0.036 |
| 760.592 | 8.0 | PC(34:1) | HMDB08263 | [M + H+]+ | 760.585081 | 759.577805117 | 0.01 | 9 | 4.74 | 0.027 |
| 788.615 | 8.6 | PC 36:1 | HMDB08038 | [M + H+]+ | 788.616381 | 787.609105245 | 0.00 | 2 | 5.81 | 0.045 |
| 786.606 | 8.5 | PC(36:2) | HMDB00593 | [M + H+]+ | 786.600731 | 785.593455181 | 0.00 | 6 | 5.27 | 0.044 |
| 784.591 | 7.4 | PC(36:3) | HMDB08591 | [M + H+]+ | 784.585081 | 783.577805117 | 0.01 | 7 | 4.55 | 0.038 |
| 782.577 | 6.5 | PC(36:4) | HMDB08014 | [M + H+]+ | 782.569431 | 781.562155053 | 0.01 | 10 | 2.37 | 0.046 |
| 762.506 | 8.7 | PE 38:7 | HMDB09456 | [M + H+]+ | 762.506831 | 761.499554797 | 0.00 | 1 | 4.99 | 0.028 |
| 760.489 | 8.1 | PE 38:8 | HMDB09393 | [M + H+]+ | 760.491181 | 759.483904733 | 0.00 | 3 | 4.94 | 0.026 |
| 792.565 | 5.4 | PG (36:2) | HMDB10605 | [M+NH4+]+ | 792.574908 | 774.54108526 | 0.01 | 12 | 2.70 | 0.041 |
| 962.687 | 7.6 | PG (49:8) | lipids maps | [M + NH4+]+ | 962.6844 | | 0.00 | 2 | 2.19 | 0.026 |
| 932.632 | 5.5 | DGDG 34:3 | lipids maps | [M + NH4+]+ | 932.6305 | 914.5957 | 0.00 | 1 | 1.72 | 0.025 |
| 749.521 | 7.9 | MGDG 34:5 | lipids maps | [M + H+]+ | 749.5199 | 748.5126 | 0.00 | 2 | 0.70 | 0.017 |
| 792.563 | 5.4 | MGDG 36:6 | lipids maps | [M + NH4+]+ | 792.562 | 774.5272 | 0.00 | 1 | 2.65 | 0.042 |
| 381.297 | 2.8 | MG (20:3) | HMDB11547 | [M+H+]+ | 381.299936 | 380.292659768 | 0.00 | 8 | 1.80 | 0.030 |
| 615.500 | 9.2 | DG 36:5 | HMDB56211 | [M + H+]+ | 615.498301 | 614.491001 | 0.00 | 2 | 1.5 | 0.008 |
| 656.622 | 9.7 | DG (37:0) | Lipids maps | [M + NH4+]+ | 656.6187 | | 0.00 | 4 | 0.16 | 0.015 |
| 538.520 | 7.4 | Ceramide (d18:1/16:0) | | [M + H+]+ | 538.519371 | 537.512095015 | 0.00 | 1 | 0.59 | 0.018 |
| 399.362 | 5.2 | Episterol | HMDB06847 | [M + H+]+ | 399.362142 | 398.354866094 | 0.00 | 1 | 0.29 | 0.007 |
| 415.393 | 5.7 | b-Sitosterol | HMDB00852 | [M + H+]+ | 415.393442 | 414.38616623 | 0.00 | 1 | 0.12 | 0.004 |

| | | | | | | | | | | |
|---|---|---|---|---|---|---|---|---|---|---|
| 413.379 | 5.6 | Stigmasterol | HMDB00937 | M+H | 413.377792 | 412.370516166 | 0.00 | 2 | 0.13 | 0.017 |
| 411.363 | 5.3 | 5-Dehydroavenasterol | HMDB06852 | [M+H+]+ | 411.362142 | 410.354866094 | 0.00 | 2 | 0.17 | 0.031 |
| 692.634 | 16.3 | Sitosteryl ester (18:3) | HMDB06736 | [M + NH4+]+ | 692.634005 | 674.60018174 | 0.00 | 0 | 0.49 | 0.031 |
| 690.623 | 15.7 | Stigmasteryl ester (18:3) | Lipids maps | [M + NH4+]+ | 690.6183 | | 0.00 | 7 | 0.28 | 0.024 |
| 694.650 | 16.9 | Sitosteryl ester (18:2) | HMDB06734 | [M + NH4+]+ | 694.649655 | 676.615831804 | 0.00 | 0 | 0.48 | 0.031 |
| 431.388 | 5.1 | a-tocopherol | HMDB01893 | [M + H+]+ | 431.388357 | 430.381080844 | 0.00 | 0 | 0.56 | 0.017 |
| 392.287 | 3.56 | Carboxy-a-chromanol | HMDB12866 | [M + H+]+ | 391.284286 | 390.277009704 | 0.00 | 3 | 1.14 | 0.037 |